PHYSICAL REVIEW D **96,** 083510 (2017)

Spectrum of the axion dark sector

Matthew J. Stott,[1,*] David J. E. Marsh,[1,†] Chakrit Pongkitivanichkul,[1,2,3,‡] Layne C. Price,[4,§] and Bobby S. Acharya[1,5,‖]

[1]*Theoretical Particle Physics and Cosmology Group, Department of Physics, King's College London, University of London, Strand, London WC2R 2LS, United Kingdom*

[2]*The Center for Future High Energy Physics, Institute of High Energy Physics, Beijing 100049, China*

[3]*Department of Physics, Khon Kaen University, Khon Kaen 40002, Thailand*

[4]*McWilliams Center for Cosmology, Department of Physics, Carnegie Mellon University, Pittsburgh, Pennsylvania 15213, USA*

[5]*The Abdus Salam International Centre for Theoretical Physics, Strada Costiera 11, Trieste 34151, Italy*

(Received 28 June 2017; published 11 October 2017)

Axions arise in many theoretical extensions of the Standard Model of particle physics, in particular the "string axiverse." If the axion masses, m_a, and (effective) decay constants, f_a, lie in specific ranges, then axions contribute to the cosmological dark matter and dark energy densities. We compute the background cosmological (quasi)observables for models with a large number of axion fields, $n_{\rm ax} \sim \mathcal{O}(10\text{–}100)$, with the masses and decay constants drawn from statistical distributions. This reduces the number of parameters from $2n_{\rm ax}$ to a small number of "hyperparameters." We consider a number of distributions, from those motivated purely by statistical considerations to those where the structure is specified according to a class of M-theory models. Using Bayesian methods, we are able to constrain the hyperparameters of the distributions. In some cases, the hyperparameters can be related to string theory, e.g., constraining the number ratio of axions to moduli, or the typical decay constant scale needed to provide the correct relic densities. Our methodology incorporates the use of both random matrix theory and Bayesian networks.

DOI: 10.1103/PhysRevD.96.083510

I. INTRODUCTION

The Standard Model of particle physics is an overwhelming triumph of 20th Century physics. Combined with the general theory of relativity (and a model for neutrino masses), it is able to describe all terrestrial phenomena over a vast range of energy scales, and it has been verified with exquisite precision in the 21th Century by the work conducted at the Large Hadron Collider [1]. The Standard Model fails spectacularly, however, when applied on cosmological scales. Observations of the cosmic microwave background (CMB) temperature and polarization anisotropies, for example, imply that the present-day energy density of the Universe is dominated by dark matter (DM) and dark energy (DE) [2]. The particle content of the Standard Model contains no candidate for DM [3], and the value of the DE density, if assumed to be solely due to the cosmological constant, Λ, cannot be explained [4].[1]

These problems at the heart of particle and cosmological physics today force us to explore a wide range of theories beyond the Standard Model. Many such theories invoke ideas combining a combination of extra dimensions of spacetime and supersymmetry (SUSY), with the leading such theory being string/M-theory (e.g., Ref. [5]). The extra dimensions are compact in these models, which in turn leads, in the low-energy, $(3+1)$-dimensional description, to the existence of massless pseudoscalar axionlike fields (which, for simplicity, we now refer to as simply "axions") [6,7].[2]

The number of axions depends on the topology of the compact dimensions. In realistic compactifications of string theory, this can easily be in the range of $\mathcal{O}(10)$ to $\mathcal{O}(100)$, or more (e.g., Ref. [8]). The axions generically acquire masses, m_a, due to nonperturbative quantum effects (e.g., instantons [9,10]), and as such, the masses depend exponentially on parameters of the UV theory, such as the size of extra dimensions. In the context of string theory, there are many effects which can be used to generate potentials for the axion fields such as world sheet or brane instantons. On the other hand, the axion "decay constants," f_a, are expected to be of order of the UV scale [11]. Large decay constants lead to suppressed couplings between axions and the Standard Model. This leads to the theoretical expectation that there should exist some large number of light, stable, axions given the potential complexity of the extradimensional manifold, an idea known as the "string axiverse" [12].

*matthew.stott@kcl.ac.uk
†david.marsh@kcl.ac.uk
‡chakpo@kku.ac.th
§laynep@andrew.cmu.edu
‖bobby.acharya@kcl.ac.uk

[1]Cosmology, of course, also presents two other huge problems for the Standard Model: the baryon asymmetry and the generation of initial conditions (inflation). We will not discuss these problems in detail.

[2]There is also the presence of scalar moduli to account for. We will discuss moduli stabilization in due course.

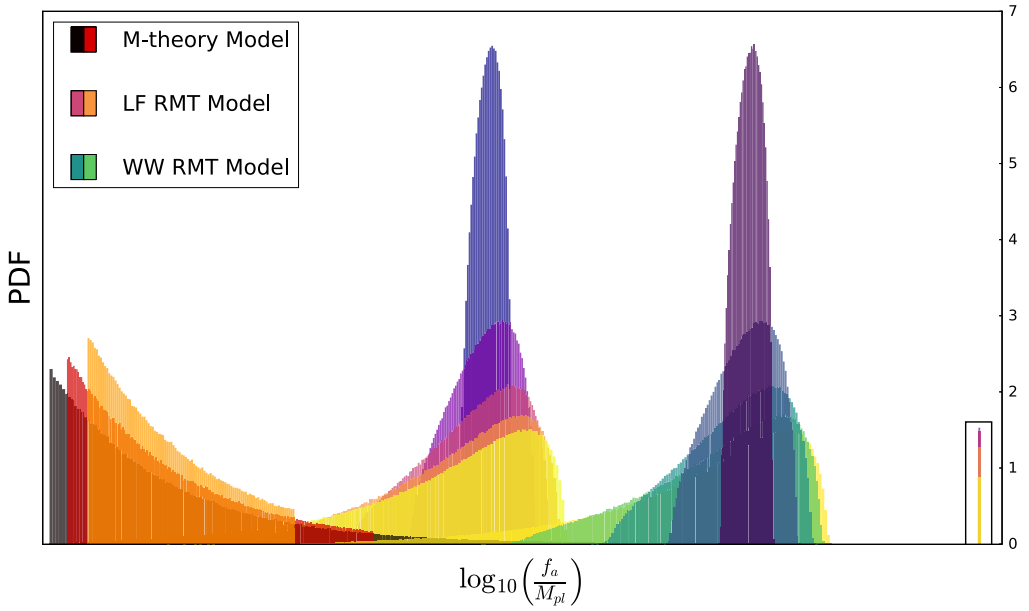

FIG. 1. String axiverse RMT model axion decay constant spectra: Probability density plots displaying the spectra for the axion decay constants, f_a, defined as the eigenvalues of the kinetic matrix in Eq. (8) constructed using 7500 iterations with $n_{\rm ax} = 100$. The shape of the spectrum determines the initial axion field range as well as affects the axion mass distribution after rotating to the canonical basis. The highlighted (black rectangle) values demonstrate the enhancement of the eigenvalue spectra width when using nonzero mean, non-Gaussian distributions (log-flat RMT (LF RMT) model, Sec. III C 3) for the kinetic matrix. For visual clarity, we include an arbitrary normalization offset on the distribution mean. In practice, the normalization is given by the Planck scale, $M_{\rm pl}$, and the mean is determined by a free model parameter of the order of the fundamental scale.

Light, stable axions are excellent DM candidates and can also contribute to the DE density, with a rich phenomenology (for a review of axion cosmology, see Ref. [13]). However, a large number of axion fields brings with it $2n_{\rm ax}^2$ parameters coming from the kinetic and mass matrices present in an effective field description, making a brute force treatment of the cosmology difficult. Natural questions which arise are as follows. What is the typical DM and DE cosmology which emerges from a string axiverse model? Under what conditions do string axiverse models give rise to realistic cosmologies? In order to address these problems, we present an initial study in the context of string axiverse cosmology for simplified axiverse models relating to both the problems of DM and DE, utilizing the frameworks of Bayesian networks and random matrix theory (RMT). In this study, we present five different models, characterized by their corresponding distributions for the elements of both the kinetic matrix (which is related to the Kähler metric) and mass matrix of a multiaxion field theory. The distributions for f_a and m_a, after rotation of the matrices to the canonical diagonal basis, determine the cosmology of string axiverse theories, and we present constraints on the hyperparameters of these distributions from the DM and DE densities.

One of our models, inspired by the Jeffreys prior, incorporating scale invariance of the physical quantities, is a statistical straw man: log-flat eigenvalue distributions, "maximally ignorant" of any underlying fundamental theory. Another straw man assumes a trivial kinetic matrix, with the mass matrix eigenvalue distribution derived from the Marčhenko-Pastur law for random matrices (loosely related to axion models [14,15]). The other three models assume nontrivial distributions in the kinetic matrix, giving rise to nontrivial distributions for the axion decay constants, f_a, in the diagonal basis. Our most physically motivated model for the matrix distributions is derived from considering the string axiverse arising in M-theory compactified on G_2-manifolds [16]. The distributions of the decay constants for these models are shown (in arbitrary units) in Fig. 1 [we define the decay constants *before* accounting for "alignment" (see Sec. II D)]. The form of the resulting mass distributions after rotations of the matrices differ from the straw-man models and are discussed throughout this paper. Table I describes each of the models we consider in this study and their associated location in the paper.

We make no discussion in this work of the possible couplings between axions and the Standard Model, or any production modes for axions other than vacuum realignment. This is the simplest possible model-independent approach to the axiverse in a cosmological context. See Refs. [13,17] for discussion of other axion production modes and detection of axions through nongravitational interactions. In this work, we focus on very long-lived, light axions, as candidates for DM and DE. Heavier, unstable axions have long been considered as good candidates to drive inflation, embedding natural inflation [18] in the string landscape. A top down approach to the issues of

TABLE I. String axiverse models used throughout this study with their corresponding short-hand notation. Also detailed are their sections of appearance in the text giving the properties of their construction as well as their DM/DE cosmology considerations.

Model	Label	Section
I. Scale invariant	*SI*	*Sec. III B*
i. Dark matter	SI DM	"
ii. Dark energy	SI DE	"
II. Marčenko-Pastur	*MP RMT*	*Sec. III C 1/C 2*
i. Dark matter	MP DM	Sec. IV A 1/ V B 1
ii. Dark energy	MP DE	Sec. IV A 2/ V B 1
III. Wishart/Wishart	*WW RMT*	*Sec. III C 2/C*
i. Dark matter	WW DM	Sec. IV B 1
ii. Dark energy	WW DE	Sec. IV B 2
IV. Log-flat/log-flat	*LF RMT*	*Sec. III C 3/C 3*
i. Dark matter	LF DM	Sec. IV C 1
ii. Dark energy	LF DE	Sec. IV C 2
V. M-theory	*MT RMT*	*Sec. III D/B 1*
i. Dark matter	MT DM	Sec. IV D 1/V B 2
ii. Dark energy	MT DE	Sec. IV D 2

cosmic inflation was tackled in Ref. [18] by incorporating the potential effects of the presence of two axion fields. This was achieved via an alignment mechanism known as the Kim-Nilles-Peloso (KNP) mechanism, which served to increase the effective field range, with each individual axion maintaining a consistent sub-Planckian range. The KNP alignment mechanism was later extended to $n_{\rm ax} \geq 2$ axions for multinatural inflation, providing a more generalized approach applicable to the string landscape in both Refs. [19,20]. Recent work on the vacuum decay rate statistics in N-dimensional field space, with landscapes well suited for inflationary model building, subject to possible alignment effects was explored in Refs. [21,22], where the authors identified the potential stability of such random axionic landscapes.

The paper is organized with the following structure. Section II presents an initial look at axions in string theory as well as detailing our effective model for string axiverse cosmology, introducing the key concepts of the kinetic matrix, $\mathcal{K}_{ij}$, and mass matrix, $\mathcal{M}_{ij}$, along with the initial field conditions. Section III presents a set of random matrix theory models for $\mathcal{K}_{ij}$ and $\mathcal{M}_{ij}$. We also present in this section a random matrix approach to G_2 compactifications of M-theory. Our results begin in Sec. IV, where we present example cosmologies for all of our models with either fixed values of the underlying parameters or gridded scans of multidimensional parameter space. Section V presents constraints on the random matrix parameters from a Markov chain Monte Carlo (MCMC) analysis of the quasiobservables from the CMB using Bayesian networks; we cover only a subset of the possible models, with a complete treatment left for future work. We conclude with discussions of our study in Sec. VI.

Appendix A presents details of our scheme for the numerical solutions to the equations of motion and more details about the assumed cosmology. Appendix B reviews the form of the superpotential arising in both M-theory and Type-IIB string theory along with details of the possible connection between random matrix theory and Type-IIB string theory on Calabi-Yau manifolds. Appendix C introduces the principle concepts of random matrix theory we incorporate in our RMT models as well as the basics of the Marčhenko-Pastur density function for sample covariance matrices and potential extensions/deviations from this law for different matrix ensembles. Finally, Appendix D contains some novel examples of outlier cosmologies.

Our numerical code, AxionNet, is written in PYTHON and is available to download from https://github.com/DoddyPhysics/AxionNet.

II. AXIONS

A. String axions: A single field example

Axions respect a perturbative shift symmetry, $\theta \to \theta + \text{const}$, of Goldstone bosons. For geometric axions, this symmetry comes from the higher-dimensional gauge symmetries of supergravity. Nonperturbative effects generically break this shift symmetry down to a discrete subgroup. Axions are characterized using two parameters: the axion decay constant, f_a, and the energy scale of the associated nonperturbative physics, Λ_a. The effective four-dimensional Lagrangian for the dimensionless axion field with a spacetime metric signature, $(-,+,+,+)$, is

$$\mathcal{L} = -\frac{f_a^2}{2}\partial_\mu\theta\partial^\mu\theta - \Lambda_a^4 U(\theta), \tag{1}$$

where $U(\theta)$ is some periodic potential of the dimensionless fields, θ. In the dilute instanton gas approximation, the field potential is given by

$$V(\theta) = \Lambda_a^4 U(\theta) = \Lambda_a^4(1-\cos\theta). \tag{2}$$

The nonperturbative physics present an exponential dependence on the instanton action S,

$$\Lambda_a^4 = \mu^4 e^{-S}. \tag{3}$$

The parameter μ is a mass scale determined by the geometric mean of the SUSY breaking scale and the "fundamental" scale such as the string or Planck scale. The canonically normalized axion field is

$$\phi = f_a\theta, \tag{4}$$

from which we see that the axion decay constant, f_a, sets the scale of periodicity in the potential. For small field displacements $\theta < 1$, performing a local Taylor expansion about the vacuum $\theta = 0$ up to quadratic order yields the axion mass term

$$m_a = \frac{\Lambda_a^2}{f_a}. \tag{5}$$

For small field displacements, f_a disappears as an explicit parameter in the Lagrangian. However, because of its role in the periodicity of the potential, it still appears as the natural range of field values for ϕ. In the ensuing discussion, we use f_a as the scale of the initial conditions.

B. String axiverse: An effective theory

For multiple fields arising in typical string axiverse models, we must consider cross-couplings in the field kinetic terms present in the nontrivial axion field space metric $\mathcal{K}_{ij}$. In SUSY theories, this is related to the Kähler metric, which, for axions paired with Kähler moduli, is given by $\frac{\partial^2 K}{\partial\tau_i\partial\tau_j}$, where K is the Kähler potential and τ_i represent the moduli fields (see Ref. [5] for a more general description). In supergravity, the basis for the axion fields is such that the kinetic matrix is both nondiagonal and not canonically normalized, where the general Lagrangian takes the form

$$\mathcal{L} = -M_{\rm pl}^2\mathcal{K}_{ij}\partial_\mu\theta_i\partial^\mu\theta_j - M_{\rm pl}^2\mathcal{M}_{ij}\theta_i\theta_j. \tag{6}$$

The mass matrix is determined as usual from the Kähler potential and the superpotential, W. For simplicity, we expand the potential to the mass term and will not use the full general form of the cosine potential, which expresses the entries of $\mathcal{M}_{ij}$ in terms of the instanton charge matrix, $\mathcal{Q}$. We discuss this briefly later, and a full treatment will be the subject of future work.

We diagonalize the Lagrangian by beginning with the diagonalization of $\mathcal{K}_{ij}$,

$$\mathcal{K} = U^T\mathrm{diag}(\mathcal{K})U = \frac{1}{2}U^T\mathrm{diag}(f_a)\mathrm{diag}(f_a)U, \tag{7}$$

where we define the axion decay constants, f_a, from the eigenvalues of $\mathcal{K}_{ij}$ in the original (nondiagonal) basis. We discuss how this choice relates to the axion initial conditions in the next subsection. The decay constants thus defined are (in Planck units)

$$\vec{f_a} = \sqrt{2\mathrm{eig}(\mathcal{K})}. \tag{8}$$

We next define the canonically normalized field:

$$\tilde{\phi} = M_{\rm pl}\mathrm{diag}(f_a)U\theta. \tag{9}$$

Inserting this definition, we find the Lagrangian for the canonical fields:

$$\mathcal{L} = -\frac{1}{2}\partial_\mu\tilde{\phi}_i\partial^\mu\tilde{\phi}_j - \frac{1}{2}\tilde{\phi}_i\tilde{\mathcal{M}}_{ij}\tilde{\phi}_j. \tag{10}$$

The new mass matrix is given by

$$\tilde{\mathcal{M}} = 2\mathrm{diag}(1/f_a)U\mathcal{M}U^T\mathrm{diag}(1/f_a). \tag{11}$$

The new mass matrix is diagonalized by

$$\tilde{\mathcal{M}} = V^T\mathrm{diag}(m_a^2)V. \tag{12}$$

Defining the mass-eigenstate fields,

$$\phi = V\tilde{\phi} = M_{\rm pl}V\mathrm{diag}(f_a)U\theta. \tag{13}$$

The fully diagonalized Lagrangian is

$$\mathcal{L} = -\frac{1}{2}\partial_\mu\phi_i\partial^\mu\phi_i - \frac{1}{2}\mathrm{diag}(m_a^2)\phi_i\phi_i. \tag{14}$$

Equation (14) is the canonical mass-eigenstate basis with the mass spectrum dependence coming from the initial forms of $\mathcal{K}_{ij}$, $\mathcal{M}_{ij}$, and the various rotations in field space. As is the case in the single axion example, the axion decay constants coming from diagonalization of $\mathcal{K}_{ij}$ now only play a role in setting the natural initial displacements of the axion fields.

C. Axion cosmology

We work in a homogeneous and isotropic universe with a flat Friedmann-Lemaître-Robertson-Walker (FLRW) geometry,

$$\mathrm{d}s^2 = -\mathrm{d}t^2 + a^2(t)\mathrm{d}\vec{x}^2, \tag{15}$$

where $a(t)$ is the cosmological scale factor, normalized to unity today, defining the cosmological redshift $a(z) = 1/(1+z)$. The equations of motion for the axion fields follow from the canonical action for matter,

$$S_m = \int \mathrm{d}^4x\sqrt{-g}\mathcal{L}, \tag{16}$$

with g the FLRW metric determinant. Axions obey the Klein-Gordon equation of motion,

$$\ddot{\phi}_i + 3H\dot{\phi}_i + m_{a,i}^2\phi_i = 0, \tag{17}$$

where the dot denotes the derivative with respect to the cosmic time. The Friedmann constraint for the Hubble parameter, $H = \dot{a}/a$, is

$$3H^2M_{\rm pl}^2 = \sum_i \rho_i, \tag{18}$$

where the sum over i extends over all axions, ordinary matter, dark matter, radiation, and the cosmological constant. See Appendix A for more details.

We solve the axion field equations in cosmic time and use the Friedmann constraint to find $a(t)$, which determines the evolution of the standard fluid components via their equation of state. The combined equation of state for the axions is given by

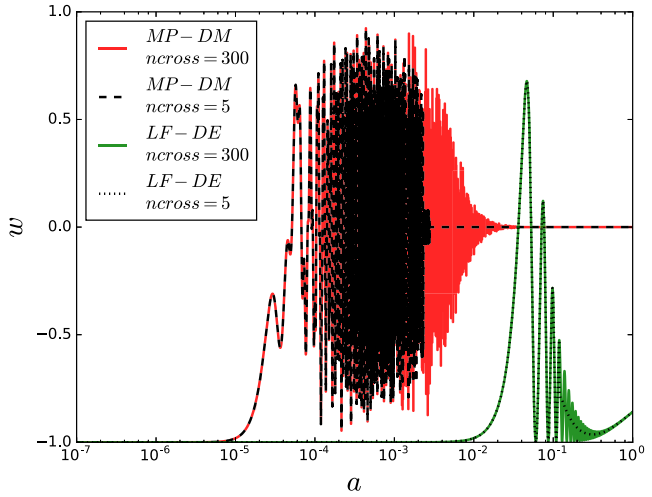

FIG. 2. Evolution of the collective axion equation of state: The collective axion equation of state, w_a, as a function of the cosmic scale factor, a, for axions behaving as either the total dark matter or total dark energy in different RMT models. $n_{\rm cross}$ referrers to the numerical precision; see Appendix A.

$$w_a = \frac{P_a}{\rho_a} = \frac{\frac{1}{2}\sum_i^N \dot{\phi}_i^2 - V}{\frac{1}{2}\sum_i^N \dot{\phi}_i^2 + V}. \tag{19}$$

The total equation of state today determines the acceleration parameter, $\ddot{a}$.

Figure 2 shows the collective equation of state for example multifield evolutions involving $n_{\rm ax} = 10$ axions for both dark matter and dark energy cosmologies in different RMT models. The dashed and dotted lines detail our approximations where we show the effect on the collective equation of state for the axion population when we restrict the individual equations of state for each field to a fixed number of oscillatory crossings used as an accuracy parameter we denote as $n_{\rm cross}$. The amplitude of the total equation of state is damped from the effects of multiple fields with nondegenerate associated scales in the population, oscillating between the values of ≤ 1 and ≥ -1. In the limit $n_{\rm ax} = 1$, the equation of state will continue to oscillate between -1 and 1. We find that $n_{\rm cross} = 5$ captures a significant proportion of the total field behavior as compared to increased values of $n_{\rm cross}$. See Appendixes A 3 and A 4 for details of our process used and the choice of approximation.

The axion fields are initially overdamped setting the fields in slow roll, $\dot{\phi}_i \approx 0$, with an almost constant equation of state, $w_a \approx -1$. This type of field evolution demonstrates the ability of axions to behave as candidates in quintessence or inflationary models. As the Hubble rate, H, decreases, the fields overcome the Hubble friction present as a damping term in their equations of motion, at a time $t^i_{\rm osc} \approx H^{-1}$ satisfying the condition $m_{a,i} \approx H$. The ith axion field now begins to coherently oscillate about the minimum of its potential with an amplitude determined by its initial misalignment angle. In this phase, the axions will begin to dilute slower and scale as pressureless matter where the equation of state begins to oscillate about $w_a = 0$ and a phase of underdamping begins. The axion pressure now averages to zero, and the energy density begins to scale as $\rho_a \propto a^{-3}$, leaving the axion as a suitable dark matter candidate. The left-hand panel of Fig. 3 details an example evolution of the components of the energy density through numerical integration of the equations of motion for $n_{\rm ax} = 10$ fields in the

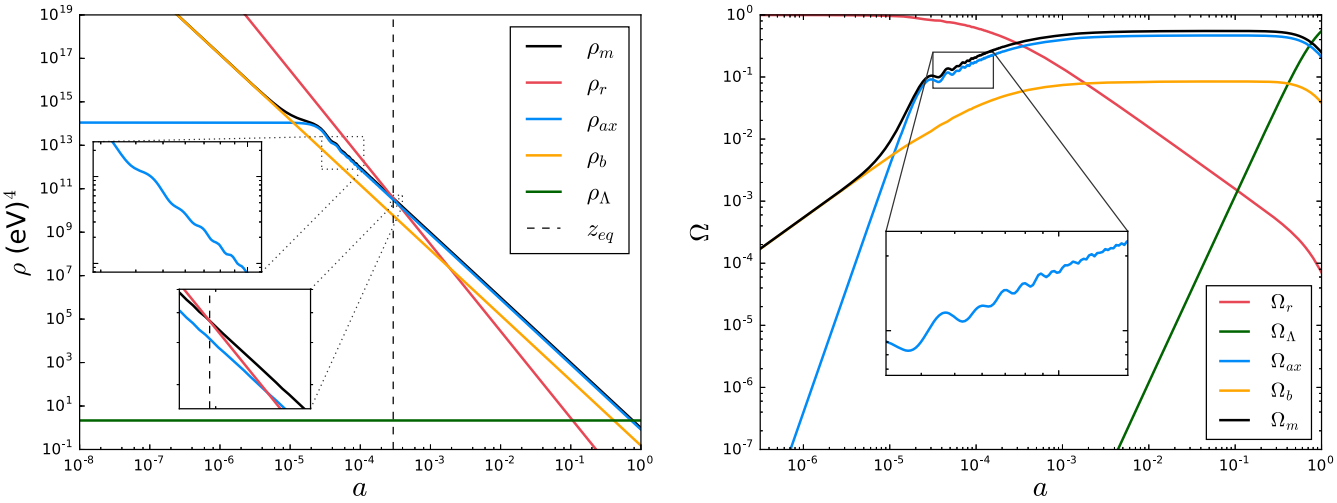

FIG. 3. Evolution of the cosmological densities and cosmological density parameters: *Left panel*: Plot for the evolution of cosmological densities, ρ, as a function of the cosmic scale factor, a, for $n_{\rm ax} = 10$ axions behaving as the total dark matter in the MP RMT model. *Right panel*: Plot for the evolution of the contributions to the critical density, $\Omega_i = \rho_i/3H^2$, as a function of the cosmic scale factor, $a(t)$. Each panel details the evolution of the MP RMT axions plus the standard ΛCDM parameters Ω_r, Ω_Λ and Ω_b. *Left figure upper inset*: Enhanced view of the effect of multifield oscillations on the total axion density, ρ_{ax}. *Left figure lower inset*: Comparative matter-radiation equality with crossings of $\rho_m = \rho_b + \rho_{ax}$ and ρ_r at $z_{\rm eq} = 3393$ defined in Table II. *Right figure inset*: Enhanced view of the effect of multifield oscillations on the axion density parameter $\Omega_{\rm DM}$ contributing to the critical density.

universe as well as the remaining standard ΛCDM parameters. The evolution of the associated density parameters is plotted in the right-hand panel.

At any given time, fields with $H \gtrsim m_{a,i}$ will behave as a contribution to the total effective dark energy density, $\Omega_{\rm DE}$, and fields with $H \lesssim m_{a,i}$ behave as a contribution to the total dark matter density, $\Omega_{\rm DM}$. We classify axions as either DM or DE components of the energy density of the universe according to the description in Appendix A. We use this to determine $\Omega_m = \Omega_b + \Omega_{\rm DM}$ and $\Omega_{\rm DE,tot} = \Omega_\Lambda + \Omega_{\rm DE}$. The evolution of ρ_m with redshift determines the redshift of matter-radiation equality, $z_{\rm eq}$.

D. Initial conditions

The role of the axion decay constants, for our purposes, is to fix the natural initial field displacements and thus the axion relic density from vacuum realignment [23–25]. In the (generic) case of multiple axions where the number of instantons providing the axion masses is larger than the number of axions, the notion of a single "axion decay constant" is not well defined.[3]

Expanding the potential to the mass term alone, the dimensionful scales that control the evolution and relic densities are the initial displacements of the canonical fields. In all cases, we set our initial conditions on the axion fields as

$$\phi_i^{\rm ini} = \mathcal{F}_{ij}\vartheta_j, \tag{20}$$

for some (random) matrix $\mathcal{F}_{ij}$, where ϑ is a random vector with elements in the range $[0, \pi]$ (as expected for an initially massless field with a discrete shift symmetry and a symmetric potential).

We set the initial conditions on ϑ_i to uniformly sample the field space in some basis. We do this by noting that there is some basis where the ϑ_i forms a cubic lattice. We uniformly sample in this cubic basis, since this is operationally very simple. However, we note that this is not a uniform sampling of the field space in the "charge basis" defined by the charge matrix, $\mathcal{Q}$, an integer matrix of which the entries reside in a charge lattice in the cosine potential, $V(\theta) = \sum_{X,i}\Lambda_X[1 - \cos(\mathcal{Q}_i^X\theta_i)]$. We leave investigations of this interesting question, which is intimately related to the notions of alignment and charge quantization, for future work. For other discussions of this point, and sampling of initial conditions in general, see Refs. [15,26–29]. We define the matrix $\mathcal{F}_{ij}$ for two different possibilities for the cubic basis. Consider the set of transformations that turn the initial fields, θ, into the canonically normalized fields, ϕ, in index notation:

$$\frac{\phi_i}{M_{\rm pl}} = V_{ij}{\rm diag}(f_a)_{jk}U_{kl}\theta_l. \tag{21}$$

[3]We thank Thomas Bachlechner for discussion on this point.

In general, we should expect that in the cubic basis both $\mathcal{K}_{ij}$ and $\mathcal{M}_{ij}$ are off diagonal, and so $\vartheta_i = \theta_i$. On the other hand, it could be the case that the cubic basis is the same basis as the one in which $\mathcal{K}_{ij}$ is diagonal. In that case, it is natural to set $\vartheta_i = U_{ij}\theta_j$. We allow for both possibilities in our numerical explorations (though for the MP and MT models, where $\mathcal{K}_{ij}$ is diagonal by construction, the two choices are the same).

For completeness of discussion, we still seek to define a measure on the initial field displacements that is somewhat equivalent to the usual notion of a "decay constant," We define such a measure by the following vector for the general case,

$$\tilde{\varphi}_i \coloneqq |V_{ij}{\rm diag}(f_a)_{jk}U_{kl}\langle\vartheta\rangle_l|, \tag{22}$$

where $\langle\vartheta\rangle$ is the vector of $\pi/2$ values representing the average of ϑ. For the case of the cubic basis with diagonal $\mathcal{K}_{ij}$, we define our measure as

$$\varphi_i = |V_{ij}{\rm diag}(f_a)_{jk}\langle\vartheta\rangle_k|. \tag{23}$$

The overall scale of our initial conditions is set by the eigenvalues of $\mathcal{K}_{ij}$ giving the elements f_a. However, rotations can shift these values onto different canonical fields, allowing for N-flation type enhancement by the Pythagorean sum. The initial field conditions coming from f_a to ϕ, $\tilde{\varphi}$ and φ are shown in Fig. 4. In the upper and lower left-hand panels, we show the initial field displacements of the form in Eq. (4) for both the WW RMT and LF RMT models where the bulk of the spectrum is initially limited to sub-Planck scale values (upper and lower left panels). ϕ is defined using Eq. (20) where $\mathcal{F}_{ij} = {\rm diag}(\sqrt{2f_a^2})_{ij}$ such that $\phi_i = {\rm diag}(\sqrt{2}f_a)_{ij}\langle\vartheta\rangle_j$. In the upper panels, we see that the initial field displacements quickly converge to a negatively skewed distribution on a logarithmic scale when using a *white* Wishart matrix for $\mathcal{K}_{ij}$ (see Sec. III C 2). Selecting a new basis identified by a further rotation acting on $\mathcal{F}_{ij}$ does not alter the initial field displacements where we observe a degeneracy across all values of $\beta_\mathcal{K}$.

When a *spiked* Wishart matrix is used for $\mathcal{K}_{ij}$ (see Sec. III C 3), the repulsed eigenvalues shown for ϕ "enhance" the potential initial field conditions when selecting a new basis for sampling. Said alternatively, the convergence of the spectra via the unitary rotations is "slower" in this model maintaining features of the initial matrix spectra for $\mathcal{K}_{ij}$. The spectra for each choice of basis are distinct in their output as shown in the central and right lower panels. In the basis for φ, lower values of $\beta_\mathcal{K}$ maintain the hard edge of the nonrotated spectra (lower left panel) with values of $\beta_\mathcal{K} \to 1$ providing larger probability densities for field displacement transcending the $M_{\rm pl}$ limit. The two models converge when finally selecting $\tilde{\varphi}$ as the choice of basis.

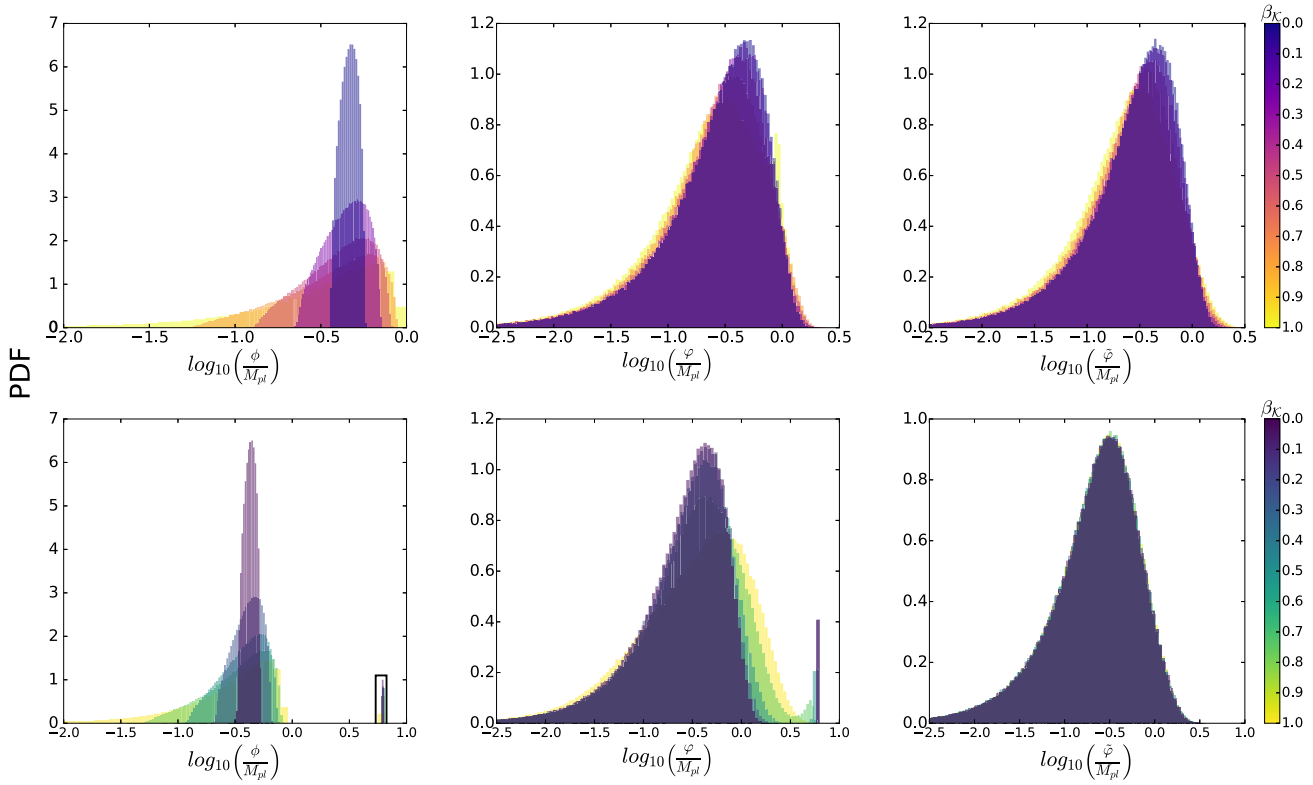

FIG. 4. String axiverse RMT model initial field displacement spectra: Probability density plots for the initial axion field displacements defined in each basis outlined in Eqs. (8), (22) and (23) for 5000 iterations using $n_{\rm ax} = 75$. *Upper panels*: Zero centered mean, Gaussian distributions used for the elements of the kinetic matrix $\mathcal{K}_{ij}$ [WW RMT model (Sec. III C 2)]. *Lower panels*: Nonzero centered mean, non-Gaussian distributions used for the elements of the kinetic matrix $\mathcal{K}_{ij}$ [LF RMT model (Sec. III C 3)]. The highlighted (black rectangle) values demonstrate the enhancement of the spectral width in the LF RMT model.

III. STRING AXIVERSE

A. Random matrix approach to the string axiverse

1. Generalities

A simplified approach to modeling the *string axiverse* is to use random matrix theory to encode the structure of the kinetic matrix and mass matrix appearing in the effective model description in the Lagrangian of Eq. (6), without detailed knowledge of the underlying Kähler potential and superpotential. The power of random matrix theory is the notion that large, complicated systems present the properties of universality, depending only on the symmetry classes of these systems. A key observation can be made that when the dimensional order of these matrices is increased their spectra begin to stabilise with their properties determined by one of several limiting laws such as Wigner's celebrated semicircle law. At a very basic level, random matrix theory and the universality that emerges from it can be considered a generalization of the central limit theorem. See Appendix C for further discussion on the generalities of random matrix theory. Accessible introductions to these topics can be found on Terry Tao's blog[4] and in the book by Mehta [30].

In each class, the matrices we consider will all have elements drawn from the same statistical distribution. Our matrices are not block diagonal, with blocks containing different scales. Physically, therefore, there are no separate sectors; all the axions we consider receive their masses from effects of the same order. Universality then dictates that our distributions will, up to outliers, be classified by a single (mean) scale and spread (variance and other moments). The lack of bimodality means that the mass distributions are unlikely to furnish us simultaneously with axions classified as DM [$m_a \gtrsim H(z_{\rm eq}) \sim 10^{-27}$ eV] and DE [$m_a \lesssim H(z_0) \sim 10^{-33}$ eV], while at the same time having no cosmologically problematic axions at the intermediate scale [31].

Given these considerations, we will restrict ourselves to only considering two classes of random matrices constructed in the form of Eq. (C2) without any loss of generality for our concerns. First is the well-motivated case of matrices residing in the Wishart ensemble of real sample covariance matrices. The limiting spectrum of normalized Wishart matrices $W = \frac{1}{p} X^T X$, where X is a $(n \times p)$ rectangular matrix and $p \geq n$ is given by the Marčhenko-Pastur law (see Appendix C 2) with spectral properties determined by an aspect ratio, $n/p \in (0, 1]$ (see

[4] https://terrytao.wordpress.com/

below). The universality of the Marčhenko-Pastur law deems it will hold for arbitrary distributions of zero mean and unit variance. When constructing our kinetic and mass matrices in this form, we shall designate them as a white Wishart matrix parametrized by $\beta = 1$ in the standard *beta* ensemble for random matrices (see Appendix C 1). (White) Wishart matrices often occur in many applications of random matrix theory and can play a key role in areas such as multidimensional Bayesian analysis [32,33]. The generalized construction of Wishart matrices via higher order convulsions have spectra described by the *Fuss-Catalan* distributions which could prove an interesting extension in future work [34]. See Appendix C for further discussion.

Second, we will investigate the properties of nonuniversality and extremal fluctuations in the asymptotic behavior of singular values in random matrix models using a non-Gaussian distribution for the entries of the submatrices, X. Matrices constructed in this manner are subject to an eigenvalue repulsion in the form of singular eigenvalues away from a bulk region of the distribution. The bulk of these distributions is governed by the Marčhenko-Pastur density function. Further discussion can be found in Appendix C or Refs. [35–38] of spiked Wishart covariance models with these properties. We will not consider in detail the finer properties of the analysis associated to the largest eigenvalues for sample covariances matrices with spiked populations through their moments or the nature of the Baik, Ben Arous and Pèchè phase transition which can lead to such phenomena [39]. We will treat our models at the level of the statistical distributions used to construct our submatrices only highlighting the features and spectral properties their eigenvalue distributions may exhibit. We will designate a matrix constructed in this way as a spiked Wishart matrix.

To summarize, for any given random matrix model, we construct both $\mathcal{K}_{ij}$ and $\mathcal{M}_{ij}$ as normalized positive-definite matrices in the following way,

$$A_{hj}, B_{hj} \in \mathbb{R}^{n\times p}, \tag{24}$$

$$\mathcal{K}_{ij} = \frac{1}{p} A^T_{ih} A_{hj} \in \mathbb{R}^{n\times n}, \tag{25}$$

$$\mathcal{M}_{ij} = \frac{1}{p} B^T_{ih} B_{hj} \in \mathbb{R}^{n\times n}, \tag{26}$$

where the entries of the submatrices A_{hj} and B_{hj} in Eq. (24) are random entries drawn from a given statistical distribution, $\Omega(\mu, \sigma)$.

In our models of the string axiverse, by construction, $\mathcal{K}_{ij}$ and $\mathcal{M}_{ij}$ are square matrices with a dimension determined by the number of axions, $(n_{\rm ax}, n_{\rm ax})$. By definition, the submatrices in our RMT models, A_{hj} and B_{hj}, need not be square. This defines the incorporation of our aspect ratio shaping parameters $\beta_{\mathcal{K}}$ and $\beta_{\mathcal{M}}$ where the submatrices A_{hj} and B_{hj} are both rectangular with the defined dimensions $(n_{\rm ax}, n_{\rm ax}/\beta_{\mathcal{K}})$ and $(n_{\rm ax}, n_{\rm ax}/\beta_{\mathcal{M}})$, respectively. The shaping parameters are explicitly defined as

$$\beta_{\mathcal{K}} = n_{\rm ax}/p_{\mathcal{K}}, \tag{27}$$

$$\beta_{\mathcal{M}} = n_{\rm ax}/p_{\mathcal{M}}, \tag{28}$$

where $p_{\mathcal{K},\mathcal{M}} \geq n_{\rm ax}$. When we select the two shaping parameters to be the same value determined by $p_{\mathcal{K}} = p_{\mathcal{M}}$ (which we will in general through this study), we shall refer to this using the notation $\beta_{\mathcal{K},\mathcal{M}}$. See Appendix B 3 for a discussion on the role of these parameters in the context of realizations of the axiverse in string theory along with the likely values they take.

B. Scale-invariant measure on eigenvalues

For a straw-man model, and as a baseline with which to compare our physically motivated models, we consider a log-flat prior using the motivations of scale invariance on the positive, real, *physical* and dimensionful parameters coming from $\mathcal{K}_{ij}$ and $\mathcal{M}_{ij}$, that is, on the decay constants in the diagonal basis along with normalization factors of $\sqrt{2}$ and masses in the canonical diagonal basis. Such a prior is well motivated in the in context of axiverse literature [12] and is inspired by the Jeffreys prior. The axion decay constants could also span several decades [40,41]. We use the log-flat prior for both of these unknown dimensionful quantities as a *maximally ignorant* approach.

We begin in the mass-eigenstate basis [Eq. (14)] where both $\mathcal{K}_{ij}$ and $\mathcal{M}_{ij}$ are diagonal and consider only the eigenvalues of both the kinetic and mass matrix in this basis. The axion parameters are drawn from

$$\log_{10}(\mathrm{eig}(\mathcal{K}_{ij})) \in \mathcal{U}[k_{\rm min}, k_{\rm max}], \tag{29}$$

$$\log_{10}(\mathrm{eig}(\mathcal{M}_{ij})) \in \mathcal{U}[m_{\rm min}, m_{\rm max}]. \tag{30}$$

The uniform distribution is unnormalized and is only a proper prior for our considerations once the end points of the distribution are fixed by the controlling limits. By definition, this breaks the scale invariance of our prior; however, we retain motivations for bounded limits in concordance with the literature. The values

$$\mathrm{eig}(\mathcal{K}_{ij}) = f^2_{a,i}, \tag{31}$$

$$\mathrm{eig}(\mathcal{M}_{ij}) = m^2_{a,i} \tag{32}$$

represent the elements of the diagonalized kinetic and mass matrix, respectively. The limits $k_{\rm min}$ and $k_{\rm max}$ in general are associated with lower and upper bounds on nonperturbative physics scales. The upper and lower bounds, $m_{\rm min}$ and

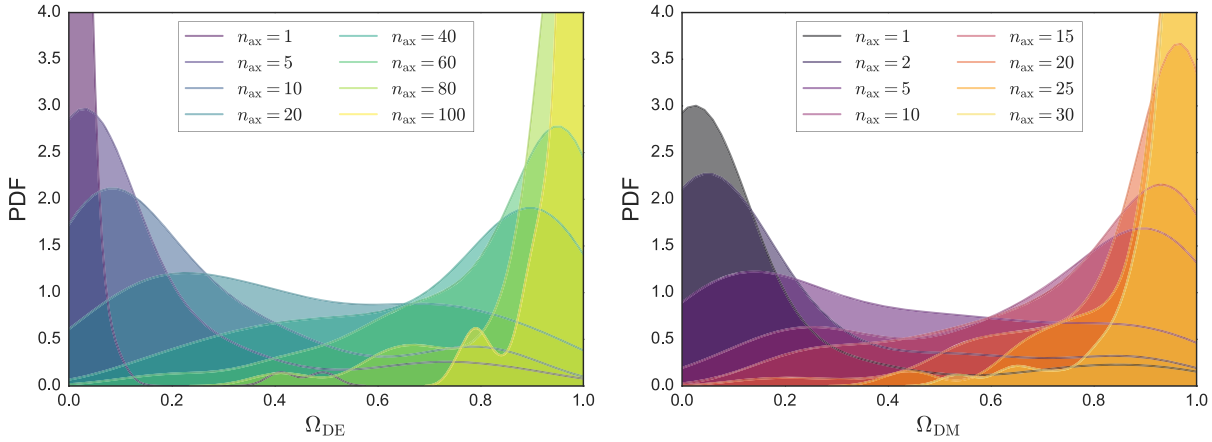

FIG. 5. Dark energy and dark matter cosmologies with scale-invariant measure on physical parameters: *Left panel*: kernel density estimation plot for the axion dark energy density parameter, $\Omega_{\rm DE}$, with $n_{\rm ax} = \mathcal{O}(1) \to \mathcal{O}(100)$ with log-flat priors on both the physical parameters, m_a^2 and f_a^2, sampled in the window detailed in Eqs. (33) to (35). *Right panel*: kernel density estimation plot for the axion dark matter density parameter, $\Omega_{\rm DM}$, with $n_{\rm ax} = \mathcal{O}(1) \to \mathcal{O}(10)$ with log-flat priors on both the physical parameters, m_a^2 and f_a^2, sampled in the window detailed in Eqs. (36) to (38).

$m_{\rm max}$, represent a portion of the axion mass window suited for extracting fields behaving as either DE or DM. In the left-hand panel of Fig. 5, we show the KDE plot in the context of axions behaving as DE with the following parameter priors:

$$n_{\rm ax} = \mathcal{O}(1) \to \mathcal{O}(100), \tag{33}$$

$$\log_{10}(\mathrm{eig}(\mathcal{K}_{ij})/M_{\rm pl}) \in \mathcal{U}[-4.0, -0.5], \tag{34}$$

$$\log_{10}(\mathrm{eig}(\mathcal{M}_{ij})/M_H) \in \mathcal{U}[-2.0, 2.0]. \tag{35}$$

Correspondingly, the right-hand panel of Fig. 5 shows the KDE plot for axions behaving as DM using the following priors:

$$n_{\rm ax} = \mathcal{O}(1) \to \mathcal{O}(10), \tag{36}$$

$$\log_{10}(\mathrm{eig}(\mathcal{K}_{ij})/M_{\rm pl}) \in \mathcal{U}[-4.0, -0.5], \tag{37}$$

$$\log_{10}(\mathrm{eig}(\mathcal{M}_{ij})/M_H) \in \mathcal{U}[6.0, 16.0]. \tag{38}$$

The requirement for axion population sizes with at least $n_{\rm ax} \approx \mathcal{O}(10)$, in order to give a realistic chance of finding cosmologies returning values of $\Omega_{\rm DE}$ sitting in the rough window $\Omega_{\rm DE} = (0.6 \to 0.8)$, is evident in the left-hand panel of Fig. 5. The right-hand panel of Fig. 5 shows that an increase in the field population size quickly leads to the domination of axion DM when utilizing a significant mass window. We use the information in both panels of Fig. 5 to indicate the potential for multiple axions giving the required values of $\Omega_{\rm DM}$ and $\Omega_{\rm DE}$ while maximising the size of the population. In general, our RMT models will consider more localized scale windows, and as such, we select a population size of $n_{\rm ax} = 20$ to serve as a good common ground between both types of cosmology.

C. Random matrix theory models

For a more physically realistic approach, we should expect our axion parameters to be encoded in some kind of matrix structure, with a nontrivial role played by the rotations between different bases. This is due to the fact there is some physical meaning to the basis in which Dirac quantization occurs, which in general is not the same as the diagonal basis. In general, this RMT structure will give localized physical parameter distributions, where we shall suspend the exploration of coupled dark sector cosmologies as a focus of future work beyond the simple example above. The following sections detail the introduction of random matrices for the string axiverse, highlighting the potential random matrix theory has to consider a more complete picture of the axion landscape

Our study consists of three models with their foundations in the universal behavior of asymptotic RMT plus an approach to realizations of the string axiverse in G2 compactified M-theory. Below, we outline our treatment of both the kinetic and mass matrix and associated parameters in these models. In the right-hand panels of Fig. 6, we present the eigenvalue spectra of the mass matrix in the mass-eigenstate basis for each model using arbitrary prior configurations. In the left-hand panels, we show an approximated theoretical density function fit for the form of the finite-dimensional matrix spectra in our models.

1. MP RMT model (unit $\mathcal{K}_{ij}$/white Wishart $\mathcal{M}_{ij}$)

This model is based on the N-flation model presented in Ref. [15] (see Appendix B 2) whereby we encode our uncertainty using a spectrum of masses governed by the

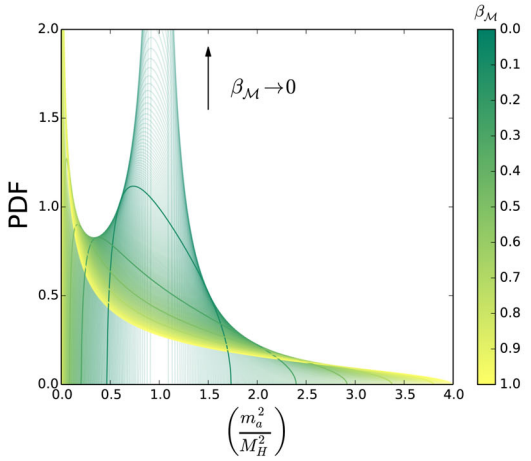

(a) **MP RMT:** Marčhenko-Pastur density function for 250 values of $\beta_{\mathcal{M}} \in (0, 1]$ centred about $\langle m_a^2 \rangle = M_H^2$.

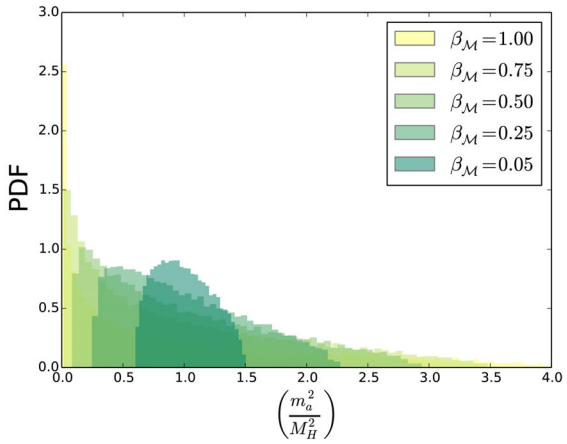

(b) **MP RMT:** Probability density plots for the eigenvalues m_a^2 of $\mathcal{M}_{ij}$ centred about $\langle m_a^2 \rangle = M_H^2$.

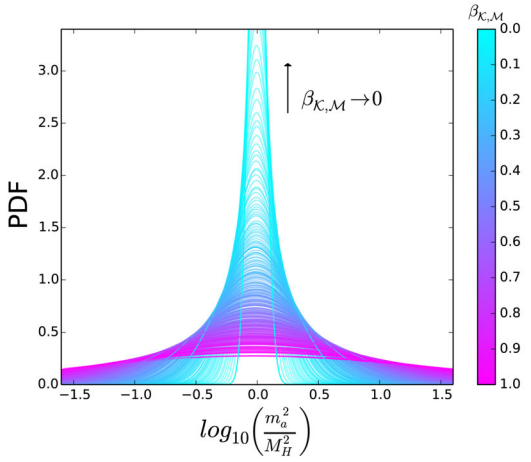

(c) **WW RMT:** Log-normal density function fit using 250 values of $\beta_{\mathcal{K},\mathcal{M}} \in (0, 1]$ centred about $\langle m_a^2 \rangle = M_H^2$.

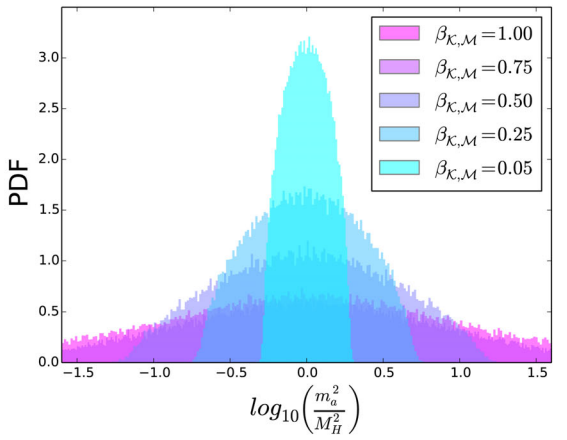

(d) **WW RMT:** Probability density plots for the eigenvalues m_a^2 of $\mathcal{M}_{ij}$ centred about $\langle m_a^2 \rangle = M_H^2$.

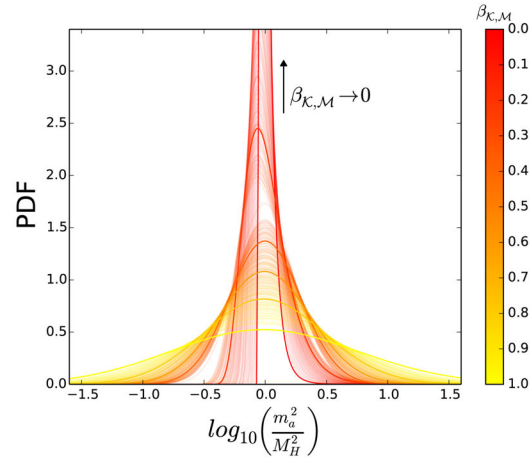

(e) **LF RMT:** Log-normal density function fit using 250 values of $\beta_{\mathcal{K},\mathcal{M}} \in (0, 1]$ centred about $\langle m_a^2 \rangle = M_H^2$.

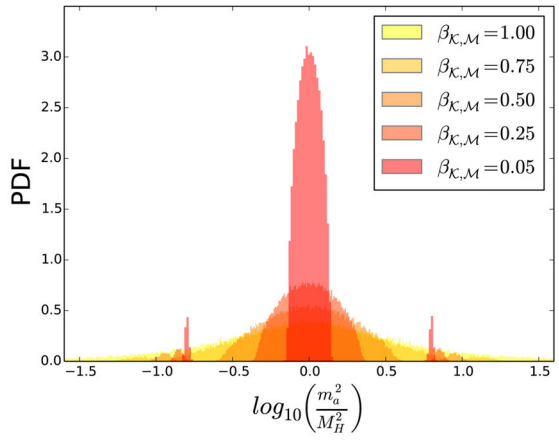

(f) **LF RMT:** Probability density plots for the eigenvalues m_a^2 of $\mathcal{M}_{ij}$ centred about $\langle m_a^2 \rangle = M_H^2$.

FIG. 6. Theoretical mass squared value spectra density function fits and associated $\mathcal{M}_{ij}$ eigenvalue probability densities for RMT models: *Left-hand panels:* Theoretical density function fits for each of the RMT models outlined in Secs. III C 1–III C 3 for 250 values of $\beta_{\mathcal{K},\mathcal{M}} \in (0, 1]$. *Right-hand panels:* Probability density plots for the eigenvalue spectrum of the rotated mass matrix, $\mathcal{M}_{ij}$, constructed using 1000 iterations and an axion population size $n_{\rm ax} = 50$.

Marčhenko-Pastur density function for a population of N uncoupled axions. We need only to consider the matrix structure for the mass matrix, $\mathcal{M}_{ij}$, where, unlike our other models in the subsequent sections, we begin in the following basis,

$$\mathcal{L} = -\frac{1}{2}\partial_\mu\phi_i\partial^\mu\phi_j - \frac{1}{2}\phi_i\mathcal{M}_{ij}\phi_j, \tag{39}$$

where our mass matrix is constructed as

$$\mathcal{M}_{ij} = \left(\frac{n_{\rm ax}}{\beta_{\mathcal{M}}}\right)B^T_{ih}B_{hj}, \tag{40}$$

$$B_{hj} \in \sigma_{\mathcal{M}} \times \mathcal{N}(0,1). \tag{41}$$

Our parameters in this model for $\mathcal{M}_{ij}$ consist of the scaling factor $\sigma_{\mathcal{M}}$ which sets the value of $\langle m_a^2\rangle$ and distribution shaping index $\beta_{\mathcal{M}}$. In this basis, the role of the kinetic matrix is such that $\mathcal{K}_{ij}$ is unitary providing only trivial rotations to the fields ($U_{kl} = \mathbb{1}$) and mass matrix following the process outlined in Sec. II B. Following the considerations in Ref. [15] when setting the initial field conditions, the treatment of the kinetic terms is replaced by considering the axion vacuum expectation values (vevs) in the mass-eigenstate basis using an equal field condition scale parameter, $\bar{f}$, along with the initial misalignments. The initial field conditions in this model are defined as

$$\phi_i = V_{ij}\bar{f}\mathbb{1}\theta_l. \tag{42}$$

Figure 6(a) shows the theoretical eigenvalue spectrum of $\mathcal{M}_{ij}$, following the Marčhenko-Pastur density function for 250 varying values of $\beta_{\mathcal{M}}$. In Fig. 6(b), we show the probability density convergence of the eigenvalue spectrum to the Marčhenko-Pastur law for a large number of fields ($n_{ax} = 1000$). The MP RMT model parameters are

$$n_{\rm ax}, \quad \sigma_{\mathcal{M}}, \quad \beta_{\mathcal{M}}, \quad \bar{f}.$$

2. WW RMT model (white Wishart $\mathcal{K}_{ij}$/white Wishart $\mathcal{M}_{ij}$)

It has also been suggested that the kinetic matrix, $\mathcal{K}_{ij}$, may too be well approximated by a matrix belonging to the Wishart ensemble on the basis of universality and symmetry [26,42,43]. For the purposes of alignment, the fundamental domain of such a matrix benefits from properties of eigenvector delocalization and has well-motivated features for inflationary models. In this model, we include a kinetic matrix constructed with the same approach for the mass matrix in Sec. III C 1, where

$$\mathcal{K}_{ij} = \left(\frac{n_{\rm ax}}{\beta_{\mathcal{K}}}\right)A^T_{ih}A_{hj}, \tag{43}$$

$$A_{hj} \in \sigma_{\mathcal{K}} \times \mathcal{N}(0,1), \tag{44}$$

which in turn introduces the distribution shaping parameter $\beta_{\mathcal{K}}$. We begin in the basis defined in Eq. (6). In this basis, the matrix structure for $\mathcal{K}_{ij}$ gives an axion decay constant spectrum governed by the Marčhenko-Pastur law up to canonical normalization factors. The mass matrix, $\mathcal{M}_{ij}$, is now subject to nontrivial unitary rotations used to diagonalize $\mathcal{K}_{ij}$. In Fig. 6(d), we show the rotated mass matrix spectrum for fixed values of $\beta_{\mathcal{K},\mathcal{M}}$. We use Fig. 6(c) to display the approximate reduction of the spectral width for 250 different values of $\beta_{\mathcal{K},\mathcal{M}} \in (0,1]$ via a log-normal density function fit on the mass spectra.

In the limit $\beta_{\mathcal{K},\mathcal{M}} = 1$, the mass probability distributions are well modelled by a log-normal density function. When $\beta_{\mathcal{K},\mathcal{M}} \neq 1$, the mass spectrum is better approximated by truncated log-normal density functions as the edges of the distribution are hardened, simultaneously reducing the spectral width of the distribution. In the limit $\beta_{\mathcal{K},\mathcal{M}} \to 0$, we observe the convergence to a semicircular distribution within a significantly more localized mass window. The WW RMT model parameters are

$$n_{\rm ax}, \quad \sigma_{\mathcal{M}}, \quad \sigma_{\mathcal{M}}, \quad \beta_{\mathcal{K}}, \quad \beta_{\mathcal{M}}.$$

3. LF RMT model (spiked Wishart $\mathcal{K}_{ij}$/spiked Wishart $\mathcal{M}_{ij}$)

Our final RMT model will focus on the case in which we relax the condition that our submatrices A_{hj} and B_{hj} are formed using statistical distributions defined with zero mean, where

$$A_{hj}, B_{hj} \in \sigma_{\mathcal{K},\mathcal{M}} \times \Omega(\emptyset, \sigma). \tag{45}$$

Our choice statistical distribution takes a log-flat prior on the elements of the submatrices in Eq. (45), using the motivations of scale invariance highlighted in Sec. III B, as displayed in Eqs. (46) and (47). The random matrices $\mathcal{K}_{ij}$ and $\mathcal{M}_{ij}$ now fall under a class of matrices which exhibit the properties of a rank-1 spiked Wishart matrix (see Appendix C). The eigenvalue spectrum of these matrices presents a bulk distribution governed by the Marčenko-Pastur law with one single outlier of the order $\lambda_{\rm max} \sim \mathcal{O}(n_{\rm ax})$ for a $n_{\rm ax} \times n_{\rm ax}$ dimensional matrix. Figure 7 shows the normalized mass spectrum before basis selection rotations using $n_{\rm ax} = 300$, demonstrating these features in the spectrum. The axion decay constants in this model present a distribution of the form in Fig. 1 (log-scale) and 7 (linear scale) up to canonical normalization factors. An interesting feature of this model could be the realization of an eigenvalue repulsion manifesting itself in the form of a single large decay constant traversing fundamental scales

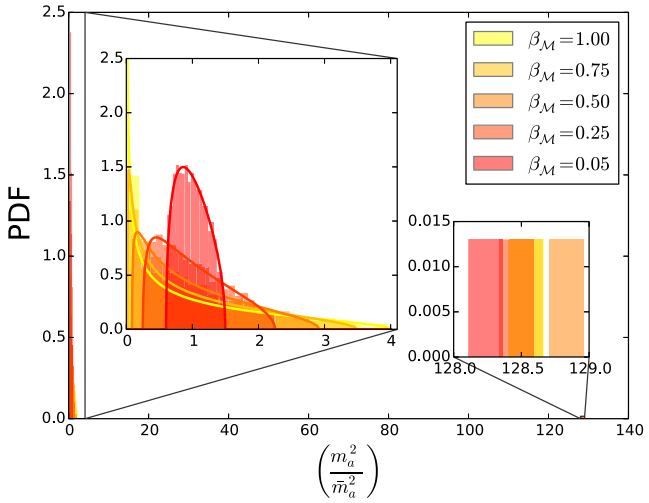

FIG. 7. LF RMT model nonrotated mass spectrum: Eigenvalue spectrum of m_a^2 values for a 300×300 matrix, $\mathcal{M}_{ij}$, before basis selection rotations in the LF RMT model demonstrating the spiked Wishart spectral properties of the initial mass matrix. The bulk of the eigenvalue spectrum is governed by the Marčenko-Pastur law (*left inset*), which is partnered with one single outlying eigenvalue of $\mathcal{O}(N)$ (*right inset*).

while the bulk of the distribution is contained in the subfundamental limit.

In order to construct our matrices, we choose that each submatrix is parametrized by two upper and lower limit parameters for the elements in each matrix, denoted by $k_{\min}$, $m_{\min}$ and $k_{\max}$, $m_{\max}$. The elements of each submatrix A_{hj} and B_{hj} are drawn from

$$\log_{10} A_{hj} \in \mathcal{U}[k_{\min}, k_{\max}], \tag{46}$$

$$\log_{10} B_{hj} \in \mathcal{U}[m_{\min}, m_{\max}]. \tag{47}$$

In accordance with the previous WW RMT model, the eigenvalue spectrum of $\mathcal{K}_{ij}$ is subject to nontrivial rotations from the unitary rotations acting on $\mathcal{K}_{ij}$ where we also observe a log-normal distribution convergence of the mass spectrum in the mass-eigenstate basis in the limit $\beta_{\mathcal{K},\mathcal{M}} = 1$. Unlike the WW RMT model when $\beta_{\mathcal{K},\mathcal{M}} \neq 1$, the outlying eigenvalues present in the mass matrix in the initial basis cause the formation of two outlying regions with eigenvalues separated from the bulk region of the spectrum in the mass-eigenstate basis. The total spectral width of the eigenvalues is not reduced for values of $\beta_{\mathcal{K},\mathcal{M}} \neq 1$ as displayed in Fig. 6(d), demonstrating the importance of the outlying eigenvalues in the initial basis. This model retains a nonzero probability density for fields with masses away from the bulk of the spectrum as shown in Fig. 6(f).

Following the treatment used in Fig. 6(c), we show the theoretical log-normal density function fit for 250 values of $\beta_{\mathcal{K},\mathcal{M}} \in (0, 1]$ for the LF RMT model in Fig. 6(e). The separation of the distribution into three populations, a bulk and two repulsed regions when $\beta_{\mathcal{K},\mathcal{M}} \neq 1$, induces a skew in the log-normal density functions. This does not provide a very accurate theoretical fit for the total form of the mass spectrum; however, we use this as an approximated measure of the effect of singular repulsed eigenvalues in the initial basis to compare to models without the properties of spiked population spectra. The skew in these distributions when $\beta_{\mathcal{K},\mathcal{M}} \neq 1$ gives an indication of the potential magnitude of divergence away from the cosmologies obtained when modeling both $\mathcal{K}_{ij}$ and $\mathcal{M}_{ij}$ with standard Wishart matrices. The LF RMT model parameters are

$$n_{\text{ax}}, \quad k_{\min}, \quad k_{\max}, \quad m_{\min}, \quad m_{\max}, \quad \beta_{\mathcal{K}}, \quad \beta_{\mathcal{M}}.$$

D. M-theory axiverse

In this section, we present a special type of RMT model motivated by the M-theory axiverse [16]. As we will see shortly, the matrix structure in the M-theory framework is constructed in a manner similar to the previous RMT models, guaranteeing positive definiteness in the axion masses. Since the moduli stabilization under the framework of G2 compactified M-theory has already been extensively studied in Refs. [44–46], we choose to explore the probability distribution of mass matrix eigenvalues and axion decay constants in the context of this framework. For technical details, see Appendix B 1.

To formulate the structure of $\mathcal{K}_{ij}$ and $\mathcal{M}_{ij}$, we begin with a continuation of the discussion in Appendix B 1, starting with an expansion up to quadratic order of the superpotential given in Eq. (B5) which gives the mass terms with the following mass matrix,

$$\mathcal{M}_{ij} = \sum_{k=1}^{n_{\text{ax}}} \sum_{r=1}^{N} \frac{4F\tilde{\Lambda}_r^3 b_r N_r^k}{M_S^3} e^{-b_r \sum_m^{n_{\text{ax}}} N_r^m s_m} b_r N_r^i b_r N_r^j \tag{48}$$

$$= \sum_{r=1}^{N} \frac{4F\tilde{\Lambda}_r^3 C_r}{M_S^3} e^{-S_r} \tilde{N}_r^i \tilde{N}_r^j, \tag{49}$$

where $\tilde{N}_i^j = b_i N_i^j$ is a rectangular matrix of size (n_{ax}, N), $C_r = \sum_k^{n_{\text{ax}}} \tilde{N}_r^k$ and $S_r = \sum_m^{n_{\text{ax}}} \tilde{N}_r^m s_m$. The dimensions of the $\tilde{N}_i^j$ are controlled by the axion population size, n_{ax}, and the number of instantons, N. This expression allows us to parametrize the mass matrix term as the product of two rectangular matrices,

$$\mathcal{M}_{ij} = \frac{1}{N} A_{ir} A_{jr}. \tag{50}$$

This leaves us with the following form for the submatrix,

$$A_{ir} = \left(2\sqrt{\frac{F\tilde{\Lambda}_r^3 C_r}{M_S^3}}\right) e^{-S_r/2} \tilde{N}_r^i, \tag{51}$$

where $i, j = 1, \ldots, n_{\rm ax}$ and $r = 1, \ldots, N$. Note that A_{ir} is a rectangular matrix of size $(n_{\rm ax}, N)$ where the normalization factor $1/N$ is introduced to provide a consistent construction structure compared to the generalized form of the matrices we consider in our RMT models. Since $N > n_{\rm ax}$, this implies that the shape parameter, $\beta_{\mathcal{M}}$, should take values of $\beta_{\mathcal{M}} < 1$.

An analysis of the kinetic terms allows us to find the axion decay constants, f_a. In the moduli sector, the Kähler potential takes the form

$$K = -\ln(\mathcal{V}_X), \tag{52}$$

where $\mathcal{V}_X$ is a homogeneous function of the moduli s_i, of degree α depicting the volume of the hidden manifold in 11-dimensional Planck length. One important feature of the Kähler potential is that it leads to a nontrivial Kähler metric (which in this case is also the axion kinetic matrix) $\mathcal{K}_{ij} \equiv \frac{\partial^2 K}{\partial z_i \partial z_j}$ which is a homogeneous function of degree minus 2. We can assume the simplest form parametrizing the nontrivial kinetic matrix is

$$\mathcal{K}_{ij} = \frac{a_i a_j}{s_i s_j}, \tag{53}$$

where a_i are constants and s_i represent the moduli fields. However, a generic matrix usually contains negative eigenvalues. To avoid such an issue, we will allow for the further simplification of the kinetic matrix such that $\mathcal{K}_{ij}$ is diagonal,

$$\mathcal{K} = \mathrm{diag}[(a/s)]. \tag{54}$$

It has been shown that such a form for the kinetic matrix can relieve tensions arising from dark radiation constraints in string axiverse models [47]. For convenience, we introduce a rescaling of the parameters so that all the physical parameters we consider are dimensionless,

$$F \to F/M_H^2, \tag{55}$$

$$\tilde{\Lambda}_i \to \tilde{\Lambda}_i/M_S, \tag{56}$$

$$\mathcal{M}_{ij} \to \mathcal{M}_{ij}/M_H^2, \tag{57}$$

$$\tag{58}$$

such that

$$\mathcal{M}_{ij} = \sum_{r=1}^{N} 4F\tilde{\Lambda}_r^3 C_r e^{-S_r} \tilde{N}_r^i \tilde{N}_r^j, \tag{59}$$

where we note that the moduli and axion fields are expressed with respect to the string scale.

The results of moduli stabilization in M-theory show that the moduli vacuum expectation value should range between values of $\sim(10 \to 100)$ in units of the string scale [44–46]. It is then natural to assume that our choice of prior should be a uniform distribution where

$$P(s_i) = \mathcal{U}(s_{\rm min}, s_{\rm max}), \tag{60}$$

with $s_{\rm min} \approx 10$, $s_{\rm max} \approx 100$. We also explore the values of the moduli vevs using a Gaussian distribution in some of our example cosmologies in Sec. IV D:

$$P(s_i) = \mathcal{N}(\bar{s}, \sigma_s). \tag{61}$$

There is no assumption made on the topology of the manifold such that the Kähler metric parameters are fixed to

$$a_i = 1. \tag{62}$$

The axion decay constants are then distributed between

$$f_{a,i} = \sqrt{2}a_i/s_i \sim (10^{-2}\text{–}10^{-1}). \tag{63}$$

The shape of the M-theory axion decay constant spectrum using arbitrary limits of the moduli vev distribution in Eq. (60) is shown in Fig. 1. The volume of the corresponding 3-cycles is calculated from

$$V_X^i = \mathrm{Im}(F_i) = \sum_{k=1}^{n_{\rm ax}} N_i^k s_k = \frac{1}{2\pi}\sum_{k=1}^{n_{\rm ax}} \tilde{N}_i^k s_k, \tag{64}$$

where F_i are the gauge kinetic functions (see Appendix B 1) and in the final step we make the assumption that the membrane instanton integers are equal to unity ($b_i = 2\pi$). Since we are considering M-theory models which are grand unified theories (GUTs) in their low-energy limits, at least one of the gauge kinetic functions must give rise to the expected value of the grand unified coupling constant $\alpha_{\rm GUT} = 1/V_X \approx 1/25$.

The distribution of $\tilde{N}_i^k$ is uniform from 0 to $\tilde{N}_{\rm max}$ such that

$$P(\tilde{N}_i^k) = \mathcal{U}(0, \tilde{N}_{\rm max}). \tag{65}$$

For some of our example cosmologies in Sec. IV D, the values of $\tilde{N}_i^k$ are sampled using a Gaussian distribution:

$$P(\tilde{N}_i^k) = \mathcal{N}(\bar{N}, \sigma_N). \tag{66}$$

In Fig. 8, we show the enhanced probability density for retrieving values of $V_X \approx 25$ when using $\tilde{N}_{\rm max} \approx 0.6$. Increasing the value of $\tilde{N}_{\rm max}$ serves to increase the spread of the distributions for V_X at values centered around $V_X > 25$ which are too high for GUT coupling constant unification. Due to the uniform nature of the distributions,

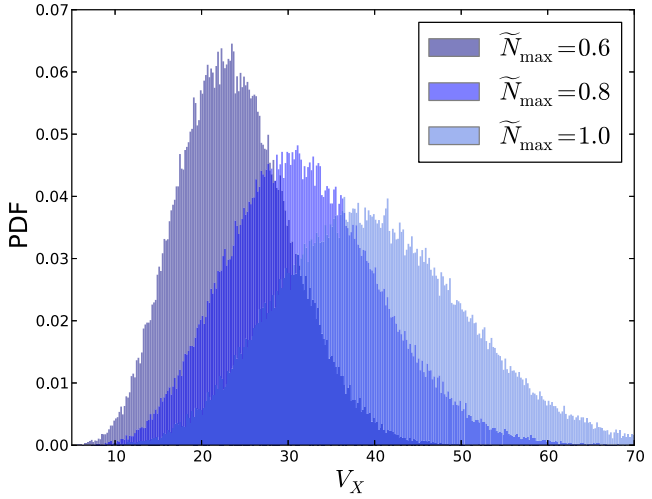

FIG. 8. MT RMT model 3-cycle volume distribution spectra: Probability density plots for the 3-cycle volume using $\tilde{N}_{\max} = 0.6$, 0.8, 1.0 with an axion population size, $n_{\rm ax} = 10$. The moduli vev is uniformly distributed between 10 to 100 in units of the string scale, $P(s_i) = \mathcal{U}(10, 100)$. The probability density of retrieving the GUT value, $V_X = 25$, is found to be enhanced for values of $\tilde{N}_{\max} \approx 0.6$.

we can chose to parametrize the axion mass distribution using the average value of 3-cycle volume distribution $\langle V_X \rangle$ instead of $\tilde{N}_{\max}$ as they are related by

$$\langle V_X \rangle = \frac{n_{\rm ax} \tilde{N}_{\max} \langle s \rangle}{4\pi}. \tag{67}$$

The values of the other mass scales and coefficients coming from the form of the mass matrix defined in Eq. (59) are taken as the following values,

$$\tilde{\Lambda}_i = \Lambda = \mathcal{O}(1), \tag{68}$$

$$F = 5.4 \times 10^{104} \left(\frac{m_{3/2}}{1 \text{ TeV}} \right), \tag{69}$$

where the large value of F is imposed by our choice of units. The mass scales in the mass matrix, $\mathcal{M}_{ij}$, are measured in units of M_H, and the scale of the quantities which give the value of F come naturally from a SUSY/high-energy physics/string theory perspective. These choices are made to account for the fact that nonperturbative scales are expected to show up around the string scale. The SUSY breaking order parameter is approximated using $m_{3/2} M_{\rm Pl}/M_H^2$ where the gravitino mass is assumed to be of order 1 TeV from naturalness arguments. In practice, we will use a single scale parameter, $F\Lambda^3 \sim \mathcal{O}(10^{105})$, which we allow to vary in our MCMC analysis.

In each panel in Fig. 9, we construct the probability density plots for the axion mass spectrum using 10,000 points in the parameter space. The left-hand panel of Fig. 9 shows the effect of varying $\beta_{\mathcal{M}}$ for fixed values of $\langle V_X \rangle$. As $\beta_{\mathcal{M}} \to 0$, it shifts to the mass spectrum to be centered around higher mass scales while also decreasing the spread of the masses. In the right-hand panel of Fig. 9, we show the expected result that larger values for the average volume lead to the axion masses centered about smaller values with a wider spread. For both of these configurations, we see axion masses covering many orders of magnitude, which is a key result common to many string axiverse models.

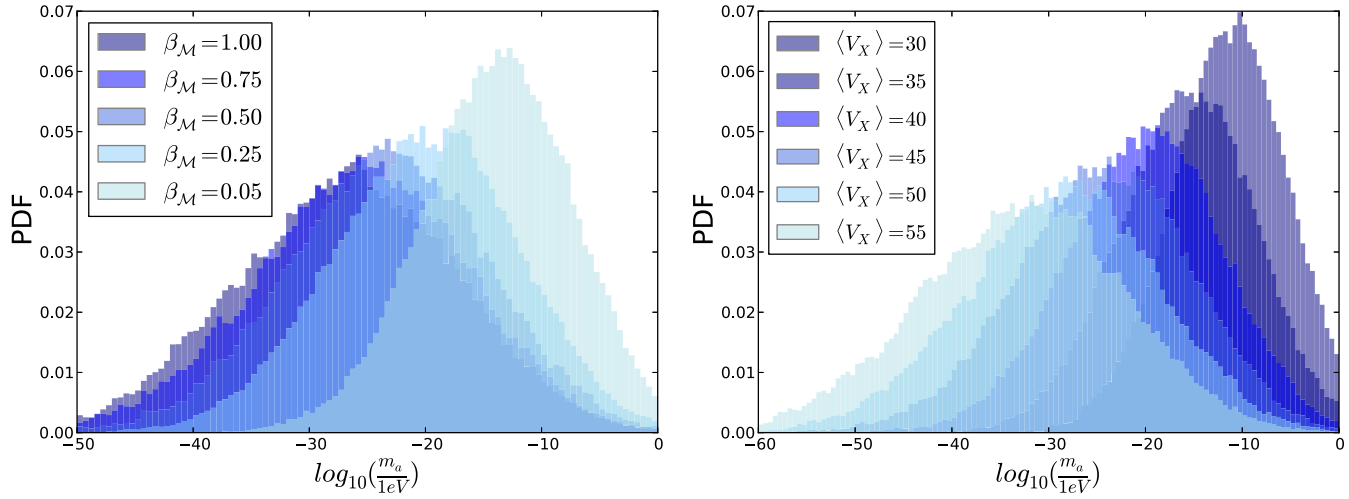

FIG. 9. MT RMT model mass spectra: *Left panel*: Probability density plots for axion masses using the fixed value $\langle V_X \rangle = 25$ for $\beta_{\mathcal{M}} = 1.00$, 0.75, 0.50, 0.25, 0.05. *Right panel*: Probability density plots for axion masses with fixed $\beta_M = 0.5$ for $\langle V_X \rangle = 30$, 35, 40, 45, 50, 55. Both panels are constructed using 10,000 iterations in the case of an axion population size, $n_{\rm ax} = 10$.

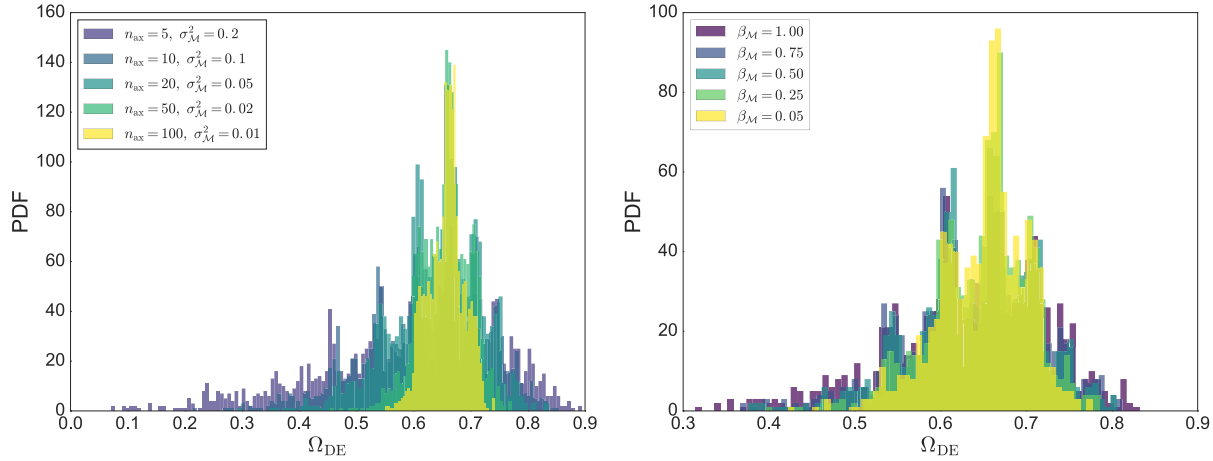

FIG. 10. MP RMT model DE cosmology examples: *Left panel*: Probability density plots for $n_{\rm ax} = \mathcal{O}(1) \to \mathcal{O}(100)$ with fixed values of $\sigma^2_{\mathcal{M}}$ according to the approximation in Eq. (72) with further fixed parameter values $\beta_{\mathcal{M}} = 0.5$ and $\bar{f} = 1$. *Right panel*: Approximate degeneracy for values of $\beta_{\mathcal{M}} \in (0, 1]$ for the axion dark energy density parameter $\Omega_{\rm DE}$ using $n_{\rm ax} = 20$ axions with fixed parameter values $\sigma^2_{\mathcal{M}} = 0.05$ and $\bar{f} = 1$.

IV. RESULTS I: DARK SECTOR COSMOLOGIES

We define two example cosmologies via contributions to the total energy density at the present time:

(i) *Dark matter cosmology.*—We will refer to the effective dark matter density as $\Omega_{\rm DM}$ coming from a population of axions. The total matter density parameter is therefore $\Omega_m = \Omega_b + \Omega_{\rm DM}$ where we decompose the total density into four components $\Omega = \Omega_b + \Omega_{\rm DM} + \Omega_\Lambda + \Omega_r$. We initially look for values of $\Omega_{\rm DM}$ falling in the very rough bounds, $0.2 \lesssim \Omega_{\rm DM} \lesssim 0.4$, in our example cosmologies with proper constraints addressed later.

(ii) *Dark energy cosmology.*—We will refer to the effective dark energy density as $\Omega_{\rm DE}$ coming from a population of axions. We set $\Omega_\Lambda = 0$ where we decompose the total density into three components $\Omega = \Omega_{\rm DE} + \Omega_m + \Omega_r$. We initially look for values of $\Omega_{\rm DE}$ falling in the very rough bounds $0.6 \lesssim \Omega_{\rm DE} \lesssim 0.8$.

We define the rough limits of the axion masses we require for each cosmology as the following. If axions are to account for the total dark matter, axion field oscillations should roughly begin in the radiation dominated era. This requires at least one axion with a mass larger than the Hubble rate at matter-radiation equality, which defines the mass limit,

$$m_a \gtrsim 10^{-27}\ \text{eV}. \tag{70}$$

The energy density of fields above this limit scales just as nonrelativistic matter throughout the matter dominated era, fixing them as plausible dark matter candidates. Axions behaving as dark energy are limited to masses defined by the upper mass bound,

$$m_a \lesssim 10^{-32}\ \text{eV}, \tag{71}$$

as motivated by Ref. [31].

Our example figures in Secs. IV A to IV C contain data for 2500 example cosmologies. Our contour density plots are constructed using 50×50 gridded scans in multidimensional parameter space with Gaussian filtering and cubic spline interpolation. The M-theory examples in Sec. IV D use 10×10 (Figs. 17 and 19) and 20×20 (Fig. 18) gridded scans with cubic spline interpolation, consisting of ten samples at each point, giving a total of 1000 and 4000 cosmologies respectively.

A. MP RMT model

In Figs. 10 and 11, we present our first example cosmologies in the simplest RMT model containing the

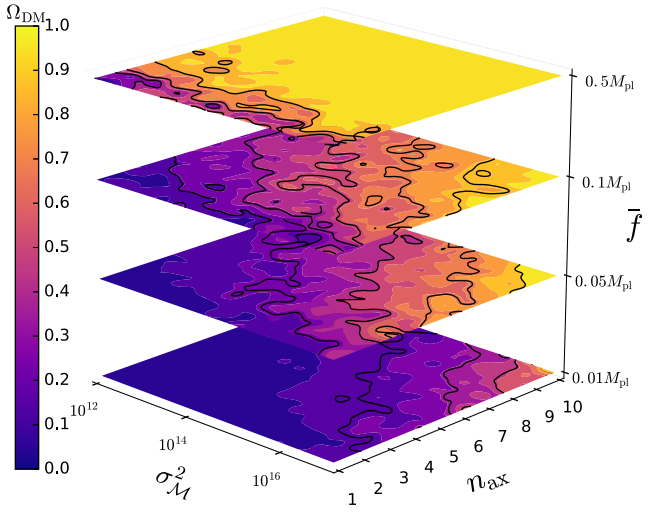

FIG. 11. MP RMT model DM cosmology example: Contour density plots for the axion dark matter density parameter $\Omega_{\rm DM}$ for $\sigma^2_{\mathcal{M}}$ and $n_{\rm ax} = \mathcal{O}(1 \to 10)$ using different fixed values of the initial field displacement scaling, $\bar{f}$.

smallest number of parameters to consider. The matrix eigenvalues have a bounded spectral width governed by the Marčenko-Pastur distribution law. When fixing our mass spectrum shape with $\beta_{\mathcal{K},\mathcal{M}} = 0.5$, this sets a configuration where each field provides approximately degenerate contributions to the total energy density up to variations in both the initial fields misalignment and random rotations from our choice of basis due to the absence of any treatment of $\mathcal{K}_{ij}$. The scale of the mass distribution defining the nature of the fields, fixed by $\sigma^2_{\mathcal{M}}$, acts as a free scaling parameter to switch between each type of cosmology.

1. MP DM

In Fig. 11, we display contour density plots for different mass distribution scales against the axion population size at fixed values for the initial field condition scaling. We demonstrate the emergence of axion dark matter density domination at the present time with large initial field displacement scalings, $\bar{f} \approx M_{\rm pl}$ for $n_{\rm ax} \gtrsim 1$. See Appendix D for a visual example of the evolution of the cosmological densities in these configurations.

In each of our RMT models, the form of the mass matrix is such that a population of axions behaving as the total dark matter requires initial field oscillations onset at a scale where the requirements on the heaviest axion mass in the population set the order of the total mass scale, $\sigma^2_{\mathcal{M}} \gg M_H$. The equal field conditions, $\bar{f}$, along with the uniform sampling of θ restrict the total number of axions, $n_{\rm ax}$, allowed in the population at any given mass scale. Only when $n_{\rm ax} \approx 1$ do we recover the potential for values of $\Omega_{\rm DM}$ consistent with expectations presenting an approximate degeneracy along the total mass scale interval we consider. Larger population numbers feel both the linear sum of field density contributions along with the convergence of the initial misalignments in our prior sampling to their averaged value, $\langle\theta\rangle \approx \pi/2$, giving the large region of parameter space returning values of $\Omega_{\rm DM} \gtrsim 0.8$.

A significant increase in the potential for larger population sizes returning values of $0.2 \leq \Omega_{\rm DM} \leq 0.4$ is seen by relaxing the scaling of the initial field displacements to $\bar{f} = \mathcal{O}(0.1 M_{\rm pl})$ as demonstrated in the lower panels. The degeneracy relationship between the number of fields allowed in the population and the mass distribution scale becomes more apparent in the second and third panels. As expected, larger values of $n_{\rm ax}$ quickly return values of $\Omega_{\rm DM}$ far in excess of what is required as the mass distribution scale is increased. Our simple example highlights this when $\bar{f} = 0.1 M_{\rm pl}$, mass distributions with $\sigma^2_{\mathcal{M}} \approx 10^{12}$ require a population size, $n_{\rm ax} \approx 10$ whereas Distributions with $\sigma^2_{\mathcal{M}} \approx 10^{17}$ require $n_{\rm ax} \approx 1$for acceptable values of $\Omega_{\rm DM}$. The lower panels shift the preferred values of $\sigma^2_{\mathcal{M}}$ as we reduce the scaling for the initial field displacements.

2. MP DE

It is easy to find parameters of the MP model that give rise to DE as the requirements are simple. Our MP DE cosmologies begin with the approximation that the mass scale at which axion field oscillation begins follows the simple limiting constraint, $\langle m_a^2 \rangle \lesssim M_H^2$. We maximize the range of the initial field conditions by fixing $\bar{f} = M_{\rm pl}$ as well as fixing the shape of the distribution with $\beta_{\mathcal{M}} = 0.5$. When searching for a population of nonoscillating fields, we approximate the value of $\sigma^2_{\mathcal{M}}$ for a significant number of low mass axions driving a phase of acceleration using

$$\sigma^2_{\mathcal{M}} \approx \frac{\sigma^2_{M_H}}{n_{\rm ax}} \approx \frac{1}{(5 \to 100)} \approx 0.2 \to 0.01. \tag{72}$$

In the left-hand panel of Fig. 10, we display the probability densities for $n_{\rm ax} = \mathcal{O}(1 \to 100)$ for corresponding values of $\sigma^2_{\mathcal{M}}$ determined by Eq. (72). Seemingly larger values of $n_{\rm ax}$ tailor the potential for desirable values of $\Omega_{\rm DE}$ by reducing the spread. A population size of $n_{\rm am} = 100$ returns a high probability density of cosmologies with values of $\Omega_{\rm DE}$ contained in the window of interest. As $n_{\rm ax} \to \mathcal{O}(100)$, the initial field misalignments in the population will converge to their averaged value $\langle\theta\rangle$ where the linear combination of the field density contributions cause the probability density of the dark energy density parameter to converge toward the modal value. Decreasing the value of $n_{\rm ax}$ increases the chance of returning cosmologies failing the acceleration criterion, $\ddot{a} > 0$ at $z = 0$ used in Sec. V B.

Using the relationship in Eq. (72), we address the role of the final parameter in this model, $\beta_{\mathcal{M}}$. The right-hand panel of Fig. 10 shows the spread of $\Omega_{\rm DE}$ values for fixed values of $\beta_{\mathcal{M}}$, distributed about $\sigma^2_{M_H}/n_{\rm ax} = 1/20$. We highlight the approximate degeneracy across our five fixed values of $\beta_{\mathcal{M}}$. Given the statistical sampling of $\beta_{\mathcal{M}}$ with either a uniform distribution or Gaussian sampling as shown in Appendix B 3, only extremal values will induce limited variations to the spread of $\Omega_{\rm DE}$ as compared to $\beta_{\mathcal{M}} = 0.5$ with each value retaining a mean value of $\Omega_{\rm DE} \approx 0.65$.

B. WW RMT model

In Fig. 12, we display contour density plots for intervals of two-dimensional parameter space for each parameter in the WW RMT model.

1. WW DM

The parameters in this model which we allow to run are scanned over the following intervals,

$$\log_{10}(\sigma^2_{\mathcal{K}}) \in [-4.0, -1.0], \tag{73}$$

$$\log_{10}(\sigma^2_{\mathcal{M}}) \in [12.00, 17.0], \tag{74}$$

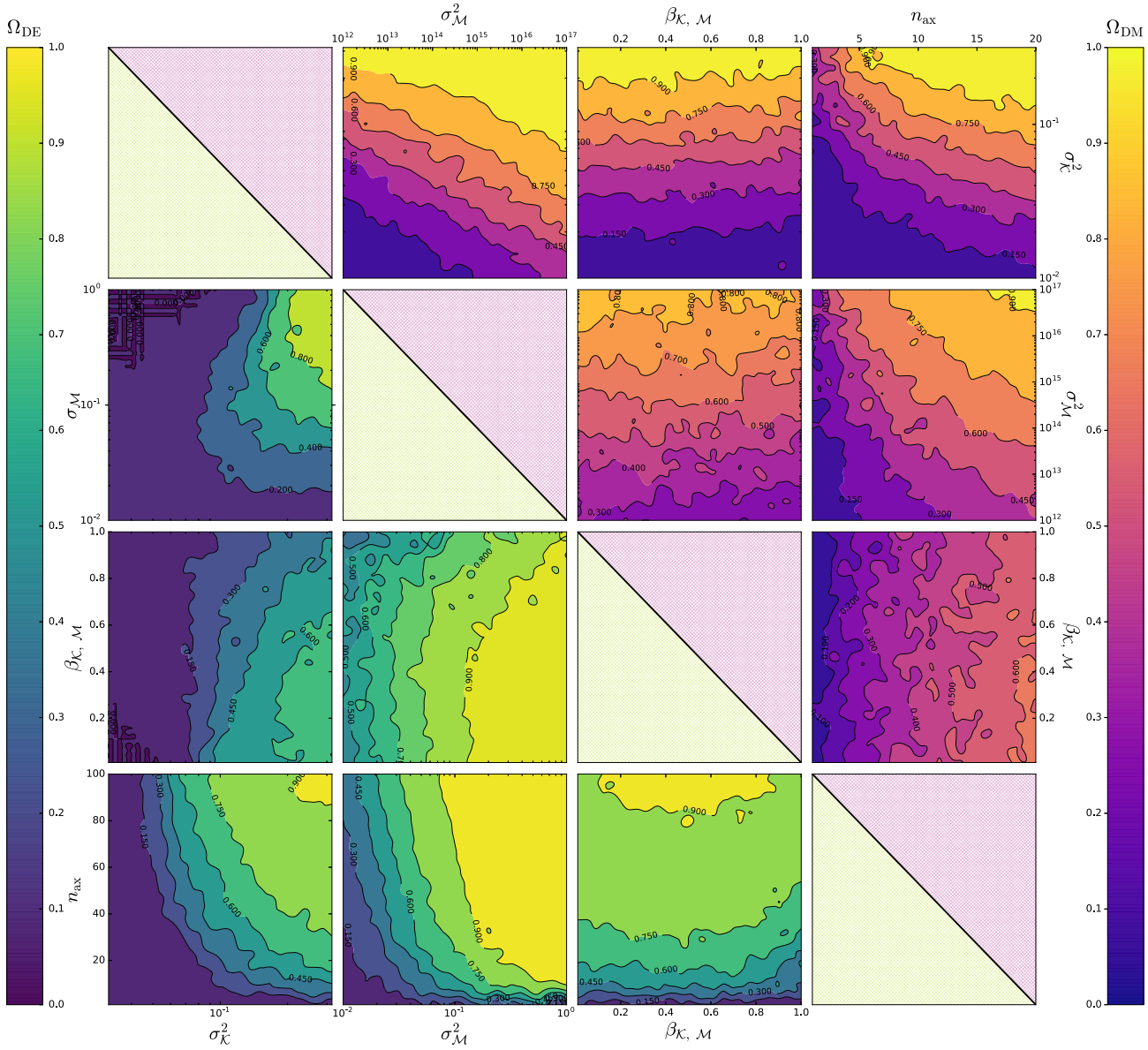

FIG. 12. WW RMT model DM and DE cosmology examples: Contour density plots for two-dimensional slices of the model parameter space for each parameter in the WW RMT model. *Upper-triangle panels*: Example contours for excluded regions of parameter space for the axion dark matter density parameter, $\Omega_{\rm DM}$, using the intervals outlined in Eqs. (73)–(75) along with fixed values in Eqs. (77)–(80). *Lower-triangle panels*: Example contours for excluded regions of parameter space for the axion dark energy density parameter, $\Omega_{\rm DE}$, using the intervals outlined in Eqs. (81)–(83) along with fixed values in Eqs. (85)–(88).

$$\beta_{\mathcal{K},\mathcal{M}} \in [0.01, 1.0], \tag{75}$$

$$n_{\rm ax} \in [1, 20], \tag{76}$$

where we use the following values if parameters remain fixed:

$$\log_{10}(\sigma^2_{\mathcal{K}}) = -2.60, \tag{77}$$

$$\log_{10}(\sigma^2_{\mathcal{M}}) = 5.70, \tag{78}$$

$$\beta_{\mathcal{K},\mathcal{M}} = 0.5, \tag{79}$$

$$n_{\rm ax} = 20. \tag{80}$$

In the top row of panels, we show the banding of dark matter density while increasing the distribution scale of our kinetic matrix, $\sigma^2_{\mathcal{K}}$. As seen in the upper left panel, the probability density for axion dark matter domination widens as the distribution scale of the initial mass matrix, $\sigma^2_{\mathcal{M}}$, leaves the lower dark matter mass limit. Indeed, it is expected that the limited spectral width of the matrix

spectra in these models is such that we should not expect large amounts of freedom to reposition ourselves in the parameter space before traversing into the bounds of the contours with nondesirable quantities of dark matter. The limited widths of the *purple* and *mauve* bands indicate the freedom we have to center the decay constant spectra at fixed mass scales. The gradient of the bands corresponds to the notion that in general one would expect dark matter densities far-in excess of the value required when considering axion populations at the mass scale limit detailed in Eq. (A9), unless we compensate the distribution scales for $\mathcal{K}_{ij}$. Indeed, we would expect, sub-GUT scales for our kinetic matrix distributions in this model when addressing a significant population size, $n_{\rm ax}$.

The convergence of the contour bands to values of $\Omega_{\rm DM} \lesssim 0.9$ is shown in the upper right panel for a spectrum of high scale decay constants when $n_{\rm ax} \lesssim 5$. Correspondingly, the panel below details the convergence in the same regard as the mass matrix scale increases. The bands widen when considering a larger number of fields $n_{\rm ax} \approx \mathcal{O}(10)$, at lower mass scales in the approximate regions (purple and mauve) for fixed $\sigma^2_{\mathcal{K}}$. Likewise, at lower values of $\sigma^2_{\mathcal{K}}$, we see a widening when $n_{\rm ax} \approx \mathcal{O}(10)$. The simplicity of the matrix structure we use will provide very comparable results between the WW RMT and MP RMT models, with approximate comparisons to be drawn from the middle right-hand panels of Fig. 12 and the panel second from the top in Fig. 11. Indeed, it is expected the averaging of the field contributions with $n_{\rm ax} \gtrsim \mathcal{O}(10)$ will give comparable results when using the equal initial field conditions for the field vevs in Eq. (42), given the bounded spectra for f_a when partnered with the random rotations and sampling on the misalignments.

2. WW DE

Our WW DE examples reside in the lower triangle of panels in Fig. 12. Unlike this model's dark matter counterpart, the requirement for nonoscillating fields with the limiting upper mass bound in Eq. (71) at the approximate scale $\sigma^2_{\mathcal{M}} \approx M_H$ will be more susceptible to both the freedom in the distribution for f_a and the shape of the rotated mass spectra. Our parameters allowed to run are scanned over the following intervals,

$$\log_{10}(\sigma^2_{\mathcal{K}}) \in [-2.0, 0.0], \tag{81}$$

$$\log_{10}(\sigma^2_{\mathcal{M}}) \in [-2.0, 1.0], \tag{82}$$

$$\beta_{\mathcal{K},\mathcal{M}} \in [0.01, 1.0], \tag{83}$$

$$n_{\rm ax} \in [1, 100], \tag{84}$$

where if parameters remain fixed we use the following values:

$$\log_{10}(\sigma^2_{\mathcal{K}}) = -0.60, \tag{85}$$

$$\log_{10}(\sigma^2_{\mathcal{M}}) = -1.65, \tag{86}$$

$$\beta_{\mathcal{K},\mathcal{M}} = 0.5, \tag{87}$$

$$n_{\rm ax} = 20. \tag{88}$$

In the upper left, lower left and lower central panels, we show the relationship between the population size and the scale of each of the distributions for the physical parameters. In general, we do require scaling parameters of the order $\sigma^2_{\mathcal{K}} \approx M_{\rm pl}$ and $\sigma^2_{\mathcal{M}} \approx M_H$ (upper left panel) with the regions of parameter space with either $\sigma^2_{\mathcal{K}} \lesssim 0.1 M_{\rm pl}$ or $\sigma^2_{\mathcal{M}} \lesssim 0.1 M_H$ quickly providing insufficient dark energy density unless the population size is increased to $n_{\rm ax} \to \mathcal{O}(100)$ (lower left and central panels).

In the upper and left central panels, we show the preference for the incorporation of the full tail of the distributions corresponding to values of $\beta_{\mathcal{K},\mathcal{M}} \to 1$ as the defining scales of the distributions are increased. The reduction of the spectral width gives a degeneracy in the contours for values of $\beta_{\mathcal{K},\mathcal{M}} \lesssim 0.5$ which can be seen more prominently in the upper central panel following fixed values for $\sigma^2_{\mathcal{M}}$. The preferential defining shape of the submatrices is dependent on the distribution scales. In the left central panel, we see the recovery of a full degeneracy across all values of $\beta_{\mathcal{K},\mathcal{M}}$ when the initial conditions for the fields are at insufficient scales required for any form of axion dark energy presence at the current time.

Finally, in the lower right panel, we show the relationship between the shape of the distribution and the axion population size. Fixed population sizes give a degeneracy for values $\beta_{\mathcal{K},\mathcal{M}} \lesssim 0.5$. The contour curvature as $n_{\rm ax} \to \mathcal{O}(100)$ potentially corresponds to a spreading of the mass spectrum, increasing the probability density of lighter fields. It could also potentially correspond to the inclusion of heavier oscillating late time dark matter-like fields at $z = 0$ as the tails of the distributions are sampled for large $n_{\rm ax}$.

C. LF RMT model

The LF RMT model examples in this section investigate potential differences in our example cosmology outputs from the $\mathcal{O}(n)$ enhanced eigenvalues present in each of the spectra for our physical quantities when compared to the limited bulk spectra in the previous models. It is worth noting by construction our examples should see very little variation compared to the WW RMT models output due to the order of magnitude of our axion population number we select. We will leave the study of large population numbers where our largest eigenvalues could obtain significant enhancements in the form of both large singular decay constants and a widening of the spectral width of the mass

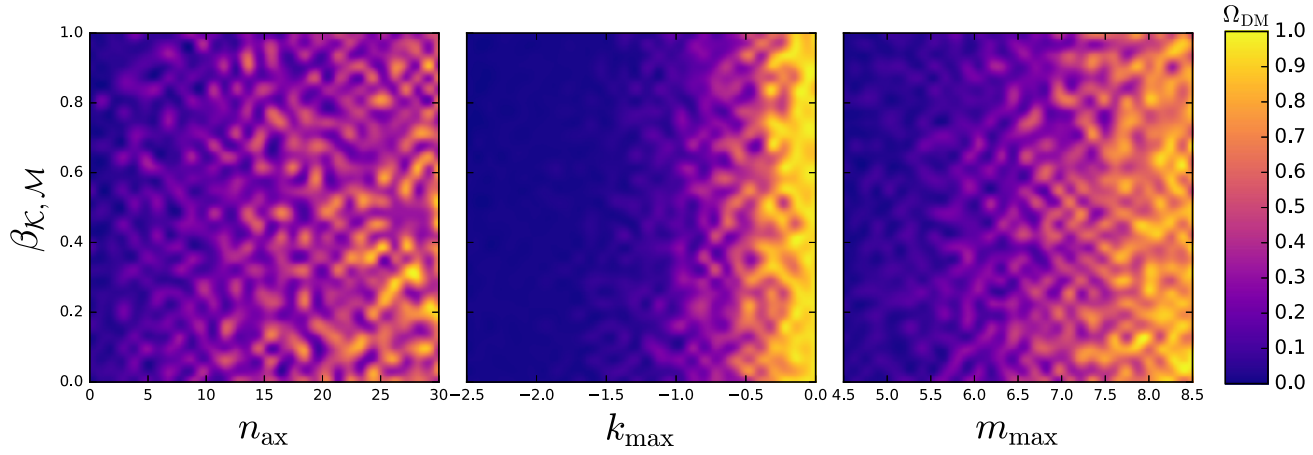

FIG. 13. LF RMT model DM cosmology example: Density heat maps for the axion dark matter density parameter, $\Omega_{\rm DM}$, for values of $\beta_{\mathcal{K},\mathcal{M}} \in (0, 1]$ along with the remaining model parameters. We use $n_{\rm ax} = [1 - 30]$ axions and varied limits on both the decay constant spectra parametrized by $k_{\rm max}$ and the mass spectra parametrized by $m_{\rm max}$.

distribution for future study. We choose to limit the number of parameters we consider in our examples in this model by fixing the values of our lower bounds on our distributions controlled by $k_{\rm min}$ and $m_{\rm min}$ throughout. The values of $\langle f_a \rangle$ and $\langle m_a \rangle$ are scaled by changing the values of $k_{\rm max}$ and $m_{\rm max}$ accordingly.

1. LF DM

We are interested in the role of a spectrum of high scale decay constants in the low mass axion window for LF DM, to explore the possible effects of the largest eigenvalues in both spectra. Our LF DM parameter intervals are defined as

$$k_{\rm max} \in [-2.5, 0.0], \tag{89}$$

$$m_{\rm max} \in [4.5, 8.5], \tag{90}$$

$$\beta_{\mathcal{K},\mathcal{M}} \in [0.01, 1.0], \tag{91}$$

$$n_{\rm ax} \in [1, 30], \tag{92}$$

with the defined fixed values

$$k_{\rm min} = -5.0, \tag{93}$$

$$k_{\rm max} = -1.0, \tag{94}$$

$$m_{\rm min} = 4.0, \tag{95}$$

$$m_{\rm max} = 6.0, \tag{96}$$

$$n_{\rm ax} = 20, \tag{97}$$

$$\beta_{\mathcal{K},\mathcal{M}} = 0.5. \tag{98}$$

The values in Eq. (93) are chosen to fix the lowest scale for $\langle f_a \rangle$ for the bulk of the spectrum to sub-GUT values when $k_{\rm max}$ is at its lowest value. The upper limit of $k_{\rm max}$ corresponds to the decay constant scale, $\langle f_a \rangle = \mathcal{O}(0.1 M_{\rm pl})$. Our lower limit on $m_{\rm min}$ in Eq. (95) is to ensure we have fields oscillating with masses $m_a > 10^6 M_H$. The maximum fixed value of $m_{\rm max}$ corresponds to fields drawn about mass distribution centered around $\langle m_a \rangle \approx \mathcal{O}(10^7 M_H)$ with the upper limit $m_{\rm max}$ giving a mass distribution scale, $\langle m_a \rangle \approx \mathcal{O}(10^9 M_H)$.

Figure 13 details regions of two-dimensional parameter space for each model parameter against values of $\beta_{\mathcal{K},\mathcal{M}}$ defined in the interval in Eq. (91). In each of the panels we reproduce the approximate degeneracy across all values of $\beta_{\mathcal{K},\mathcal{M}}$as shown in the corresponding panels in Fig. 12. It is clear that the this model will offer little deviation from the previous model considerations for dark matter cosmologies given the low number of fields we are considering and the mass scales we are considering. In the middle panel, we see the clustered heat density for large values of $\Omega_{\rm DM}$ as we scale the distribution for f_a toward $M_{\rm pl}$, once again indicating a preference away from values of $f_a \approx M_{\rm pl}$. The left-hand panel shows a measure of the potential, at fixed physical parameter scales, to find acceptable quantities of dark matter as the population size increases via the "speckled" nature of the probability densities.

2. LF DE

In both Figs. 14 and 15, we introduce a small step into the three-dimensional parameter space for $\Omega_{\rm DE}$ contour densities. We initially focus on the configuration where the scales of our dimensional quantities are determined by $m_{\rm min} = k_{\rm min}$ and $m_{\rm max} = k_{\rm max}$. This ensures that our rotated mass spectrum is centered about $\langle m_a \rangle = M_H$ with a spectral width determined by the value we fix for $k_{\rm max}$.

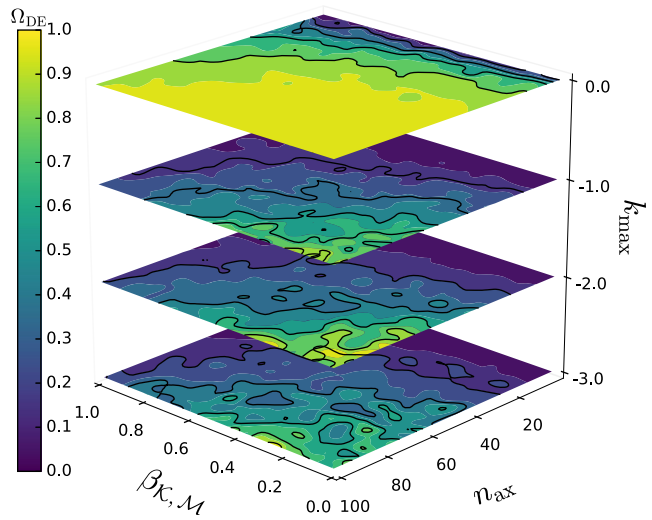

FIG. 14. LF RMT model DE cosmology example for $\boldsymbol{k}_{\rm max}$ limits: Contour density plots for the axion dark energy density parameter, $\Omega_{\rm DE}$ for $\beta_{\mathcal{K},\mathcal{M}}$ and $n_{\rm ax} = \mathcal{O}(1 \to 100)$ for different fixed values of $k_{\rm max}$.

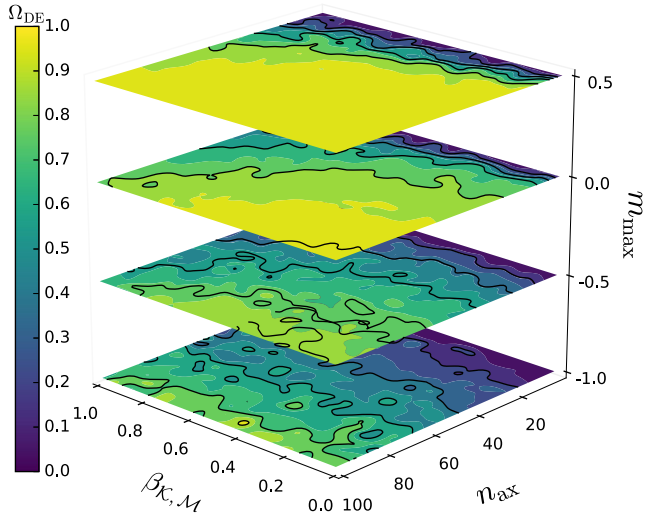

FIG. 15. LF RMT model DE cosmology example for $\boldsymbol{m}_{\rm max}$ limits: Contour density plots for the axion dark energy density parameter, $\Omega_{\rm DE}$ for $\beta_{\mathcal{K},\mathcal{M}}$ and $n_{\rm ax} = \mathcal{O}(1 \to 100)$ for different fixed values of $m_{\rm max}$.

Our LF DE parameters which we allow to run are scanned over the following intervals,

$$k_{\rm max} \in [-3.0, 0.0], \tag{99}$$

$$m_{\rm max} \in [-1.0, 0.5], \tag{100}$$

$$\beta_{\mathcal{K},\mathcal{M}} \in [0.01, 1.0], \tag{101}$$

$$n_{\rm ax} \in [1, 100], \tag{102}$$

with the following values of the fixed model parameters:

$$k_{\rm min} = m_{\rm min} = -5.0, \tag{103}$$

$$k_{\rm max} = m_{\rm max} = 0.0, \tag{104}$$

$$n_{\rm ax} = 20, \tag{105}$$

$$\beta_{\mathcal{K},\mathcal{M}} = 0.5. \tag{106}$$

Figure 14 shows the contour densities for $\beta_{\mathcal{K},\mathcal{M}}$ against $n_{\rm ax}$ for stacked decay constant distribution scales, emphasizing the previously determined preference for high scale decay constants for sufficient $\Omega_{\rm DE}$ when using mass centered distributions about M_H. Lower values of $k_{\rm max}$ slowly recover the degeneracy across all values of $\beta_{\mathcal{K},\mathcal{M}}$ providing little dark energy density. For $k_{\rm max} = 0.0$, as the population number $n_{\rm ax}$ increases significantly, a preference is made for the inclusion of the full tail of the mass spectrum as $\beta_{\mathcal{K},\mathcal{M}} \to 1$, maximizing the spread of mass values fields can take. Values of $k_{\rm max}$ minimally offset from this value require $\beta_{\mathcal{K},\mathcal{M}} \to 0$ to ensure a large population of fields have approximately degenerate and sufficient mass values ($\approx M_H$), in order to furnish our cosmologies with a sufficient quantity of dark energy density at the current time.

Correspondingly, Fig. 15 presents contour density plots for $\beta_{\mathcal{K},\mathcal{M}}$ against $n_{\rm ax}$ for stacked mass distribution scales offset with respect to the scale $\langle m_a \rangle \approx M_H$ fixed by $m_{\rm max}$. Each configuration uses a fixed distribution of high scale decay constants [Eq. (104)]. It is clear in the upper panel that distributions offset toward the upper mass limit in Eq. (71) quickly produce high probability densities for cosmologies with axion dark energy domination. Scales centered about $\langle m_a \rangle \approx M_H$ increase the width of the contour bands with acceptable values of $\Omega_{\rm DE}$ (*green* and *light green*). Large population sizes where $(n_{\rm ax} \approx \mathcal{O}(100))$ at this scale display a preference for a wider bulk in the mass distribution for values of $\beta_{\mathcal{K},\mathcal{M}} \to 1$, a feature consistent with the previous model's behavior. Mass scales offset below M_H ($m_{\rm max} = -0.5$) give a preference for $\beta_{\mathcal{K},\mathcal{M}} \to 0$ while also requiring large population sizes. A further increase in the offset below the mass scale of M_H recovers approximate degeneracies across all values of $\beta_{\mathcal{K},\mathcal{M}}$ with significantly reduced probability densities for the required values of $\Omega_{\rm DE}$.

D. MT RMT model

In this section, we look at cosmologies returning the required values of $\Omega_{\rm DM}$ and $\Omega_{\rm DE}$ drawn from the M-theory landscape where we fix the number of fields in our examples to $n_{\rm ax} = 10$ throughout. Our choice of initial scales we use consists of the values given in Eqs. (68) and (69). In order to account for gauge couplings consistent with the known elementary particles, we chose to sample

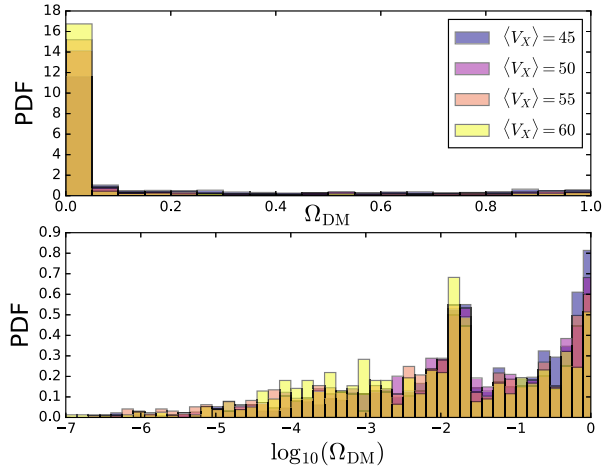

FIG. 16. MT RMT model DM cosmology example: Probability density plots for the axion dark matter density parameter, $\Omega_{\rm DM}$ for $\langle V_X\rangle = 45$, 50, 55, 60 presented in both linear and logarithmic scales.

the average values for the 3-cycle volume in the interval $\langle V_X\rangle = [25, 60]$. In Figs. 17–19, we make use of narrow prior windows incorporating Gaussian distributions in our sampling (see Sec. IV D 3).

1. MT DM

For our initial look at how axions in the M-theory axiverse model could give rise to dark matter, we begin by fixing the average value of the 3-cycle volume distribution, $\langle V_X\rangle$ to maximize the probability density of retrieving axions with masses in the window

$$10^{-32}\ \text{eV} \leq m_a \leq 10^{-25}\ \text{eV}, \tag{107}$$

which is done by selecting the following values:

$$\langle V_X\rangle = 45, 50, 55, 60. \tag{108}$$

Figure 16 gives the probability density plots for the axion dark matter density parameter, $\Omega_{\rm DM}$, for each of our selected values of $\langle V_X\rangle$ in Eq. (108).

In the upper panel of Fig. 16, we show the high probability density to return values of $\Omega_{\rm DM} \lesssim 0.05$. The lower panel of Fig. 16 details the spread of these values on a logarithmic scale with an enhanced probability density of returning values of $\Omega_{\rm DM} = \mathcal{O}(10^{-2})$. The low quantities of dark matter arise from the M-theory mass spectrum consistent with the many axiverse model spanning many decades giving a significantly lower percentage of cosmologies with values of $\Omega_{\rm DM}$ falling in the window $0.2 \leq \Omega_{\rm DM} \leq 0.4$ as compared to the localized scale RMT models of the string axiverse with far more localized spectra. The spread of the axion masses is such that for the average 3-cycle volume distribution values, $\langle V_X\rangle = 45$ and $\langle V_X\rangle = 60$, we only see an increase in the number of cosmologies with values of $\Omega_{\rm DM}$ falling in the window above go from ≈3% to ≈8.5%.

2. MT DE

Initial searches for axions with the properties of dark energy in the M-theory model show that there is no mass distribution which gives any form of satisfactory probability density for values of the dark energy density parameter, $\Omega_{\rm DE}$, falling in the bounds $0.6 \leq \Omega_{\rm DE} \leq 0.8$. This feature arises due to the nature of the axion decay constants in the model which are typically too small, $f_a \sim a/s_i \sim 10^{-2} M_{\rm pl}$. The dark energy density can be increased using a significantly larger number of axions or utilizing the alignment mechanism which could potentially sufficiently enhance the decay constants; however, our assumption on the diagonal form of the kinetic matrix in Eq. (54) does not allow for the inclusion of any such alignment mechanism. Therefore, we postpone an initial look into the possibility of sampling the M-theory axiverse models for dark energy to a topic of interest for future work.

3. M-theory toy model

In order to paint a better picture of the potential of the dark sector in the M-theory model, we consider a toy model with narrow prior probability densities of the associated hyperparameters in order to address some of the issues highlighted in previous sections. In particular, if the priors on the moduli vev s and the instanton index parameter $\tilde{N}_i^j$, which control the volume function, are narrow, our M-theory mass distributions will generically only spread over a few orders of magnitude instead of the many decades we would typically expect. As a result, the axion dark sector density parameters, $\Omega_{\rm DM}$ and $\Omega_{\rm DE}$, will also be concentrated around particular values. This configuration allows us to study correlations between mean values of the M-theory model parameters in a relatively simple manner.

We restrict the sampling of the parameters by fixing the priors distributions for s and $\tilde{N}_i^j$ to be drawn from a Gaussian distribution, $\mathcal{N}(\mu, \sigma)$. We limit the width of the prior sampling by fixing to the distribution standard deviation for s and $\tilde{N}$ to $\sigma_s = 1$ and $\sigma_{\tilde{N}} = 0.01$ respectively. For our dark matter examples, we simulate cosmologies for a range of mean values of s and $\tilde{N}_i^j$ as shown in Fig. 17. The contour density plot shows a trend of hyperbolic constraint as expected from the relation $\overline{V_X} \sim \bar{s} \times \bar{N}$. Our example cosmologies where we allow for variations in $\beta_{\mathcal{M}}$ are given in Fig. 18.

When considering dark energy, this toy model gives us quick insight on how much enhancement the decay constants could require in the M-theory model. We study this effect by parametrizing the enhancement by the factor $\tilde{f} = f'_a/f_a$. Figure 19 shows that the enhancement factor necessary to accomplish the observed dark energy is of the order $f_a \sim [10\text{–}100]$.

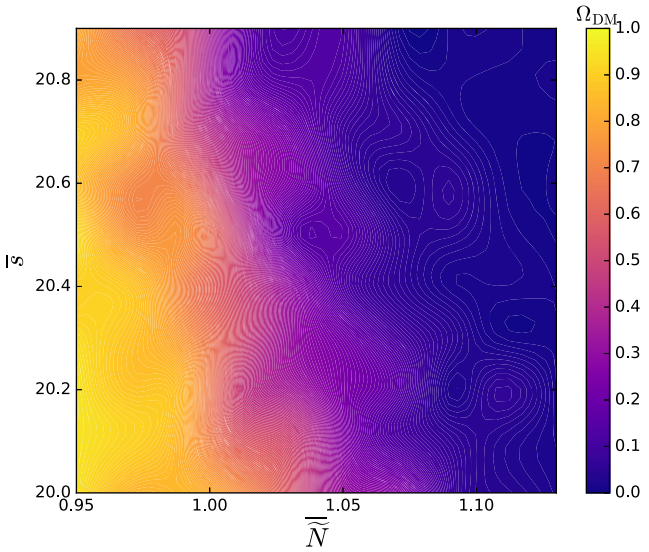

FIG. 17. MT RMT model DM cosmology example with narrow priors: Contour density plot for the axion dark matter density parameter, $\Omega_{\rm DM}$, with narrow priors for the moduli vev, s, and instanton index parameter, $\bar{\tilde{N}}$.

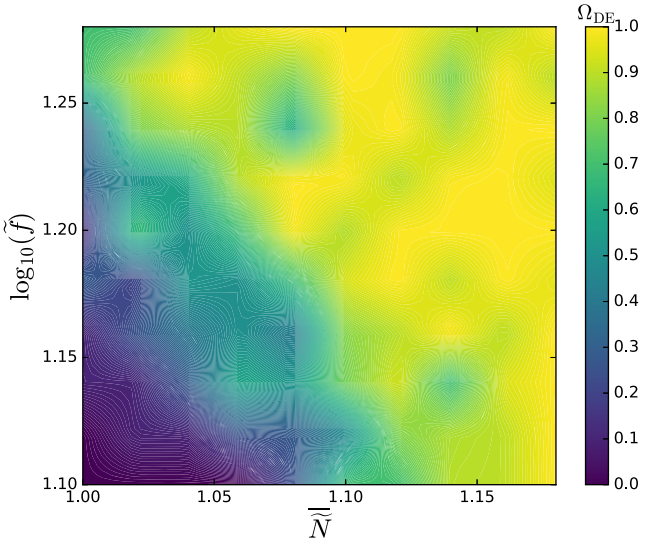

FIG. 19. MT RMT model DE cosmology example with narrow priors: Contour density plot for the axion dark energy parameter, $\Omega_{\rm DE}$ using narrower priors for $\tilde{N}$ along with an enhancement factor on decay constant f_a.

V. RESULTS II: THE STRING AXIVERSE AS A BAYESIAN NETWORK

A. Bayesian networks

We present here some brief examples treating the string axiverse as a Bayesian network, following the Bayesian networks approach to inflation in Ref. [48]. A complete treatment will be presented in a forthcoming paper. A generic Bayesian network for axion cosmology is shown in Fig. 20. We apply the Bayesian network using MCMC techniques. For this purpose, we use the affine-invariant ensemble sampler [49] implemented in EMCEE [50]. Plots detailing the constraints for model hyperparameters are made using CORNER [51].

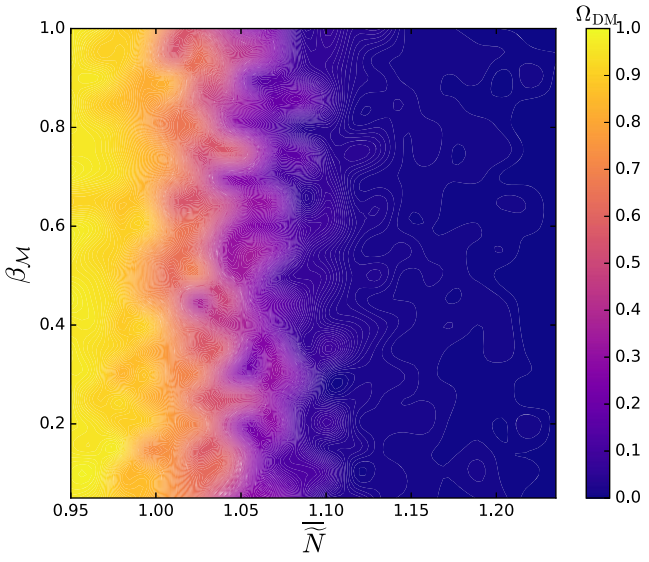

FIG. 18. MT RMT model DM cosmology example with narrow priors: Contour density plots for the axion dark matter parameter, $\Omega_{\rm DM}$ for $\beta_{\mathcal{M}}$ and using narrower priors on the instanton index parameter $\bar{\tilde{N}}$.

The cosmological parameters are $\vec{p} = (\Omega_r h^2, \Omega_{\rm mat} h^2, \Omega_\Lambda h^2)$. In principle, the cosmological parameters are determined stochastically from the hyperparameters of a higher level distribution, though in practice here we take these as fixed Dirac delta distributions determined by the model under consideration. The matter density $\Omega_{\rm mat} = \Omega_b + \Omega_c$ contains ordinary cold dark matter (CDM) and baryons, and the total matter density includes in addition the contribution from axions that have begun oscillations: $\Omega_m = \Omega_{\rm mat} + \Omega_a^{\rm osc}$. The axion model parameters fixed by the theory are $\{m_i\}$ and $\{\phi_i\}$. Given the complete set of model parameters, the quasiobservables are found deterministically by solving the equations of motion. For more details on the numerics, see Appendix A.

The level 1 (L1) theory hyperparameters stochastically determine the model parameters $\{\phi_i\}$ and $\{m_i\}$. Model selection (theory L2) sets the model, the number of axions and the prior distributions for the L1 hyper parameters. The theoretical modeling from L1 to the model parameters accounts for treating the axion potential as a pure mass matrix and in fixing the moduli. Theoretical modeling and cuts going from L1 to the quasiobservables includes a cut on the maximum m_a and the choice of cosmological model.

The quasiobservables are the fractional densities in each part of the dark sector, the Hubble parameter, the redshift of matter-radiation equality and the acceleration of the scale factor. In principle, we could consider also the evolution of the background quantities with redshift. For simplicity in the

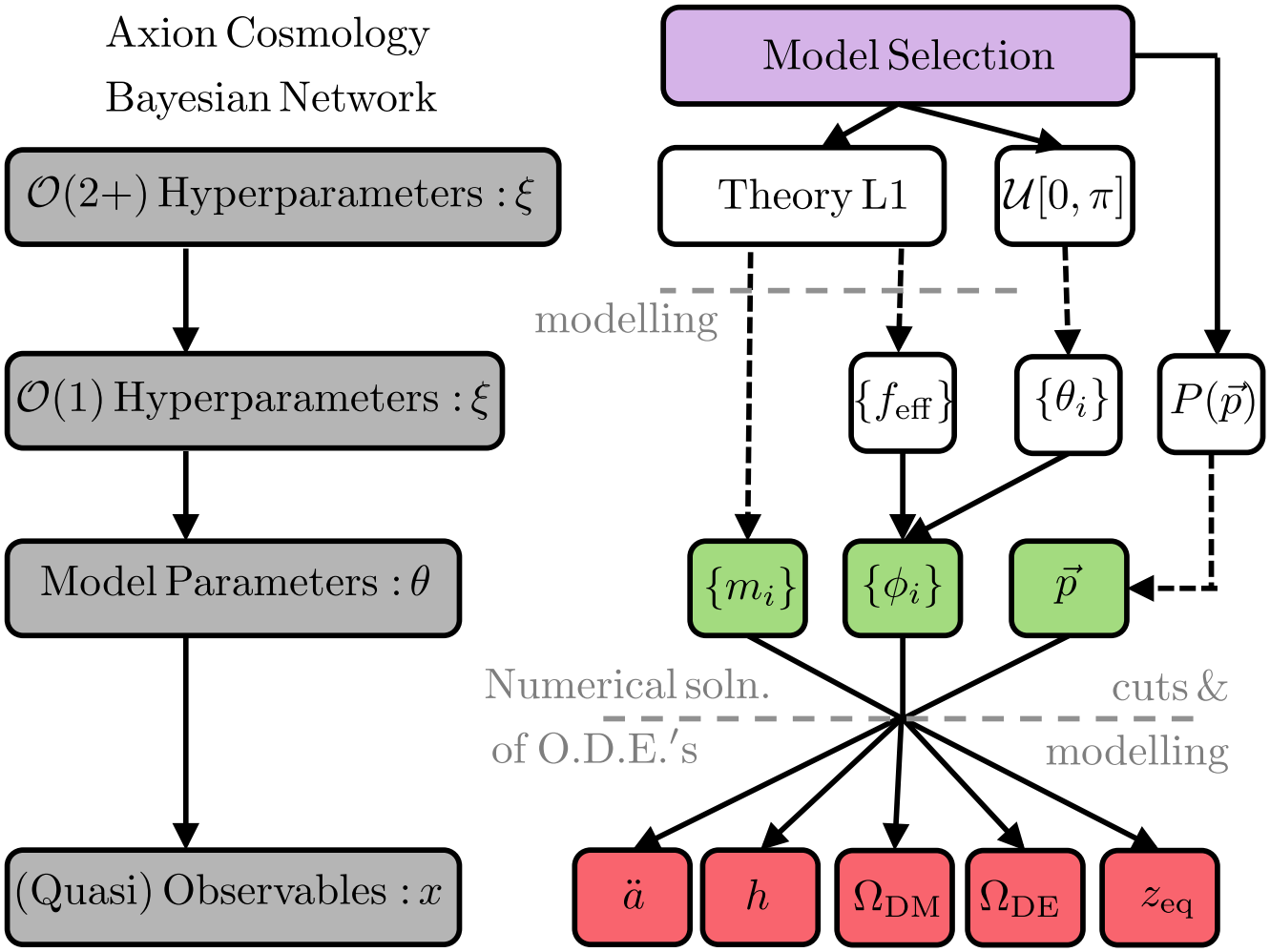

FIG. 20. A Generic Bayesian network for axion cosmology: Arrows indicate the direction of dependence, with dashed arrows indicating stochastic dependence and solid arrows indicating deterministic dependence.

examples shown, we simply apply a Gaussian likelihood to Ω_m, h, and $z_{\rm eq}$, assuming the *Planck* (2015) TT + lowP results [2] presented in Table II. We assign axions to the matter or DE density according to whether the equation of state has begun oscillating. We also apply a cut demanding an accelerating expansion of the universe, $\ddot{a} > 0$.

Our treatment of the quasiobservables should be considered only as giving approximate constraints on the models. Our models can have nontrivial effects on the equation of state for dark energy, $w(z)$, and for light DM axions also on structure formation and the CMB power spectrum [31], which are not accounted for in the simplified quasiobservables with Gaussian likelihood.

In ordinary ΛCDM, Ω_m, $z_{\rm eq}$ and h are not independent. However, in axion models, the change in the equation of state at late times can alter these relationships by the creation of additional matterlike axion density after $z_{\rm eq}$. Our use of $z_{\rm eq}$ as an independent quasiobservable from the matter density and h serves as an approximation of the constraints of Ref. [31], which disfavor large energy densities of ultralight axions that begin oscillating after equality. We ignore covariance between the quasiobservables for the same reason that dependences are not the same in axion models as in ΛCDM.

Our quasiobservables are particularly simple. A more advanced compression of the CMB, baryonic acoustic oscillation and growth data appropriate for DE models is given by the treatment of Refs. [53,54]. In this treatment, the CMB data are compressed into a vector of measurements for the matter densities, matter power spectrum amplitude and the angular size of the sound horizon, including covariance. Use of a wide variety of data sets will be possible by integrating our random axion models into COSMOSIS [55].

B. Constraints on the string axiverse

All the constraints shown hold the number of axions fixed at $n_{\rm ax} = 20$. Numerical accuracy settings are defined in Appendix A. All EMCEE walkers are initialized from the priors, and chains are run to convergence as evaluated according to the spectral method of Ref. [56].

TABLE II. The full range of parameters used in this study including the cosmological input parameters along with the model-dependent RMT parameters and theoretical M-theory parameters. Our cosmological density and parameter data come from the *Planck 2015 TT+lowP* likelihood's in Ref. [2] with our CMB temperature defined using COBE data in Ref. [52].

Parameter	Definition	Prior/value	Eq. Ref.
	Cosmological		
$n_{\rm ax}$	Number of axion fields	$\mathcal{O}(1$–$100)$	⋯
f_a	Axion decay constant	$\mathcal{O}(10^{-4}M_{\rm pl} - M_{\rm pl})$	Eq. (8)
m_a	Axion mass	$[10^{-35}$ eV, 10^{-15} eV$]$	Eq. (12)
θ_i	Initial field misalignment	$\mathcal{U}[0,\pi]$	Eq. (4)
ϕ_i	Initial axion field conditions	$\mathcal{F}_{ij}\theta_j$	Eq. (20)
$\dot{\phi}_i$	Initial field derivative	0	Eq. (17)
$\mathcal{F}_{ij}$	Decay constant matrix	Model dependent	Eq. (20)
a	Cosmic scale factor	$(10^{-8} \to 1)$	⋯
H_0	Present-day Hubble rate	hM_H	⋯
M_H	Hubble mass scale, 100 km s $-$ 1 Mpc^{-1}	2.13×10^{-33} eV	⋯
$M_{\rm pl}$	Reduced Planck mass, $1/\sqrt{8\pi G}$	2.435×10^{27} eV	⋯
$\Omega_{\rm DM}$	Axion dark matter density parameter	(0,1)	⋯
$\Omega_{\rm DE}$	Axion dark energy density parameter	(0,1)	⋯
	Planck 2015 TT+lowP parameters		
	Used as quasiobservable data		
h	Present-day Hubble rate	0.6731 ± 0.0096	[2]
Ω_m	Total matter fraction	0.315 ± 0.013	[2]
z_{eq}	Redshift of matter-radiation equality	3393 ± 49	[2]
	Fixed in a given model		
$\Omega_b h^2$	Physical baryon density (all)	0.022	[2]
$\Omega_c h^2$	Physical dark matter density (DE models)	0.12	[2]
$\Omega_\Lambda h^2$	Physical dark energy density (DM models)	0.31	[2]
$T_{\rm CMB}$	CMB temperature (COBE, all)	2.725 K	[52]
	Random matrix theory models		
$\sigma^2_{\mathcal{K}}$	Kinetic matrix distribution scale	$[10^{-3}M_{\rm pl}, 1M_{\rm pl}]$	Eq. (44)
$\sigma^2_{\mathcal{M}}$	Mass matrix distribution scale	$[10^{-4}M_H, 10^{36}M_H]$	Eq. (41)
$\beta_{\mathcal{K},\mathcal{M}}$	Submatrix dimension parameter	(0.0, 1.0]	Eq. (27)/(28)
$\bar{f}$	MP RMT model equal field condition scale	$[10^{-9}M_{\rm pl}, 1M_{\rm pl}]$	Eq. (42)
$k_{\rm min}$	LF RMT model kinetic matrix element distribution lower bound	-5.0	Eq. (46)
$k_{\rm min}$	LF RMT model kinetic matrix element distribution upper bound	$[-3.0, 0.0]$	Eq. (46)
$m_{\rm min}$	LF RMT model mass matrix element distribution lower bound	-5.0 (DE), 4.0 (DM)	Eq. (47)
$m_{\rm max}$	LF RMT model mass matrix element distribution upper bound	$[-1.0, 8.5]$	Eq. (47)
	M-theory model		
$F/(M_H^2)$	SUSY order parameter, $m_{3/2}M_{\rm pl}$	$5.4 \times 10^{104}(m_{3/2}/1$ TeV$)$	Eq. (55)
$m_{3/2}$	Gravitino mass	10 TeV	⋯
Λ	Instanton mass scale, string units	$[10^{-5}, 1]$	Eq. (55)
s	Averaged value for moduli vevs, string units	$\mathcal{U}[10,100]/\mathcal{N}(\bar{s},\sigma_s)$	Eq. (60)/(61)
$\tilde{N}_{\rm max}$	Instanton index parameter	[0.6,1.6]	Eq. (65)
a_0	Axion decay constant scale	1	Eq. (62)

1. MP RMT model for DM and DE

The first set of example constraints we show is the simplest both in model and computational terms. We take the Marčenko-Pastur Law model and tailor it to provide DE with a fixed number of axions $n_{\rm ax} = 20$. We fix the matter density to $\Omega_{\rm mat}h^2 = 0.148$, including dustlike CDM and baryons.

The L1 hyperparameters have the following priors (fixed L2 parameters):

$$\bar{f} \in \mathcal{U}[0.0, 5.0], \tag{109}$$

$$\sigma_{\mathcal{M}} \in \mathcal{U}[0.0, 10.0], \tag{110}$$

$$\beta_{\mathcal{M}} \in \mathcal{U}(0.0, 1.0]. \tag{111}$$

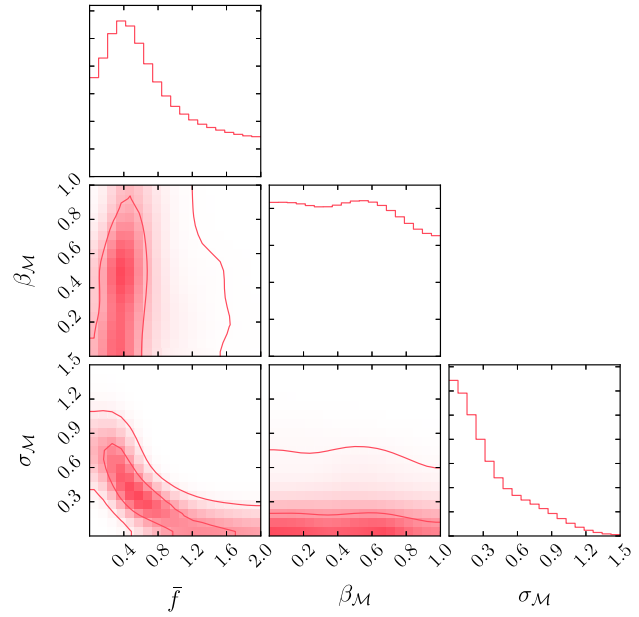

FIG. 21. Constraints on the MP RMT model for DE: Contours 1 and 2σ in the posterior distribution after imposing likelihoods and cuts on the quasiobservables. Demanding acceleration with $\Lambda = 0$ gives the bound $\sigma_{\mathcal{M}} < 0.9 M_H = 1.9 \times 10^{-33}$ eV (95% C.L.) from requiring the total equation of state $w < -1/3$ with the fields in slow roll at $z = 0$.

After applying Gaussian likelihoods to h, $z_{\rm eq}$ and Ω_m and a cut for $\ddot{a} > 0$, we find the constraints shown in Fig. 21. The mass parameter and $\bar{f}$ are constrained to values consistent with the DE density. The cut on acceleration with the requirement $\Lambda = 0$ leads to a maximum allowed value of $\sigma_{\mathcal{M}}$. This model shows no preference on $\beta_{\mathcal{M}}$; with a linear prior on $\sigma_{\mathcal{M}}$ near M_H, the width of the mass distribution is not important.

The degeneracies in the MP DE are demonstrated in Fig. 22. We show random samples drawn for different values of $(\bar{f}, \sigma_{\mathcal{M}})$ with $\beta_{\mathcal{M}} = 0.5$ and demonstrate how the quasiobservable distributions shift. The models moving along the degeneracy direction give accelerated expansion and consistent values of $\Omega_{\rm DE}$ which change relatively little. Perpendicular to this direction, the DE density is too low if the mass is too large (oscillations begin before $z = 0$), or the decay constant is too low (the field displacement is too small). This has a knock effect of making the acceleration parameter negative in these models.

Next, we consider the computationally more challenging but physically more interesting case of the Marčenko-Pastur Law model for DM. The model is more computationally challenging than the DE model due to the required switch in the equations of motion and following of axion field oscillations before the switch [an average run of AxionNet for this model takes $\mathcal{O}(20\text{s})$ in wall-clock time]. We fix the (nonaxion) matter density to the baryon density,

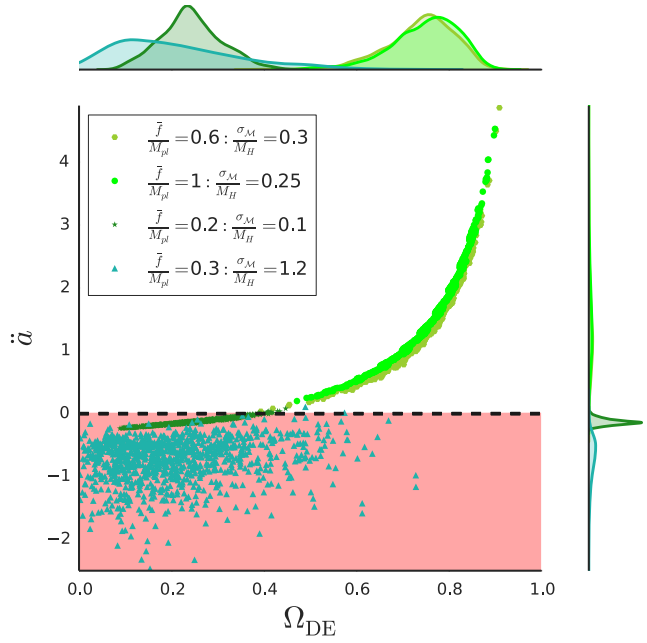

FIG. 22. Degeneracies in the MP RMT model for DE: We show random samples form four locations in the $(\bar{f}, \sigma_{\mathcal{M}})$ plane at fixed $\beta_{\mathcal{M}} = 0.5$, marked in Fig. 21. Along the degeneracy direction, the quasiobservable distributions do not change much. Across this direction, models are disfavored, with the quasiobservables distributions moving in opposite directions on either side.

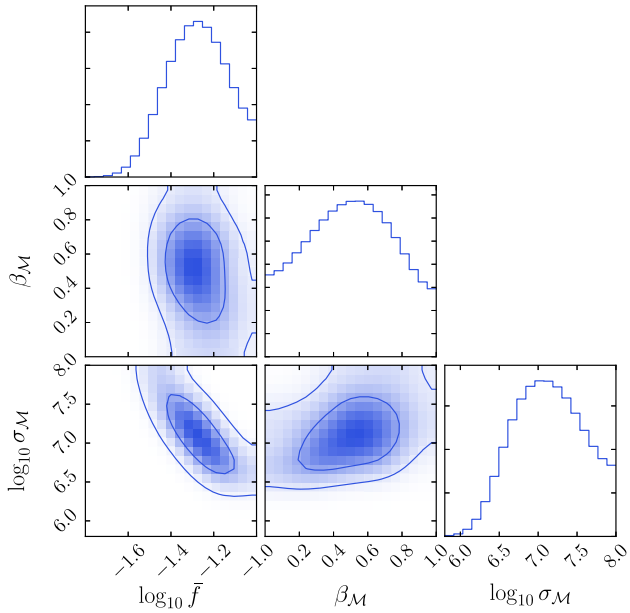

FIG. 23. Constraints on the MP RMT model for DM: Contours 1 and 2σ in the posterior distribution after imposing likelihoods and cuts on the quasiobservables. Fixing $z_{\rm eq}$ with only baryons as additional matter leads to the constraint $\log_{10}\sigma_{\mathcal{M}} > 6.6 \Rightarrow \sigma_{\mathcal{M}} > 4 \times 10^{-27}$ eV (95% C.L.) from requiring the fields to be oscillating with $w = 0$ prior to this epoch. There is a mild preference for $\beta = 0.5$.

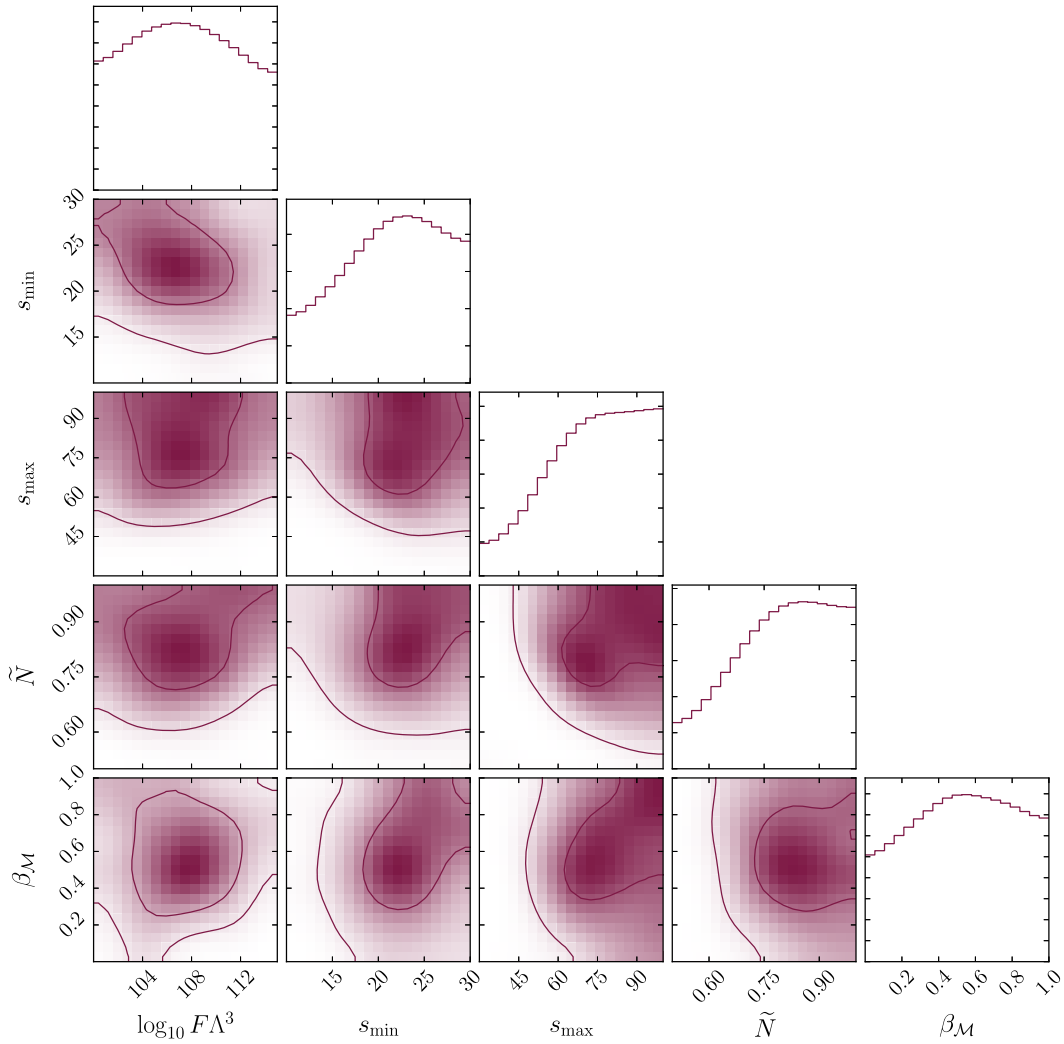

FIG. 24. Constraints on MT RMT model DM: Contours 1 and 2σ in the posterior distribution after imposing likelihoods and cuts on the quasiobservables. One sided constraints on parameters are driven by the simultaneous requirements of not overproducing DM and maintaining an accelerating universe at $z = 0$. The constraints are one sided due to the best-fit region being very narrow, with a plateau in the likelihood away from this region where the axion density drops to zero, $z_{\rm eq}$ is fixed by the baryons alone, and acceleration is guaranteed by the cosmological constant.

$\Omega_b h^2 = 0.022$, and we fix the physical cosmological constant density to $\Omega_\Lambda h^2 = 0.31$ (this gives the central Planck value for $\Omega_\Lambda = 1 - \Omega_m$ when $h = 0.673$).

The L1 hyperparameters have priors:

$$\log_{10} \bar{f} \in \mathcal{U}[-9.0, -1.0], \tag{112}$$

$$\log_{10} \sigma_{\mathcal{M}} \in \mathcal{U}[0.0, 8.0], \tag{113}$$

$$\beta_{\mathcal{M}} \in \mathcal{U}(0.0, 1.0]. \tag{114}$$

The posterior distributions are shown in Fig. 23. The constraint on the matter density parameter, Ω_m, fixes a direction in the $(\bar{f}, \sigma_{\mathcal{M}})$ space. The constraint on $z_{\rm eq}$ leads to a minimum allowed value of $\sigma_{\mathcal{M}}$. Interestingly, this model shows a mild preference for $\beta_{\mathcal{M}} = 0.5$. The preference for $\beta_{\mathcal{M}} = 0.5$ is possibly driven by the preference for a *not-too-wide* mass distribution. Preventing the occurrence of axions with $m_a < H(z_{\rm eq})$ selects against $\beta_{\mathcal{M}} = 1$ and a wide distribution. There is no strongly preferred mass for DM above this scale, and so $\beta_{\mathcal{M}} = 0$ is disfavored to keep the distribution from becoming singular. The minimum value of $\bar{f}$ depends on the maximum value of $\sigma_{\mathcal{M}}$, fixed by obtaining the relic density.

In both the above considered Marčenko-Pastur models, we observe a constraint on the characteristic axion mass and decay constant. The location of the constraint on the mass is fixed by the quasiobservables and the problem under consideration: either by the condition on $\ddot{a}$ for $h \approx 0.7$ for axion DE or by the conditions on $z_{\rm eq}$ and Ω_m for axion DM. The modal value of $\bar{f}$ in the Marčenko-Pastur model is determined by the required energy density in axions and is

thus dependent on our *fixed* parameter $n_{\rm ax} = 20$. In the DE example, the modal value (after binning on the linear prior) is $\bar{f} = 0.3M_{\rm pl}$, reduced from the naive value $\bar{f} = M_{\rm pl}$ in a single axion model by the "N-flation" $1/\sqrt{n_{\rm ax}}$ effect (cf. constraints on axions as quintessence [57]). There is a similar effect in the DM example, where $\bar{f}$ is lowered from the value needed in a single field $m^2\phi^2$ model for the DM relic density (e.g., Ref. [13]). A model with varying $n_{\rm ax}$ would display a degeneracy in the $(\bar{f}, n_{\rm ax})$ plane.

2. Dark matter from the M-theory axiverse

The M-theory axiverse, with its log-normal mass distribution and very wide spread, means that the constraints must be read carefully (in a preliminary investigation, we found the same considerations apply to the log-flat matrix elements model). The constraints on the M-theory model parameters for the case of uniform distributions in s and $\tilde{N}$ are shown in Fig. 24.

The constraints on the M-theory model are primarily derived from not overproducing DM. With decay constants typically of order the GUT scale, axions with masses $m_a \gtrsim 10^{-18}$ eV typically provide too much DM density ("anthropically constrained" [12]). This leads to minimum values of $s_{\rm min}$ and $s_{\rm max}$, with large moduli giving large instanton actions, low axion masses and correspondingly lower relic densities. There is also a lower bound on $\tilde{N}$, which sets the scale of the instanton charges and also leads to lower axion masses.

The vast majority of the M-theory DM models within the 2σ allowed region in Fig. 24 produce a cosmology with quasiobservables: $(h, \Omega_m, z_{\rm eq}) \approx (0.57, 0.06, 520)$, with $\ddot{a} > 0$ provided by the cosmological constant and the matter density provided by the baryons. While this is a bad fit to the data, it is a better fit than a model with, for example, total DM domination at $z = 0$, $\ddot{a} < 0$ and $z_{\rm eq} \approx 10^5$, which results if heavy axions "overclose" the Universe by providing too much DM. This is not to say that there are not examples of M-theory models that do provide good fits to the data. For example, it is easy to find a model in our chains with hyperparameters $(\log_{10} F\Lambda^3, s_{\rm min}, s_{\rm max}, \tilde{N}, \beta_{\mathcal{M}}) \approx (105, 26, 54, 0.7, 0.9)$ and quasiobservables $(h, \Omega_m, z_{\rm eq}) \approx (0.7, 0.3, 3000)$. We have checked that this general trend also applies in the alternative Gaussian priors on s and $\tilde{N}$ and also using the alternative quasiobservable $\Omega_d h^2$ for the axion DM instead of the total matter content including baryons.

This one-sided behavior in the constraints, and with many samples being poor fits, can be understood by considering the results of grid-based sampling in a simplified model. We took the Gaussian priors model for s and $\tilde{N}$, holding $\sigma_s = 1$, $\sigma_N = 0.01$ fixed and varying $\bar{s} \in [20, 21]$, $\bar{N} \in [0.5, 0.55]$ with $n_{\rm ax} = 20$. We sampled each point in parameter space ten times and interpolated the average quasiobservables on a linear grid.

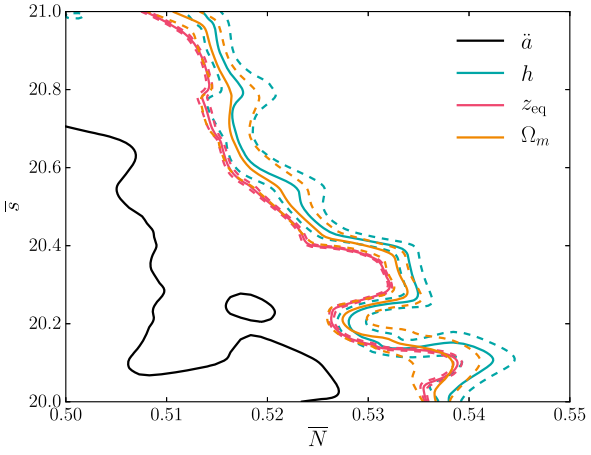

FIG. 25. Grid sampling of MT RMT model DM: Solid (dashed) contours show the mean ($\pm 2\sigma$) values of the quasiobservables on a grid based sampling of $(\bar{N}, \bar{s})$ for $n_{\rm ax} = 20$. For small $\bar{N}$, $\ddot{a} < 0$ leading to zero likelihood (cut), while for large $\bar{N}$, $\ddot{a} > 0$. For large $\bar{N}$, the axion density goes to zero, but the likelihood plateaus due to the inclusion of the baryons and the cosmological constant.

Figure 25 shows the results of this sampling. The contours show the location of $\bar{x} \pm 2\sigma_x$ for quasiobservable x and the location of $\ddot{a} > 0$. We see that there is only a very narrow region of parameter space where the quasiobservables all have values near the means. For small $\bar{N}$, the likelihood goes to zero due to the cut on $\ddot{a}$. On the other hand, for large $\bar{N}$, the likelihood plateaus. As the axion DM density drops to zero, the baryon contribution leads to minimum values of $z_{\rm eq}$ and h. Thus, the whole region of parameter space with large $\bar{N}$ is equally disfavored and has large prior volume. This leads to a one-sided constraint on parameters driven by $\ddot{a} > 0$, which is in turn driven by the requirement of not overproducing DM and having $z_{\rm eq}$ too large.

These observations highlight some limitations of our methodology when applied to a model with a larger number of parameters and a very small prior volume in the best-fit region. It also highlights how our use of quasiobservables does not equally disfavor all possibilities away from the best fit.

VI. DISCUSSION AND CONCLUSIONS

The existence of a "dark sector" of particles largely decoupled from the Standard Model is necessary to explain the phenomenon of dark matter and could also play a role in the accelerated expansion of the Universe as dark energy. String theory and M-theory predict the existence of a complex, multicomponent dark sector containing (among other things) many axion fields. Making definite predictions in such a landscape of possibilities seems at present impossible. However, statistical tools enable us to explore these possibilities. In the context of inflationary theory, random matrix models have proven to be a useful

simplification, owing to the universality of the eigenvalue distributions.

In the present work, we have investigated random matrix models for the axion dark sector and computed the spectrum of axion masses and initial field values. These quantities determine the resulting energy densities of dark matter and dark energy. By treating these as quasiobservables, we have been able to constrain the parameters of the random matrix models. This is the first such investigation (that we are aware of) of random multifield models applied to the problem of the dark sector. We have used the adaptable framework of Bayesian networks to perform a Monte Carlo investigation of this scenario.

We have chosen to investigate axion models for DM and DE separately. A model for axion DM *and* DE *together* requires a mass splitting at least of $\mathcal{O}(H(z_{\rm eq})/M_H) \sim 10^6$ so as not to generate too much energy density in light states [31]. Such a hierarchy cannot be generated in the models we have considered. The structure of the matrices we have assumed is that all the stable axions acquire their masses from similar sources. That is, the elements of the matrices are all drawn from the same distributions. There are no separate sectors, which would occur for matrices with mixed distributions and for block-diagonal matrices. In our models, the only effect that can lead to hierarchies in the mass spectrum is the existence of large eigenvalues, and we have not found this to be sufficient to allow axions to simultaneously provide DM and DE.

An interesting extension of our work would be to consider a *hierarchical* model, constraining the $\{m_i\}$ and $\{\phi_i\}$ distributions separately for DM and DE. With this information, one could design block-diagonal random matrix models for an entirely axionic dark sector. In a high-energy physics context, such a model could be realized if part of the axion sector was protected from the leading order instanton effects and received its mass only at some higher order.

Hierarchies can also be generated in multiaxion models with nontrivial potentials [58], where isocurvature perturbations (see below) can also be suppressed. This highlights another major simplification and limitation of our work: the use of the mass term only in the potential. While it is technically trivial to replace the mass term with some general function (such as the instanton expansion), computationally it is more challenging. First, it is necessary to impose such simplifications after oscillations (for a non-quadratic minimum, one cannot use $w_a = 0$), and second by the possibility of metastable minima leading to dynamics on widely separated time scales.

We have found, in the case of DM models, data-driven lower bounds on axion mass distributions set by the matter density and $z_{\rm eq}$. Low mass scales for axions find theoretical and phenomenological motivation also. Theoretically, as discussed, the mass scale $m_a \approx 10^{-15}$ eV emerges from fixing the GUT scale unified gauge coupling, $\alpha_{\rm GUT} \approx 1/25$, in the M-theory compactifications [16], with a similar approximate relation in string models [59]. Generation of ultralight masses has been discussed extensively recently, in string theory and supersymmetry [60], in QCD-related theories [61] and through use of discrete symmetries [62]. Constraints on the axion parameter space in the context of Peccei-Quinn symmetry breaking scales for ultralight axion cold DM in both standard and nonstandard cosmologies has been explored in Refs. [63,64] respectively. Ultralight DM has distinctive effects on cosmic structure formation that allow it to be distinguished from cold DM, and it represents a frontier of DM research [13,59]. The "anthropic window" of axion parameter space for ultralight masses constituting the total DM has been analyzed in Ref. [65]. The idea of "catastrophic boundaries" [66] in the multiverse may lead to a preference for universes "on the edge" of such a frontier.

Phenomenologically, axion masses in the range we have constrained [approximately $H_0 < m_a < H(z_{\rm eq})$], and up to 10^{-23} eV, are probed by the CMB power spectrum and large scale structure [31,67,68]. Higher masses in the range 10^{-22} eV $\lesssim m_a \lesssim 10^{-20}$ eV are motivated by their interesting effects on galaxy formation [13,59,69–71] and are probed by high redshift galaxy formation [72–75] and the Lyman-alpha forest flux power spectrum [76,77]. Still more massive axions in the range 10^{-20} eV $\lesssim m_a \lesssim 10^{-18}$ eV can be probed purely gravitationally by the 21 cm power spectrum [78].

Constraints from quasiobservables cannot be easily connected to such detailed constraints as discussed above. To even begin such a task would require the perturbation theory of multiaxion models. While technically trivial, this is a computationally challenging task that we have not attempted to take on. However, even without perturbation theory, the range of masses 10^{-18} eV $\lesssim m_a \lesssim 10^{-10}$ eV is constrained by black hole superradiance [79–83]. Incorporating the superradiance constraints into the axion mass distribution will be a relatively simple task given the adaptability of the Bayesian networks approach.

In addition to axion mass distributions, we have computed the distributions of decay constants, f_a, from the eigenvalues of the kinetic matrix. The "weak gravity conjecture" [84] (WGC) can be used to place bounds on combinations of axion decay constants and masses and broadly speaking can be said to constrain the existence of super-Planckian values for f_a (without the alignment mechanism). Overcoming this apparent constraint is a prime motivation for the introduction of multifield models of axion inflation and has in part motivated the present work on DM and DE.

We have held $n_{\rm ax}$ fixed in our example Bayesian network constraints. It would be interesting to explore in a future work how imposing the (weak or strong forms of the) WGC as a prior could lead to a lower bound on $n_{\rm ax}$ required by providing the correct energy densities in a given DM or DE

model. In the case of N-flation (and related models), the necessary minimum number of fields has been argued to be in conflict with entropy bounds in de Sitter space [85], and a similar conclusion for axion DE or DM could have profound implications.

A notable multifield axion model for DE considered previously in the literature is Ref. [86], with more detailed cosmological consequences computed in Ref. [87]. The model considered a simplified distribution for the axion masses and decay constants, equivalent to log-flat mass eigenvalues and uniform kinetic matrix eigenvalues. The model has a 1:100 "chance" of providing the correct DE density. An interesting extension considered in Ref. [86] is the use of noncanonical multi-instanton potentials to facilitate the decay of problematic heavy axion fields that otherwise provide too large energy densities.

Our random matrix approach provides a more versatile, and realistic, approach to the distributions. Our Bayesian forward model is able to quantify and extend the estimates outlined in Ref. [86] for the mass and decay constant distributions. Reference [87] considers the observables for DE models more thoroughly, such as the angular diameter distance to the CMB and improvements from future baryon acoustic oscillation measurements by the Square Kilometre Array. It would be interesting to include these in our Bayesian network.

The only concrete axiverse construction we have used to inform our random matrix models has been the M-theory model of Ref. [16]. An explicit axiverse model has also been realized in Type IIB [88], where models for N-flation and "N-quintessence" have also been constructed [89], and our methodology could easily be applied to these models also. We note, however, that in the case where these models can have a low string scale, $M_s \sim 10^{12}$ GeV, the DM abundance from vacuum realignment of light axions will be hard to achieve.

Our discussion in this paper has been set entirely in the late Universe, in particular during radiation domination post-big bang nucleosynthesis, and we have made no explicit connection between our models and inflationary theory. This neglects the very important constraints on axion DM coming from isocurvature perturbations (e.g., Refs. [90,91]). High scale inflation, in particular with an observably large tensor-to-scalar ratio, typically generates large amplitude number density perturbations in axions, which contribute to the CMB power spectrum acoustic peaks so as to shift their phase, inconsistent with observations [92,93]. The Hubble scale during inflation is constrained, for the QCD axion with typical f_a, to be $H_I \lesssim 10^8$ GeV.

The requirements on H_I are significantly loosened for ultralight axions, with isocurvature perturbations becoming negligible for $m_a \lesssim 10^{-26}$ eV [94,95]. The constraints become multiplicatively worse, however, in the case of multiple axion fields [96]. In Ref. [16], it was shown that the M-theory axiverse requires $H_I \lesssim 10^{10}$ GeV. The adaptability of the Bayesian networks approach means that including the isocurvature amplitude as a quasiobservable and H_I as a model parameter is another easily tackled problem. Such an investigation would clarify the prior dependence in the results of Ref. [96].

The study of random matrix multiaxion models has been popular for some time in inflationary theory. While inflation is well motivated by cosmological observations, it is unlikely to be possible to determine the theory precisely due to the limited information available. Dark matter, on the other hand, offers far greater prospects for precision measurement [68], and so by studying multiaxion models in the late Universe, we might discover more about physics beyond the Standard Model. In this work, we have presented the first exploration of a random matrix multiaxion model for dark matter and dark energy and have used statistical methods to bound the axion mass and decay constant distributions.

ACKNOWLEDGMENTS

We are thankful to Thomas Bachlechner, Jonathan Frazer, Eugene Lim and M. C. David Marsh for helpful discussions and correspondence. The work of M. J. S. is supported by funding from the UK Science and Technology Facilities Council (STFC). D. J. E. M. is supported by a Royal Astronomical Society Postdoctoral Fellowship. D. J. E. M. is grateful to student participants at the International Summer School for Young Physicists, Perimeter Institute, 2013, who were an inspiration during the conception of this project. L. C. P. is supported in part by DOE Grant No. DE-SC0011114.

APPENDIX A: COMPUTATIONS

We numerically solve the equations of motion for $n_{\rm ax}$ axions with fixed initial conditions and evolve the solutions forward in time using SCIPY. We rescale the fields in terms of Planck units. The cosmic time, t, is the independent variable measured in units of M_H. This naturally sets the axion mass scale in units of M_H, and the cosmological densities in component X appear in the Friedmann constraint in terms of their density today as $\Omega_X h^2$.

1. Energy densities

We define our initial and final conditions using the photon temperature as a clock. The total energy density for the relativistic degrees of freedom, ρ_r, is

$$\rho_r = \frac{\pi^2}{30} g_\star(T) T^4, \tag{A1}$$

where $g_\star(T)$ counts the relativistic degrees of freedom (e.g., Ref. [97]). We fix *today* from the CMB temperature, $T_{\rm CMB} = 2.725$ K [52]. Normalizing the scale factor such that $a(T_{\rm CMB}) = 1$, the scale factor $a(t)$ is found by integrating the Friedmann constraint.

For simplicity, we treat the total relativistic degrees of freedom as a constant, and thus we must begin our solutions after neutrino decoupling. Using the fits from Ref. [98], this occurs at $T_i \approx 23$ keV when the scale factor is $a_i \approx 10^{-8}$. After this time, the radiation energy density evolves as

$$\rho_r(a) = 3M_H^2 M_{\rm pl}^2 \frac{\Omega_r h^2}{a^4}, \tag{A2}$$

where

$$\Omega_r h^2 = \rho_r(T_{\rm CMB})/(3M_H^2 M_{\rm Pl}^2) = 4.16 \times 10^{-5}. \tag{A3}$$

Assuming radiation domination at T_i allows us to set the initial physical time,

$$t_i = (a_i^2/2)(\Omega_r h^2)^{-0.5}. \tag{A4}$$

We allow for the inclusion of a cosmological constant with fixed physical density $\Omega_\Lambda h^2$. The total (ordinary + CDM) matter density is

$$\rho_{\rm mat}(a) = 3M_H^2 M_{\rm pl}^2 \frac{\Omega_{\rm mat} h^2}{a^3}. \tag{A5}$$

The minimum value for $\Omega_m h^2$ is given by the physical baryon density, $\Omega_b h^2 = 0.022$ [2].

In the homogeneous limit, the energy-momentum tensor for the axions is described by a perfect fluid with components $T_0^0 = -\rho$ and $T_j^i = P\delta_j^i$. The energy density and pressure for a single axion are

$$\rho_a = \frac{1}{2}\dot{\phi}^2 + \frac{1}{2}m_a^2\phi^2, \tag{A6}$$

$$P_a = \frac{1}{2}\dot{\phi}^2 - \frac{1}{2}m_a^2\phi^2. \tag{A7}$$

The pressure of the matter, radiation and cosmological constant are determined by the equations of state: $P_i = w_i\rho_i$ (no sum on i) with $w_r = 1/3$, $w_m = 0$ and $w_\Lambda = -1$. The total pressure appears in the acceleration equation,

$$\dot{H} + H^2 = \frac{\ddot{a}}{a} = -\frac{1}{3}\sum_i(\rho_i + 3P_i), \tag{A8}$$

with an accelerating universe satisfying the condition $\ddot{a} > 0$. We do not solve the acceleration equation, but we compute $\ddot{a}$ using the right-hand side on Eq. (A8).

2. Initial conditions and axion mass limits

The Hubble parameter, H, provides a friction term in the Klein-Gordon equation, in which, as long as the condition $H \gtrsim m_a$ is satisfied, the axion field velocity will remain small. In the limit that the mass can be entirely neglected, the attractor solution is $\dot{\phi} = 0$. We assume this condition is met for our initial conditions. This assumption sets an upper limit for the axion masses that we can consistently consider for any given initial temperature. Demanding that $m_a < 3H(T_i)$ fixed by neutrino decoupling, we find the upper limit for the axion mass:

$$m_a < 4 \times 10^{-19}\ \text{eV}. \tag{A9}$$

In principle, we could extend to higher temperatures, and thus higher axion masses, by modeling the evolution of $g_\star$ above neutrino decoupling. We have chosen not to do this for a number of reasons. First, the particle content is not known beyond a few TeV. Second, above about 1 MeV [big bang nucleosynthesis (BBN)], the Universe need not have been radiation dominated, and there is no observational necessity to assume so. Third, in string/M-theory, we expect a nonthermal cosmology at early times dominated by the energy density of moduli coherently displaced by vacuum fluctuations during inflation. The matter dominated phase is known to alter the relic densities of axions that begin oscillating during that period [16,99].

Furthermore, when the moduli are displaced, and before they have decayed, our entire treatment of the axiverse effective theory is not valid, since the Kähler metric is dynamical. For our simple treatment to hold, we must consider axions still in slow roll after the lightest modulus field X_0 has decayed: $m_a < \Gamma_{X_0} = \mathcal{O}(1)^{m_{X_0}^3}/M_{\rm pl}^2$. For $m_{X_0} \approx 30$ TeV, so as to avoid the cosmological moduli problem [100–102], we can extract a slightly higher maximum value for the axion mass we could consider:

$$m_a < 1 \times 10^{-15}\ \text{eV}. \tag{A10}$$

Axions violating these bounds must be removed from the spectrum for our treatment to be consistent. Numerically, this is simple to achieve; we locate axions in the spectrum violating the bound and set the mass to zero. Our initial conditions then ensure that the realignment energy density in these fields remains zero.

A simple way to achieve this is to assume a large amount of entropy production and/or a short period of inflation caused by the modulus-dominated epoch prior to BBN. This will dilute the population of heavy axions that began oscillations prior to BBN. Such a scenario is relatively natural in the context of a string/M-theory cosmology with many moduli [16,103–105].

A second possibility is that these heavier axions themselves decay rapidly prior to BBN and simply contribute to setting the correct radiation content and baryon density. Theoretically, such axion decays are more problematic. Axion decays through the canonical two photon coupling are comparatively slow (see, e.g., Ref. [106]), and decays before BBN require $m_a \gtrsim 1$ keV. For axions respecting our bounds to decay, one would require much larger than expected couplings and rapid decay channels.

Alternatively, we could assume a gapped spectrum with any axions violating our bounds taken to have their masses lifted to a much higher scale to allow decays through standard channels. Another mechanism to remove heavy

axions is via the multi-instanton potential, $U(\theta) \propto (1-\cos\theta)^3$, of Ref. [86], which causes the misalignment population to redshift faster than a^{-3} due to the nonquadratic potential minimum. Whether or not the appearance of such a multi-instanton potential occurs naturally in string/M-theory models is not clear.

All the above options (removing heavy axions from the spectrum) are covered by the simple command removemasses = True in AXIONNET. We also allow for the option to reject outright (set zero likelihood) all models with large masses violating our bounds. This is controlled by a setting inside the likelihood function in AXIONNET and is operative when removemasses = False is used.

Despite the construction of the mass matrix guaranteeing positive semidefiniteness mathematically, and thus mass eigenvalues $m_a^2 \geq 0$, the huge spread in the elements of the mass matrix in the M-theory model leads to numerical precision errors and the existence of "tachyonic" $m_a^2 < 0$ eigenvalues. We have not been able to overcome this issue of numerical precision within the confines of NUMPY. We remove these tachyonic states from the spectrum just as we remove the heavy states, and they do not contribute to the energy density. Fortunately, the negative eigenvalues are guaranteed to be those for which the true values are smallest in absolute value. Since the true eigenvalue is $m_a \ll H_0$ and the field displacements $\phi_i^{\rm ini} \sim \mathcal{O}(M_{\rm pl})$, even with the correct (positive) eigenvalue, these states would not contribute significantly to the spectrum, and so removing them does not affect the results.

Options for alternative thermal histories and the evolution of $g_\star$ in AXIONNET will be the subject of future developments. The two mass limits, in Eqs. (A9) and (A10), are both far exceeding axion masses probed by our simple DM constraints, and thus the model of the Universe used above a few keV, the treatment of heavy axions and the use of constant $g_\star$ does not affect our results. These effects will be important for treatments going beyond considerations of the simple quasiobservables.

3. Axion oscillations

As the Universe expands, H decreases monotonically. When any individual field satisfies the condition $m_a \gtrsim H$, the field begins to roll toward its potential minimum and then begins coherent oscillations about it. The solution is given by

$$\phi(a > a_{\rm osc}) = \phi(a_{\rm osc})\left(\frac{a}{a_{\rm osc}}\right)^{-3/2}\cos(m_a t), \qquad \text{(A11)}$$

where $a_{\rm osc}$ occurs at approximately $H(a_{\rm osc}) \approx m_a$ (we define it more precisely shortly). As H further decreases, the time scale of the oscillation induces a very small time step in the integrator of order $(\sim m_a^{-1})$ (much smaller than the dynamical time, $t_{\rm dyn} \approx H$). This is computationally prohibitive to integrate directly given the hierarchical nature of the axion mass distribution.

Although the axion field oscillates, the energy density does not, and it obeys a simple scaling:

$$\rho_a(a > a_{\rm osc}) = \rho(a_{\rm osc})\left(\frac{a_{\rm osc}}{a}\right)^3. \qquad \text{(A12)}$$

It is a well-known fact that fields oscillating in a quadratic potential will behave as nonrelativistic matter (e.g., Ref. [107]). The pressure oscillates with a frequency $P \sim \cos(2m_a t)$, leading to a time-averaged equation of state $\langle w_a \rangle = 0$, and can be safely neglected for our purposes.[5]

The dynamical time scale in our integration is fixed to be of order the Hubble scale today, M_H. In order to be able to integrate models with $m_a \gg M_H$, we must approximate the axion evolution for time scales $t > t_{\rm osc}$. The method we choose is simply to set $w_a(t > t_{\rm osc}) = 0$ such that the energy density in heavy axions evolves exactly as a^{-3} at late times. An alternative method uses a change of coordinates in the axion phase space, as implemented in Ref. [67].

We define $t_{\rm osc}$ by allowing the equation of state in the full solution to oscillate (cross zero) a fixed number of times denoted by the parameter, $n_{\rm cross}$. We then define $t_{\rm osc}$ using $n_{\rm cross}$. This is an accuracy parameter in our numerical results, with larger values of $n_{\rm cross}$ leading to more accurate, but considerably slower, numerical computations. We find that results for the quasiobservables converge above $n_{\rm cross} = 3$, and we use $n_{\rm cross} = 5$ in the examples and constraints in the text. Care must be taken, however, as using too large a value of $n_{\rm cross}$, while improving the numerical integration accuracy, incorrectly assigns DM axions to the DE density in the quasiobservables (see below).

4. Computing the quasiobservables

Our quasiobservables are $(\Omega_m, z_{\rm eq}, \ddot{a}, h)$. We compute in physical time, t, up to some maximum time $t_{\rm f} \approx \mathcal{O}(10)$ and output a fixed number of log-spaced time steps. We begin by locating $z = 0$ in the output variables. If $z = 0$ has not been reached in ten Hubble times (which may occur for extreme cosmologies), AXIONNET outputs default quasiobservables which lead to a very low likelihood (in particular, failing the acceleration cut). This is equivalent to a cut on the age of the Universe.

Having located $z = 0$, computing h is trivial as it is given by the Friedmann constraint evaluated at $z = 0$. Computing the other variables relies on the separation of axions into DM- and DE-like based on $n_{\rm cross}$. The split at $z = 0$ trivially gives the matter density: $\Omega_m = \Omega_b + \Omega_{\rm DM}$. The acceleration is computed from the total pressure and density as

$$\ddot{a} = -\frac{a}{3}\sum_i(\rho_i + 3P_i), \qquad \text{(A13)}$$

[5]For a selection of interesting astrophysical consequences of the pressure term, see Refs. [108–111].

where the index i runs over axions and the ordinary cosmological components. The pressure for the axions with a number of crossings less than $n_{\rm cross}$ is computed directly from the fields using Eq. (A7), while for those with crossings greater than $n_{\rm cross}$, we set $P_i = 0$.

Finally, we compute $z_{\rm eq}$. At all values of z, the axions are split into the energy density components, $\rho_{\rm DM}$ and $\rho_{\rm DE}$, by selecting those that have and have not passed the $n_{\rm cross}$ criterion. We are also in possession of the radiation energy density $\rho_r(z)$ and baryon energy density $\rho_b(z)$ at every value of the redshift. We locate $z_{\rm eq}$ by simply finding numerically the point where $\rho_{\rm DM} + \rho_b = \rho_r$. We do not include $\rho_{\rm DE}$ in the definition of equality. We also find equality using the list of output times, and not using interpolation. Therefore, the location of equality will depend on the number of output times used. In our numerical examples, we use 1000 log-spaced times steps between $t_{\rm ini} = 8 \times 10^{-15}$ and $t_{\rm f}$.

APPENDIX B: CONNECTION TO STRING THEORY AND M-THEORY

1. Superpotential in M-theory

Axions generically arise in string compactifications as Kaluza-Klein modes of antisymmetric tensor fields which are present in all low-energy string/M-theory frameworks. The topology of such generic theories which can manifest realistic models in high-energy physics is complex, containing many cycles which in turn generate a *landscape* of fields. This landscape provides a source to many axionlike fields which could, in the context of cosmology, potentially be of great interest given the hierarchical nature of their associated physical parameter scales. The shift symmetries coming from the higher-dimensional gauge invariance of antisymmetric tensors leave the resulting scalar fields from string compactifications massless to any perturbative order. There are always plenty of instanton configurations arising in string theory models such as world sheet, gauge, gravitational or membrane instantons that violate the shift symmetries.

In the framework of four-dimensional supergravity, the superpotential is a holomophic function of the scalar part of the moduli superfield $z_i = t_i + is_i$ where t_i denote the axion fields and s_i denote the geometric moduli fields. We consider the following general form of the superpotential generated from nonperturbative effects,

$$W_{\rm inst} = \sum_{i=1}^{N} \tilde{\Lambda}_i^3 e^{ib_i F_i}, \tag{B1}$$

where $\tilde{\Lambda}_i$ are the mass scales associated to each of the nonperturbative effects. F_i represents the gauge kinetic functions which are linear combinations of the moduli superfields,

$$F_i = \sum_{k}^{n_{\rm ax}} N_i^k z_k = \sum_{k}^{n_{\rm ax}} N_i^k (t_k + is_k). \tag{B2}$$

The nonperturbative effects are assumed to be membrane instantons such that $b_i = 2\pi I_i$, where I_i are positive integers. In general, the number of nonperturbative effects such as string/membrane instantons present in any compactification is larger than the number of axions, which, in turn, allows for the possibility of stabilizing the axion/moduli potential. Therefore, we will assume that the number of independent terms in the superpotential is always greater than or equal to the number of axions, $N > n_{\rm ax}$. The supergravity potential is calculated using

$$V = e^{\mathcal{K}} \left(\mathcal{K}^{i\bar{j}} \frac{DW}{Dz^i} \frac{D\overline{W}}{D\bar{z}^j} - 3|W|^2 \right), \tag{B3}$$

where $\mathcal{K}$ is the Kähler potential and $\mathcal{K}^{i\bar{j}}$ is the inverse of the Kähler metric $\mathcal{K}_{ij} \equiv \frac{\partial^2 K}{\partial z_i \partial \bar{z}_j}$.

The periodic potentials arise from the interference of the instanton superpotential and the superpotential from other SUSY breaking sources, W_0. Assuming that the SUSY breaking scale is

$$F \sim \frac{DW_0}{Dz_i}, \tag{B4}$$

this gives rise to the following form for the potential,

$$\begin{aligned} V &\approx F \left(\sum_{i=1}^{n_{\rm ax}} \frac{\partial}{\partial z_i} \sum_{j=1}^{N} \tilde{\Lambda}_j^3 e^{ib_j F_j} \right) + \text{c.c.}, \\ &\approx \sum_{i=1}^{n_{\rm ax}} \sum_{j=1}^{N} \frac{2F\tilde{\Lambda}_j^3 b_j N_j^i}{M_S} e^{-b_j \sum_k^{n_{\rm ax}} N_j^k s_k} \cos\left(\sum_{k=1}^{n_{\rm ax}} b_j N_j^k t_k \right), \end{aligned} \tag{B5}$$

where M_S is the string scale.

2. Superpotential in type-IIB string theory

In this section, we review the original arguments of Ref. [15], which provide a context for the Marčenko-Pastur models in Kachru-Kallosh-Linde-Trivedi (KKLT) [112] comptactifications of Type-IIB string theory. In this setup, we find motivations for the relationship between the parameter, $\beta_{\mathcal{M}}$, and the ratio of axions to moduli. We also discuss and highlight the potential power random matrix theory could have in these physical models.

N-flation models are proposed in order to solve the issue regarding the requirement of trans-Plackian displacements of inflatons. Given their symmetry properties, axions could potentially provide a very good candidate in these models. The original model for N-flation consisted of $n_{\rm ax} \gg 1$ decoupled axion fields, each with identical masses that served to drive a period of inflation through the assisted inflation mechanism [14,113]. The fields have periodic potentials as expressed in Eq. (2), where the scales $\Lambda_{a,i}$ can

be significantly lower than the UV cutoff scale of the theory due to dimensional transmutation. The fields with identical masses undergo a common initial displacement ϕ' as they continue to roll in unison, providing an effective single field displacement of the order $\sqrt{n_{\rm ax}}\phi'$.

Further expanding on these concepts, Easter and McAllister incorporated the mathematics of random matrix theory in a more general framework in which the axion masses come from distinct spectra in Ref. [15]. In their framework, the form of the matrix used to determine a spectrum of axion masses is only dependent on the basic structure the matrix possesses, which can be extracted by the supergravity potential,

$$V = e^{k}(K^{AB}D_{A}WD_{\bar{B}}\overline{W} - 3|W|^{2}). \tag{B6}$$

The KKLT superpotential from nonperturbative effects which are generated from the associated moduli and axions is given as

$$W_{i} = \tilde{\Lambda}_{i}e^{-2\pi\rho_{i}}e^{2\pi i\phi_{i}} \equiv C_{i}e^{2\pi i\phi_{i}}, \tag{B7}$$

where C_i are constants when the moduli are fixed at their minimum. A Taylor expansion about the origin at $\phi_i = 0$ along with the F-flatness conditions $D_A W|_{\phi_i=0} = 0$ finds the mass matrix from quadratic order terms in the axion fields,

$$\mathcal{M}_{ij} = (2\pi)^{2}e^{K}(K^{AB}D_{A}C_{i}D_{B}C_{j} - 3C_{i}C_{j}), \tag{B8}$$

where

$$V = \mathcal{M}_{ij}\phi^{i}\phi^{j}. \tag{B9}$$

Note that $i, j = 1, \ldots, N$ run over the Kähler moduli, where the terms $A, B = 1, \ldots, N + L$ run over the dilaton, complex moduli and Kähler moduli. After the kinetic terms are bought into their canonical form (see Sec. II B), the mass matrix can be expressed as

$$\widetilde{\mathcal{M}}_{ij} = (2\pi)^{2}\frac{e^{K}}{f_{i}f_{j}}U_{i}^{k}(K^{AB}D_{A}C_{k}D_{B}C_{l} - 3C_{i}C_{j})U_{j}^{l}. \tag{B10}$$

Despite the complex form of $\mathcal{M}_{ij}$ in Eq. (B10), it can be shown that the characteristics of the N-flation model can be extracted from the eigenvalues of a random matrix with independent and identically distributed (i.i.d) entries. Numerically and semianalytically, it was shown that, regardless of the input distributions for K, f_i, U_i^k, C_i, $D_A C_i$ and K^{AB}, the complicated structural form of the mass matrix above can be simplified by assuming that the leading contribution to $\mathcal{M}_{ij}$ takes the following form,

$$\mathcal{M}_{ij} = B_{iA}B_{Aj}, \tag{B11}$$

where B_{iA} is defined as

$$B_{iA} = 2\pi\frac{e^{\mathrm{k}/2}}{f_{i}}U_{i}^{K}\mathcal{Z}_{Ak}, \tag{B12}$$

with $\mathcal{Z}_{Ak}$ a matrix constructed of Kähler covariant derivatives. The approximation made in Eq. (B11) is subject to the arguments that the matrix B_{iA} should be a $N \times (N + L)$-dimensional matrix constructed from i.i.d variables with zero mean and variance σ^2. The spectral properties of a matrix of this form are well known from the Marčhenko-Pastur limiting law in random matrix theory.

3. Axions and moduli in string theory

In the context of string theory, the parameter $\beta_{\mathcal{K},\mathcal{M}}$ in our study can be related to the relative number of axions to moduli appearing in the axion mass and kinetic matrices. In M-theory, $\beta_{\mathcal{K}} = 1$, while, as discussed in the main text, $0 < \beta_{\mathcal{M}} \leq 1$ is specified by the number of instantons. In (weakly coupled) Type-IIB string theories compactified on Calabi-Yau manifolds, $\beta_{\mathcal{K}} = 1$, while $\beta_{\mathcal{M}}$ is specified by the ratio of the number of axions (from the Kähler moduli) to the total number of moduli (Kähler plus complex structure plus axiodilaton).

The value $\beta_{\mathcal{K}} = 1$ in Type IIB comes from the large volume, tree level result for the Kähler potential, which is sum separable for the Kähler and complex structure moduli (e.g., Eq. (10.104) in Ref. [5]). Values of $\beta_{\mathcal{K}} \neq 1$ can arise when a mixing between the Kähler and complex structure moduli occurs. For example, in Ref. [114], the authors introduce matter fields from D-branes leading to the nontrivial mixing of all the moduli fields. Such mixing can also come from quantum corrections in α' or g_s and from non-Calabi-Yau compactification considerations.

The number of Kähler and complex structure moduli coming from Calabi-Yau 3-folds are topologically invariant and are given by the hodge numbers $h_{1,1}$ (Kähler moduli) and $h_{1,2}$ (complex structure moduli) respectively, which can be used to define the value of $\beta_{\mathcal{M}}$,

$$\beta_{\mathcal{M}} = \frac{h_{1,1}}{(h_{1,1} + h_{1,2} + 1)}. \tag{B13}$$

Following from a complete construction of reflexive polyhedra from Kreuzer and Skarke [8], the topological and geometrical information of the extra dimensions can be extracted (e.g., Ref. [115]). The data on the Hodge numbers from the Kreuzer-Skarke database are shown in the left-hand panel of Fig. 26. In the right-hand panel of Fig. 26, we show the probability density of $\beta_{\mathcal{M}}$ defined in Eq. (B13) in KKLT compactifications.

In Type-IIB string theory on a Calabi-Yau manifold, topologies with $\beta_{\mathcal{M}}$ close to zero or unity (Hodge numbers of zero or going to infinity) will be rare. Distributions with values close to $\beta_{\mathcal{M}} = 0.5$ are more expected in fitting with

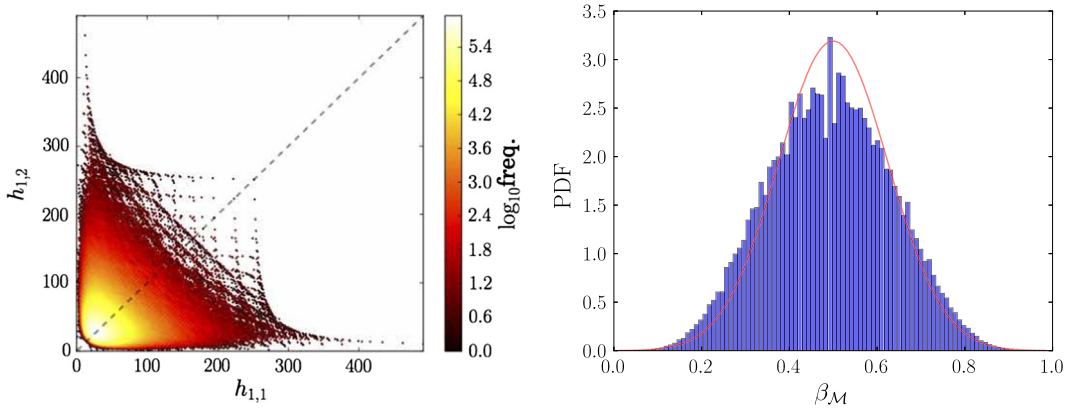

FIG. 26. Database of string compactifications and associated ratio of axions to moduli: *Left Panel:* Probability density of the hodge numbers h_{11} (Kähler moduli) and h_{12} (complex structure moduli) on Calabi-Yau manifolds from the construction of Ref. [8]. *Right Panel:* Probability density of $\beta_{\mathcal{M}}$ on Calabi-Yau manifolds. This is reasonably well fit by a Gaussian distribution with mean $\bar{\beta}_{\mathcal{M}} = 0.5$ and standard deviation $\sigma_{\beta} = 0.125$ (solid line). (Since the distribution has exactly zero probability density at the boundaries, a Gaussian fit cannot be perfect.)

the Kreuzer-Skarke database and mirror symmetry. In the M-theory limit, however, one has exactly $\beta_{\mathcal{M}} = 1$, i.e., equal numbers of axions and moduli. A final point to note about the low-energy theory is that Type IIB requires orientifold projection in order to obtain chiral fermions leading to the Betti number relation for axions vs moduli. However, some axions are also "eaten" by gauge bosons from Green-Schwarz anomaly cancellation, which alters the number of light axions [116].

APPENDIX C: RANDOM MATRIX THEORY

1. Matrix ensembles

The study of the statistical properties of the spectral behavior for sample covariance matrices in models involving high-dimensional data structures has seen prolific advancements in both their theoretical and practical applications. The most well-known random matrix ensembles consistent with modeling physical systems are the *Wigner-Dyson* or so-called *beta* ensembles of Hermitian matrices classified by the *three-fold* way [117,118] with elements distributed according to the probability function

$$P(X)DX = \mathcal{Z}e^{-\frac{N\beta}{4}TrX^{\dagger}X}DX, \tag{C1}$$

where $\mathcal{Z}$ is a distribution normalization constant and DX is the Haar measure. The parameter β is the Dyson index determined by the symmetry group of the matrix with classical values $\beta \in \{1, 2, 4\}$, [6]each with well-defined eigenvalue distributions for full matrix Wishart ensembles which give unitary, orthogonal or symplectic transformation invariance in matrix space [119–121]. These special orders of β defining the three division algebras over the real numbers correspond to correlation functions which can be explicitly expressed in terms of polynomials orthogonal to the associated invariant measure.

We are primarily interested in the class of symmetric, $(A \to O^{T}AO)$, positive-definite, real matrices with orthogonal invariance residing in the Wishart ensemble. The eigenvalue spectral distribution and limit properties of Wishart matrices play an important part in many aspects of multivariate analysis [122]. We begin with the basic matrix property that it is always possible to take any ensemble of non-Hermitian matrices and construct a random matrix in the Wishart form,

$$X_{ij} = H_{ih}^{T}H_{hj}, \tag{C2}$$

where H_{hj} is a $(n \times p)$ dimensional rectangular matrix with a shaping index, $\beta = n/p$[7] X_{ij} is defined as a positive-definite Wishart matrix in the class $W_{\mathbb{R}}(n, \Sigma_p)$ with n degrees of freedom and population covariance matrix Σ_p. Its eigenvalues, which are our derived physical quantities, are the positive real values, $\lambda_i = m_i^2$ or $\lambda_i = f_i^2$, where $\{\lambda_i \in \mathbb{R} | \lambda_i > 0\}$. When $\Sigma_p = \mathbb{1}$, this is referred to as the "null" case corresponding to the class of white Wishart matrices or the $\beta = 1$ Laguerre ensemble. The limiting normalized eigenvalue spectral density function, $P(x)$, of a white Wishart matrix is given by the Marčhenko-Pastur distribution (see Appendix C 2). It has also been shown in the limit that $\Sigma_p = \mathbb{1}$ ensembles will reproduce the Marčhenko-Pastur distribution with a total invariance over $\beta = \{1, 2, 4\}$ [123]. The asymptotic distribution for the rescaled largest eigenvalues of a white Wishart covariance

[6]The β parametrization should not be confused with the submatrix dimension parameters for $\mathcal{K}_{ij}$ and $\mathcal{M}_{ij}$ denoted as $\beta_{\mathcal{K}}$ and $\beta_{\mathcal{M}}$ used throughout this paper.

[7]See Appendix C 2 for physical motivations in the context of string theory.

matrix is determined by the *Tracy-Widom* distribution [124]. Finite-dimensional analysis of real Wishart matrices, whereby the properties of the largest eigenvalues can be extracted, incorporate determining the hypergeometric functions of matrix arguments [38,125].

2. Marčhenko-Pastur law

The Marčhenko-Pastur law is but one of several limiting laws in random matrix theory used to describe the asymptotic behavior of empirical measures of sample covariance matrices [126]. Matrices of this form can find a purpose in many areas of physics and have recently found traction in the context of string theory models. We provide a brief review of the properties of the Marčhenko-Pastur law, continuing the arguments made in Ref. [15] as discussed in Appedix B 2 in the context of axion mass spectra arising in KKLT compactifications in Type-IIB string theory.

The elements of B_{iA} in Eq. (B11) are drawn from a standard Gaussian statistical distribution such that the axion mass matrix in the canonical basis is defined in the class of Wishart matrices. Given the mass matrix is sufficiently large, the eigenvalue spectrum of m_a^2 values is governed by the Marčhenko-Pastur distribution law parametrized by the two quantities $\beta_{\mathcal{M}} = n_{\rm ax}/p$ and $\sigma_{\mathcal{M}}^2$. The closed form density expression for the Marčhenko-Pastur distribution of which the shape is encoded by $\beta_{\mathcal{M}}$ is given as

$$p(m_a^2) = \begin{cases} \frac{1}{2\pi m_a^2 \beta_{\mathcal{M}} \sigma_{\mathcal{M}}^2} \sqrt{(\gamma_+ - m_a^2)(m_a^2 - \gamma_-)}, \\ 0, \end{cases} \tag{C3}$$

where γ_+ and γ_- are defined as

$$\gamma_+ = \sigma_{\mathcal{M}}^2 (1 + \sqrt{\beta_{\mathcal{M}}})^2, \tag{C4}$$

$$\gamma_- = \sigma_{\mathcal{M}}^2 (1 - \sqrt{\beta_{\mathcal{M}}})^2. \tag{C5}$$

The density function in Eq. (C3) is defined on the compact interval $[\gamma_-, \gamma_+]$ such that $\gamma_- \geq m_a^2 \geq \gamma_+$, where the probability density drops out to zero outside this region. The eigenvalues will surely converge to the compact interval bounds in the asymptotic limit. The rate of convergence for the real case was found in the work by Johnstone [124], where he found approximations satisfactory up to dimensions as low as $n, p \approx 10$. We will therefore treat our distributions as "safe" and within the asymptotic understanding of their spectral convergence when using axion population numbers, $n_{\rm ax} \geq \mathcal{O}(10)$.

It follows that the overall scale of eigenvalues is controlled by the variance, $\sigma_{\mathcal{M}}^2$, where

$$\langle m_a^2 \rangle = \sigma_{\mathcal{M}}^2. \tag{C6}$$

In the original axiverse models for N-flation, the overall scale for the axion masses is fixed for inflationary concerns, i.e., $\sigma \sim 10^{-5} M_{\rm Pl}$, in order to enforce that density perturbations from inflation are consistent with observational limits. However, such constraints are of no interest for cosmological concerns for axions in the dark sector.

3. Eigenvalue spectra: Nonuniversality and free multiplicative convolution

a. Generalized Wishart matrices

We have currently only considered the construction of $\mathcal{K}_{ij}$ and $\mathcal{M}_{ij}$ in our effective model residing in Eq. (6) involving matrix products to first order with no level of decomposition or considerations of the free convolution of matrix ensembles.[8] This study is only concerned with a focus on the products of fixed ensembles with the entries constructed from some predefined statistical distribution; however, there are several areas which could be interesting for further study in this regard. More general considerations of the construction of Wishart matrices such as those appearing in our MP RMT and WW RMT models involve the product of random independent Gaussian matrices. See Refs. [128–131] for detailed work regarding this subject.

Following the approach in this work, a generalized construction of random matrices residing in the Wishart ensemble involves the product of $\mathcal{S}$ non-Hermitian submatrices residing in the Ginibre ensemble, $X_{ij} = H_{ih}^{(1)} H_{hl}^{(2)} H_{lj}^{(\mathcal{S})}$. The study of the singular values of these products corresponding to the root of the associated eigenvalues is of interest in generalizations of these random matrix ensembles. The spectral density functions, $P_{\mathcal{S}}(x)$ (where $\mathcal{S} \in \mathbb{N} = \{1, 2, 3, \ldots\}$), for these ensembles involving the product of an arbitrary number of matrices are asymptotically described by the *Fuss-Catalan* distributions with their moments defined by the Fuss-Catalan numbers [132]. These distributions can be expressed as the multiplicative free convolution of the Marčhenko-Pastur spectral density limit, of the order $\mathcal{S}$ such that

$$P_{\mathcal{S}}(x) = [P_1(x)^{\boxtimes \mathcal{S}}]. \tag{C7}$$

A powerful two-dimensional parametrization of the Fuss-Catalan numbers comes in the form of the *Raney* sequences. An explicit density $W_{p,r}(x)$ characterized by the indices $p, r \in \mathbb{R}$ defines a family of measures incorporating the multiplicative free measures of the Marčhenko-Pastur distribution reproducing the both the Fuss-Catalan densities and Wigner semicircle distribution for specific values of r and p.

[8] See Ref. [127] for the potential uses of additive free convolutions of matrix ensembles in the context of random Hessian construction in supergravity.

b. Spiked Wishart matrices

Recent work involving so-called *nonwhite* Wishart matrices or spiked population models has yielded interesting insight into the effects of a phase-transition phenomena [39] in the fluctuations of the largest eigenvalues of the population covariance matrix [35–38,133]. These models can make predictions beyond the traditional ensembles found in the literature. The presence of large eigenvalues in the population covariance matrix can have a significant effect of the total spectral width and limiting distributions of the sample covariance matrix in the limit $n, p \to \infty$ and have been incorporated into many interesting areas such as finance [134].

Figure 7 shows the eigenvalue spectrum for a mass matrix displaying the features of these models. Singular eigenvalues in these models will leave the support of the Marčhenko-Pastur bulk with a value $\sim\mathcal{O}(N)$ for $(N \times N)$ dimensional data structures. The determination of the true values of the largest eigenvalues in these models can be analyzed using various methods such as the stochastic operator method [135] or using the Painleve formula [136]. In general, the effects in these models will be most prevalent when considering high-dimensional data structure or in our case a high population number of axions.

APPENDIX D: OUTLYING COSMOLOGIES

In this section, we provide a picture of the evolution of the cosmological densities in the context of example cosmologies which would not pass the cuts outlined in Sec. V. In Fig. 27, we show the cosmological evolution for three example configurations using the MP RMT model for a population of axions behaving as dark matter. We allow the equal field condition scaling parameter $\bar{f}$ to approach the high scale limit, $\bar{f} \to M_{\rm pl}$ (*blue* line). The large value for $\bar{f}$ causes the population of axions to collectively "inflate" the universe for a period ($10^{-4} \lesssim a \lesssim 10^{-1}$) with the collective energy density overshooting the expected value of $z_{\rm eq}$ before it enters the scaling regime behaving as nonrelativistic matter. The evolution of the collective axion field density as dark matter begins to scale accordingly at an approximate time of $z \approx 0$ with a value of $z_{\rm eq}$ far too early in the cosmic history. Such cosmologies return axion DM domination with $\Omega_{\rm DM} \approx 0.9999$.

Decreasing the scale of $\bar{f}$ to $0.1M_{\rm pl}$ (cyan line) causes the axions to account for the correct total dark matter density at the current time where $\Omega_{\rm DM} = 0.2528$. The reduced initial field conditions cause the axions to enter the correct scaling regime with a significantly reduced redshift. The inset of Fig. 27 shows the value of $z_{\rm eq}$ falling within acceptable bounds [crossing of black $(\rho_b + \rho_{\rm ax})$ and red (ρ_r) lines]. Further decreasing $\bar{f} = 0.01M_{\rm pl}$ (green line) corresponds to an example configuration in which the total matter density is insufficient for the universe to reach redshift zero within ten Hubble times according to our numerical configurations. The lowest value of z reached corresponded to an axion dark matter density parameter value of $\Omega_{\rm DM} = 0.0119$. In Fig. 28, we show potential configurations which do not pass the acceleration criterion, $\ddot{a} > 0$, or give dominant contributions to the critical density at $z = 0$ for MP DE cosmologies. The axion density is set by the initial field displacement and axion mass, $m_a^2\phi^2$. Without a sufficient scaling of the initial field displacements (light blue and green lines), the axion masses need to be higher to account for the acceptable

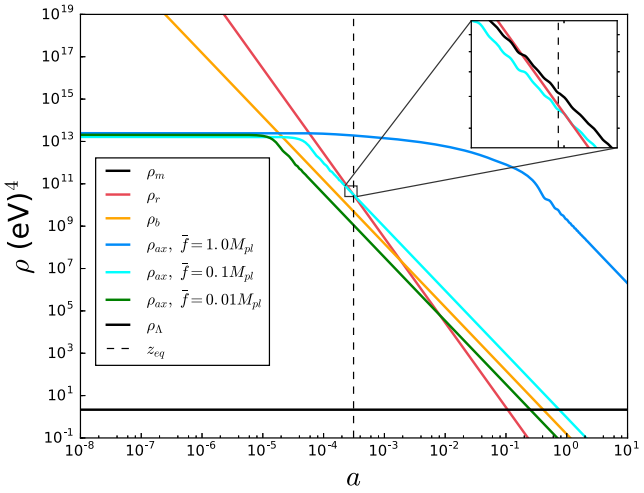

FIG. 27. MP DM example outlier cosmology density evolution: Evolution of the collective axion density, $\rho_{\rm ax}$, using $n_{\rm ax} = 20$. We highlight the effect of using different initial field condition scales set by $\bar{f}$, where values of $\bar{f} \to 1$ returning cosmologies which do not fulfill the criterion for acceptable values of $z_{\rm eq}$.

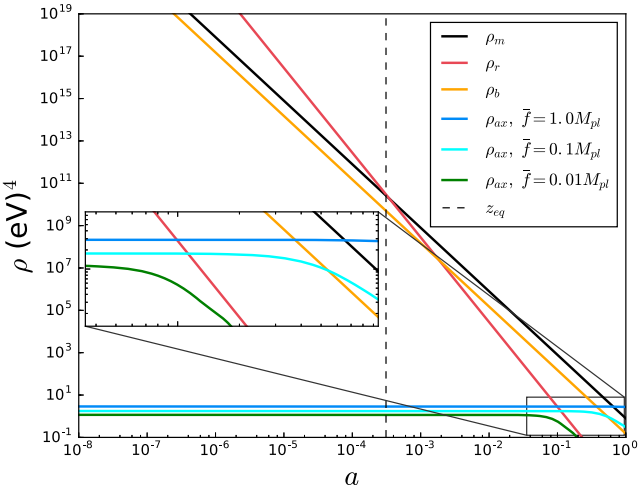

FIG. 28. MP DE example outlier cosmology density evolution: Evolution of the collective axion density, $\rho_{\rm ax}$, for $n_{\rm ax} = 20$ We highlight the effect of using different scales for $\bar{f}$ where insufficient values of $\bar{f}$ lead to outlier cosmologies which do not fulfil the acceleration criterion, $\ddot{a} > 0$.

amount of dark energy density. However, this generally causes the axion to start oscillating earlier, following the condition $m_a \leq H$, which returns smaller values of $\Omega_{\rm DE}$. Increasing the value of the scaling $\bar{f}$ in this configuration would satisfy an accelerating universe with sufficient dark energy density. The increased value of $\bar{f} = 0.1 M_{\rm pl}$ enhances the final dark energy density at $z = 0$, returning a value of $\Omega_{\rm DE} = 0.1979$. Finally, the configuration (blue line) with $\bar{f} = 1.0 M_{\rm pl}$ is sufficient for an effective dark energy cosmology returning a value of $\Omega_{\rm DE} = 0.7732$.

[1] K. Olive *et al.* (Particle Data Group Collaboration), Chin. Phys. C **38**, 090001 (2014).
[2] P. A. R. Ade *et al.* (Planck Collaboration), Astron. Astrophys. **594**, A13 (2016).
[3] G. Bertone, D. Hooper, and J. Silk, Phys. Rep. **405**, 279 (2005).
[4] S. Weinberg, Rev. Mod. Phys. **61**, 1 (1989).
[5] K. Becker, M. Becker, and J. H. Schwarz, *String Theory and M-Theory* (Cambridge University Press, Cambridge, England, 2007).
[6] E. Witten, Phys. Lett. B **149**, 351 (1984).
[7] P. Svrcek and E. Witten, J. High Energy Phys. 06 (2006) 051.
[8] M. Kreuzer and H. Skarke, Adv. Theor. Math. Phys. **4**, 1209 (2000).
[9] S. B. Giddings and A. Strominger, Nucl. Phys. **B306**, 890 (1988).
[10] S. Coleman, *Aspects of Symmetry* (Cambridge University Press, Cambridge, England, 1988).
[11] T. Banks, M. Dine, P. J. Fox, and E. Gorbatov, J. Cosmol. Astropart. Phys. 06 (2003) 1.
[12] A. Arvanitaki, S. Dimopoulos, S. Dubovsky, N. Kaloper, and J. March-Russell, Phys. Rev. D **81**, 123530 (2010).
[13] D. J. E. Marsh, Phys. Rep. **643**, 1 (2016).
[14] S. Dimopoulos, S. Kachru, J. McGreevy, and J. G. Wacker, J. Cosmol. Astropart. Phys. 08 (2008) 003.
[15] R. Easther and L. McAllister, J. Cosmol. Astropart. Phys. 05 (2006) 018.
[16] B. S. Acharya, K. Bobkov, and P. Kumar, J. High Energy Phys. 11 (2010) 105.
[17] P. W. Graham, I. G. Irastorza, S. K. Lamoreaux, A. Lindner, and K. A. van Bibber, Annu. Rev. Nucl. Part. Sci. **65**, 485 (2015).
[18] J. E. Kim, H. P. Nilles, and M. Peloso, J. Cosmol. Astropart. Phys. 01 (2005) 005.
[19] K. Choi, H. Kim, and S. Yun, Phys. Rev. D **90**, 023545 (2014).
[20] T. Higaki and F. Takahashi, J. High Energy Phys. 07 (2014) 074.
[21] G. Wang and T. Battefeld, J. Cosmol. Astropart. Phys. 04 (2016) 025.
[22] A. Masoumi and A. Vilenkin, J. Cosmol. Astropart. Phys. 03 (2016) 054.
[23] J. Preskill, M. B. Wise, and F. Wilczek, Phys. Lett. B **120**, 127 (1983).
[24] L. F. Abbott and P. Sikivie, Phys. Lett. B **120**, 133 (1983).
[25] M. Dine and W. Fischler, Phys. Lett. B **120**, 137 (1983).
[26] T. C. Bachlechner, M. Dias, J. Frazer, and L. McAllister, Phys. Rev. D **91**, 023520 (2015).
[27] T. C. Bachlechner, C. Long, and L. McAllister, J. High Energy Phys. 01 (2016) 091.
[28] R. Easther and L. C. Price, J. Cosmol. Astropart. Phys. 07 (2013) 027.
[29] D. J. E. Marsh, E. R. M. Tarrant, E. J. Copeland, and P. G. Ferreira, Phys. Rev. D **86**, 023508 (2012).
[30] M. L. Mehta, *Random Matrices* (Academic, New York, 1991).
[31] R. Hlozek, D. Grin, D. J. E. Marsh, and P. G. Ferreira, Phys. Rev. D **91**, 103512 (2015).
[32] A. Bekker and J. Roux, Commun. Stat., Theory Methods **24**, 2485 (1995).
[33] A. Dubbs, A. Edleman, P. Koev, and P. Venkataramana, J. R. Stat. Soc. Ser. B **54**, 083507 (2013).
[34] W. Młotkowski, M. A. Nowak, K. A. Penson, and K. Życzkowski, Phys. Rev. E **92**, 012121 (2015).
[35] D. Wang, Ph.D. thesis, Brandeis University, 2008.
[36] M. Y. Mo, arXiv:1011.5404.
[37] A. Bloemendal and B. Virág, arXiv:1109.3704.
[38] M. Chiani, J. Multivariate Anal. **129**, 69 (2014).
[39] J. Baik, G. Ben Arous, and S. Peche, arXiv:math/0403022.
[40] M. Honda, A. Oikawa, and H. Otsuka, J. High Energy Phys. 01 (2017) 064.
[41] T. Banks, M. Dine, P. J. Fox, and E. Gorbatov, J. Cosmol. Astropart. Phys. 06 (2003) 001.
[42] T. C. Bachlechner, C. Long, and L. McAllister, J. High Energy Phys. 12 (2015) 042.
[43] F. Ferrari, S. Klevtsov, and S. Zelditch, Nucl. Phys. **B869**, 89 (2013).
[44] B. S. Acharya, K. Bobkov, G. L. Kane, P. Kumar, and J. Shao, Phys. Rev. D **76**, 126010 (2007).
[45] B. S. Acharya, K. Bobkov, G. L. Kane, J. Shao, and P. Kumar, Phys. Rev. D **78**, 065038 (2008).
[46] B. S. Acharya and K. Bobkov, J. High Energy Phys. 09 (2010) 001.
[47] B. S. Acharya and C. Pongkitivanichkul, J. High Energy Phys. 04 (2016) 009.
[48] L. C. Price, H. V. Peiris, J. Frazer, and R. Easther, J. Cosmol. Astropart. Phys. 02 (2016) 049.
[49] J. Goodman and J. Weare, Commun. Appl. Math. Comput. Sci. **5**, 65 (2010).
[50] D. Foreman-Mackey, D. W. Hogg, D. Lang, and J. Goodman, Publ. Astron. Soc. Pac. **125**, 306 (2013).
[51] D. Foreman-Mackey, J. Open Source Software **1** (2016).
[52] D. J. Fixsen, E. S. Cheng, J. M. Gales, J. C. Mather, R. A. Shafer, and E. L. Wright, Astrophys. J. **473**, 576 (1996).
[53] É. Aubourg *et al.*, Phys. Rev. D **92**, 123516 (2015).

[54] Z. Zhai, M. Blanton, A. Slosar, and J. Tinker, arXiv: 1705.10031.
[55] J. Zuntz *et al.*, Astron. Comput. **12**, 45 (2015).
[56] J. Dunkley, M. Bucher, P. G. Ferreira, K. Moodley, and C. Skordis, Mon. Not. R. Astron. Soc. **356**, 925 (2005).
[57] V. Smer-Barreto and A. R. Liddle, J. Cosmol. Astropart. Phys. 01 (2017) 023.
[58] R. Daido, T. Kobayashi, and F. Takahashi, Phys. Lett. B **765**, 293 (2017).
[59] L. Hui, J. P. Ostriker, S. Tremaine, and E. Witten, Phys. Rev. D **95**, 043541 (2017).
[60] J. Halverson, C. Long, and P. Nath, arXiv:1703.07779.
[61] H. Davoudiasl and C. W. Murphy, Phys. Rev. Lett. **118**. 141801 (2017).
[62] J. E. Kim and D. J. E. Marsh, Phys. Rev. D **93**, 025027 (2016).
[63] L. Visinelli and P. Gondolo, Phys. Rev. D **80**, 035024 (2009).
[64] L. Visinelli and P. Gondolo, Phys. Rev. D **81**, 063508 (2010).
[65] L. Visinelli, Phys. Rev. D **96**, 023013 (2017).
[66] R. Bousso, L. J. Hall, and Y. Nomura, Phys. Rev. D **80**, 063510 (2009).
[67] L. A. Ureña-López and A. X. Gonzalez-Morales, J. Cosmol. Astropart. Phys. 07 (2016) 048.
[68] R. Hložek, D. J. E. Marsh, D. Grin, R. Allison, J. Dunkley, and E. Calabrese, Phys. Rev. D **95**, 123511 (2017).
[69] D. J. E. Marsh and J. Silk, Mon. Not. R. Astron. Soc. **437**, 2652 (2014).
[70] H.-Y. Schive, T. Chiueh, and T. Broadhurst, Nat. Phys. **10**, 496 (2014).
[71] B. Schwabe, J. C. Niemeyer, and J. F. Engels, Phys. Rev. D **94**, 043513 (2016).
[72] B. Bozek, D. J. E. Marsh, J. Silk, and R. F. G. Wyse, Mon. Not. R. Astron. Soc. **450**, 209 (2015).
[73] H.-Y. Schive, T. Chiueh, T. Broadhurst, and K.-W. Huang, Astrophys. J. **818**, 89 (2016).
[74] A. Sarkar, R. Mondal, S. Das, S. K. Sethi, S. Bharadwaj, and D. J. E. Marsh, J. Cosmol. Astropart. Phys. 04 (2016) 012.
[75] P. S. Corasaniti, S. Agarwal, D. J. E. Marsh, and S. Das, Phys. Rev. D **95**, 083512 (2017).
[76] E. Armengaud, N. Palanque-Delabrouille, C. Yèche, D. J. E. Marsh, and J. Baur, arXiv:1703.09126.
[77] V. Irsic, M. Viel, M. G. Haehnelt, J. S. Bolton, and G. D. Becker, Phys. Rev. Lett. **119**, 031302 (2017).
[78] D. J. E. Marsh, Phys. Rev. D **91**, 123520 (2015).
[79] A. Arvanitaki and S. Dubovsky, Phys. Rev. D **83**, 044026 (2011).
[80] P. Pani, V. Cardoso, L. Gualtieri, E. Berti, and A. Ishibashi, Phys. Rev. Lett. **109**, 131102 (2012).
[81] H. Kodama and H. Yoshino, Int. J. Mod. Phys. Conf. Ser. **07**, 84 (2012).
[82] A. Arvanitaki, M. Baryakhtar, and X. Huang, Phys. Rev. D **91**, 084011 (2015).
[83] H. Yoshino and H. Kodama, Classical Quantum Gravity **32**, 214001 (2015).
[84] N. Arkani-Hamed, L. Motl, A. Nicolis, and C. Vafa, J. High Energy Phys. 06 (2007) 060.
[85] J. P. Conlon, J. Cosmol. Astropart. Phys. 09 (2012) 019.
[86] M. Kamionkowski, J. Pradler, and D. G. E. Walker, Phys. Rev. Lett. **113**, 251302 (2014).
[87] R. Emami, D. Grin, J. Pradler, A. Raccanelli, and M. Kamionkowski, Phys. Rev. D **93**, 123005 (2016).
[88] M. Cicoli, M. D. Goodsell, and A. Ringwald, J. High Energy Phys. 10 (2012) 146.
[89] M. Cicoli, K. Dutta, and A. Maharana, J. Cosmol. Astropart. Phys. 08 (2014) 12.
[90] P. Fox, A. Pierce, and S. Thomas, arXiv:hep-th/0409059.
[91] L. Visinelli and P. Gondolo, Phys. Rev. Lett. **113**, 011802 (2014).
[92] E. Komatsu *et al.*, Astrophys. J. Suppl. Ser. **180**, 330 (2009).
[93] Planck Collaboration, Astron. Astrophys. **594**, A20 (2016).
[94] D. J. E. Marsh, D. Grin, R. Hložek, and P. G. Ferreira, Phys. Rev. D **87**, 121701 (2013).
[95] D. J. E. Marsh, D. Grin, R. Hlozek, and P. G. Ferreira, Phys. Rev. Lett. **113**, 011801 (2014).
[96] K. J. Mack and P. J. Steinhardt, J. Cosmol. Astropart. Phys. 05 (2011) 001.
[97] E. W. Kolb and M. S. Turner, *The Early Universe* (Addison-Wesley, Reading, MA, 1990).
[98] O. Wantz and E. Shellard, Phys. Rev. D **82**, 123508 (2010).
[99] T. Banks and M. Dine, Nucl. Phys. **B505**, 445 (1997).
[100] G. D. Coughlan, W. Fischler, E. W. Kolb, S. Raby, and G. G. Ross, Phys. Lett. B **131**, 59 (1983).
[101] T. Banks, D. B. Kaplan, and A. E. Nelson, Phys. Rev. D **49**, 779 (1994).
[102] B. de Carlos, J. A. Casas, F. Quevedo, and E. Roulet, Phys. Lett. B **318**, 447 (1993).
[103] G. Lazarides, R. K. Schaefer, D. Seckel, and Q. Shafi, Nucl. Phys. **B346**, 193 (1990).
[104] P. Fox, A. Pierce, and S. D. Thomas, arXiv:hep-th/0409059.
[105] J. Kaplan, J. High Energy Phys. 10 (2006) 065.
[106] M. Millea, L. Knox, and B. D. Fields, Phys. Rev. D **92**, 023010 (2015).
[107] M. S. Turner, Phys. Rev. D **28**, 1243 (1983).
[108] A. Khmelnitsky and V. Rubakov, J. Cosmol. Astropart. Phys. 02 (2014) 019.
[109] N. K. Porayko and K. A. Postnov, Phys. Rev. D **90**, 062008 (2014).
[110] A. Aoki and J. Soda, Int. J. Mod. Phys. D **26**, 1750063 (2017).
[111] D. Blas, D. L. Nacir, and S. Sibiryakov, Phys. Rev. Lett. **118**, 261102 (2017).
[112] S. Kachru, R. Kallosh, A. Linde, and S. P. Trivedi, Phys. Rev. D **68**, 046005 (2003).
[113] A. R. Liddle, A. Mazumdar, and F. E. Schunck, Phys. Rev. D **58**, 061301 (1998).
[114] M. Grana, T. W. Grimm, H. Jockers, and J. Louis, Nucl. Phys. **B690**, 21 (2004).
[115] R. Altman, J. Gray, Y.-H. He, V. Jejjala, and B. D. Nelson, J. High Energy Phys. 02 (2015) 158.
[116] T. W. Grimm and J. Louis, Nucl. Phys. **B699**, 387 (2004).
[117] M. A. Stephanov, J. J. M. Verbaarschot, and T. Wettig, arXiv:hep-ph/0509286.
[118] P. Bourgade, L. Erdos, and H.-T. Yau, arXiv:1104.2272.
[119] A. T. James, Ann. Math. Stat. **31**, 151 (1960).

[120] T. Ratnarajah and R. Vaillancourt, Comput. Math. Appl. **50**, 399 (2005).
[121] F. Li and Y. Xue, arXiv:0901.3379.
[122] J. Harnad, *Random Matrices, Random Processes and Integrable Systems* (Springer-Verlag, New York, 2011).
[123] I. Dumitriu, Ph.D. Thesis, Massachusetts Institute of Technology, 2003.
[124] I. M. Johnstone, Annali di statistica **29**, 295 (2001).
[125] M. Chiani, arXiv:1401.3987.
[126] V. A. Marcenko and L. A. Pastur, Math. USSR-Sbornik **1**, 457 (1967).
[127] D. Marsh, L. McAllister, and T. Wrase, J. High Energy Phys. 03 (2012) 102.
[128] W. Młotkowski, M. A. Nowak, K. A. Penson, and K. Życzkowski, Phys. Rev. E **92**, 012121 (2015).
[129] P. J. Forrester and D.-Z. Liu, J. Stat. Phys. **158**, 1051 (2015).
[130] K. A. Penson and K. Życzkowski, Phys. Rev. E **83**, 061118 (2011).
[131] W. Mlotkowski, K. A. Penson, and K. Zyczkowski, Documenta Mathematica **18**, 1573 (2013).
[132] N. Alexeev, F. Götze, and A. Tikhomirov, arXiv:1012.2743.
[133] D. Wang, arXiv:0711.2722.
[134] J. P. Bouchaud and M. Potters, arXiv:0910.1205.
[135] A. Bloemendal and B. Virág, arXiv:1011.1877.
[136] M. Y. Mo, arXiv:1101.5144.